

EVALUATION OF AN EXISTING INDUSTRIAL BUILDING RETROFITTED WITH  
FLUID VISCOUS AND VISCOELASTIC DAMPERS UNDER NO-PULSE AND  
PULSE-LIKE BASE EXCITATIONS

by

Muhammet Arif Uçkaç

B.S., Civil Engineering, Boğaziçi University, 2020

Submitted to the Institute for Graduate Studies in  
Science and Engineering in partial fulfillment of  
the requirements for the degree of  
Master of Science

Graduate Program in Civil Engineering

Boğaziçi University

2022

## ACKNOWLEDGEMENTS

Firstly, I would like to present my special thanks to Professor Serdar SOYÖZ. The contributions of Professor Serdar SOYÖZ to my academic perspective and achievement cannot be quantified. All the engineering approaches and theories that I have learned from the lectures of Professor Serdar SOYÖZ are invaluable acquisitions for me. Besides, constructive feedback, qualitative guidance, and good communication from Professor Serdar SOYÖZ during the thesis period helped me a lot in pursuing my graduate study efficiently and wishfully. I also would like to express my sincere gratitude to Professor Serdar SOYÖZ for the invaluable support for my further academic studies and plans.

Due to the precious suggestions of Professor Hilmi LUŞ during the process of determining my thesis subject, I owe a debt of sincere gratitude to him. Furthermore, I also put myself into a group of lucky ones because of finding an opportunity to listen Professor Hilmi LUŞ's lectures and his intellectual interpretations.

It is unthinkable to pass that section without presenting my special thanks to Professor Kutay ORAKÇAL. I made use of the information and methodologies learned from Professor Kutay ORAKÇAL's lectures enormously. His comprehensive and systematic style of teaching deserves high regard. Hence, I also would like to present my special thanks to Professor Kutay ORAKÇAL for his direct and indirect contributions to my work.

I would like to present my special thanks to Associate Professor Ufuk YAZGAN for accepting to be my thesis jury and allocating time.

I would like to thank Teaching Assistant Emre AYTULUN for allocating time to help me. His assistance when I needed to consult about my thesis was always ready.

My Family. All the effort you made for me is complimentary and cannot be repaid. I would like to present my furthest gratitude to you for your support in all aspects of my life and your existence.

## **ABSTRACT**

### **EVALUATION OF AN EXISTING INDUSTRIAL BUILDING RETROFITTED WITH FLUID VISCOUS AND VISCOELASTIC DAMPERS UNDER NO-PULSE AND PULSE-LIKE BASE EXCITATIONS**

A retrofitting methodology using passive control devices, was adopted in this study for the performance improvement of an existing industrial building in Malatya, Yeşilyurt. The efficiency of the methodology was investigated through the analytical model developed in SAP2000. The structure was constructed in 1989, and the design report of the structure is unreachable. Therefore, site investigations were carried out to determine the necessary dimensions and material properties as well as soil class. The structure was exposed to severe earthquakes and fire, and hence the industrial building is currently out of use because of possessing risk of life safety. Previous retrofitting studies using steel jacketing and addition of shear walls were not enough to reach the desired level of performance. For this reason, a retrofitting methodology using passive control devices, fluid viscous dampers and viscoelastic dampers, was chosen as an alternative tool for bringing the structure to the desired performance level. Firstly, within the investigation, the performance level of the structure was determined according to TBDY 2018, and the necessity of a new retrofitting methodology was demonstrated. Then, the structure's finite element model (FEM) was updated by adding the passive control devices properly. The Nonlinear Time History Analysis (NLTHA) method was used to obtain the plastic deformation demands on the members. The structure is very close to the East Anatolian Fault, and therefore near-fault effect having velocity pulse characteristics on the response was also considered in the analyses. In line with this purpose, ten different earthquake records, comprised of five no-pulse like records and five pulse-like records, were selected according to TBDY 2018, and NLTHA were conducted for the bare frame, damped with FVD frame, and damped with VE frame separately, and results were evaluated.

## ÖZET

### **AKIŞKAN VİSKOZ VE VİSKOELASTİK SÖNÜMLEYİCİLER İLE GÜÇLENDİRİLMİŞ MEVCUT ENDÜSTRİYEL BİNANIN PULS ETKİSİNE SAHİP OLAN VE OLMAYAN DEPREM YER HAREKETLERİ ALTINDA DEĞERLENDİRİLMESİ**

Bu çalışmada Malatya Yeşilyurt'ta bulunan mevcut bir endüstriyel binanın performans iyileştirmesi için pasif kontrol cihazları güçlendirme metodolojisi olarak benimsenmiştir. Metodolojinin etkinliği, sonlu eleman programı SAP2000 kullanılarak analitik model aracılığıyla araştırılmıştır. Yapı 1989 yılında inşa edilmiş olup yapının statik raporuna ulaşılamamaktadır. Bu nedenle zemin sınıfının yanı sıra gerekli boyut uzunlukları ve malzeme özelliklerinin belirlenmesi için saha araştırmaları yapılmıştır. Şiddetli deprem ve yangına maruz kalan yapı, can güvenliği riski taşıdığından şu anda kullanım dışıdır. Çelik mantolama ve perde duvarların kullanıldığı önceki güçlendirme çalışmaları istenen performans düzeyine ulaşamamıştır. Bu nedenle, yapıyı istenilen performans seviyesine getirmek için yeni bir araç olarak akışkan viskoz ve viskoelastik sönümleyiciler yeni güçlendirme metodu olarak seçilmiştir. İlk olarak yapının performans düzeyi doğrusal olmayan statik analiz yöntemi ile TBDY 2018'e göre belirlenmiş ve yeni bir güçlendirme metodolojisinin gerekliliği ortaya konulmuştur. Daha sonra yapının sonlu eleman modeli, pasif kontrol cihazları uygun şekilde eklenerek güncellenmiştir. Kesitler üzerindeki plastik şekil değiştirme taleplerinin elde edilmesinde zaman tanım alanında doğrusal olmayan hesap yöntemi kullanılmıştır. Yapı, Doğu Anadolu Fayı'na çok yakındır ve bu nedenle, yapının davranışı üzerinde hız puls etkisi de gözetilmiştir. Bu amaç doğrultusunda TBDY 2018'e uygun 5 puls etkisine sahip deprem ve 5 puls etkisine sahip olmayan deprem kaydı olmak üzere 10 farklı deprem kaydı seçilmiş ve çıplak çerçeve, akışkan viskoz sönümleyici çerçeve ve viskoelastik çerçeve için ayrı ayrı zaman tanım alanında lineer olmayan hesap yöntemi kullanılarak analizler gerçekleştirilmiş ve sonuçlar değerlendirilmiştir.

## TABLE OF CONTENTS

ACKNOWLEDGEMENTS .....	iii
ABSTRACT.....	iv
ÖZET .....	v
LIST OF FIGURES .....	viii
LIST OF TABLES.....	xiv
LIST OF SYMBOLS .....	xvi
LIST OF ABBREVIATIONS.....	xix
1. INTRODUCTION .....	1
1.1. Overview .....	1
1.2. Literature Review .....	5
1.3. Objective .....	16
1.4. Scope .....	17
2. THE STRUCTURE AND NONLINEAR STATIC ANALYSIS (NSA).....	18
2.1. General Information .....	18
2.2. Seismicity of the Region .....	20
2.3. Finite Element Model.....	24
2.3.1. Material Properties and Section Analysis.....	24
2.3.2. SAP2000 Model of the Structure .....	32
2.3.3. Loads .....	35
2.3.4. Plastic Hinges .....	35
2.4. Evaluation of the Existing Structure (NSA).....	36
3. PASSIVE CONTROL DEVICES AS A RETROFITTING METHODOLOGY .....	42
3.1. Theory and Mechanics of Fluid Viscous Dampers .....	42
3.2. Theory and Mechanics of Viscoelastic Dampers.....	45
3.3. Selection of Dampers' Mechanical Properties (Shear Constraint) .....	48
3.4. Modelling the Structure with FVDs and VEs .....	56
4. SEISMIC LOADING .....	61
4.1. No-Pulse Like Records .....	62
4.2. Pulse-Like Records .....	63
4.3. Nonlinear Time History Analysis (NLTHA) .....	64

5. NLTHA RESULTS.....	65
5.1. Plastic Rotation Demands .....	68
5.1.1. No-Pulse Like Records' Bar Charts .....	69
5.1.2. Pulse-Like Records' Bar Charts .....	74
5.1.3. Geometric Means.....	79
5.2. Change in the Modal Periods, Peak Spectral Accelerations and Total Number of Plastic Hinges.....	81
5.3. Maximum Link Forces and Links' Force-Deformation Graphs .....	83
6. EVALUATION OF THE ANALYSIS RESULTS and COMMENTS .....	90
7. CONCLUSION.....	100
7.1. Summary and Results.....	100
7.2. Future Works.....	102
REFERENCES .....	103

## LIST OF FIGURES

Figure 1.1. Working principle of passive control devices [1].....	1
Figure 1.2. Force-Displacement graph of dampers [2]. .....	2
Figure 1.3. Torre Mayor Tower [1].....	4
Figure 1.4. LAPD Recruit Training Center [1]. .....	5
Figure 2.1. General view of the structure.....	19
Figure 2.2. Side view of the structure. ....	20
Figure 2.3. Front view of the structure.....	20
Figure 2.4. Seismicity map of Turkey [27]. .....	21
Figure 2.5. Seismicity of the region [28]. .....	21
Figure 2.6. Horizontal elastic design spectrum TBDY 2018 [29]. .....	23
Figure 2.7. Horizontal elastic design spectrum of the region. ....	24
Figure 2.8. Column fire damage. ....	25
Figure 2.9. Column damage.....	26
Figure 2.10. View from the inside of the factory building. ....	27
Figure 2.11. Another view from the inside of the factory building. ....	27
Figure 2.12. Stress-Strain Relation of confined and unconfined concrete 5A.1 of TBDY 2018.....	28
Figure 2.13. Stress-Strain relation of reinforcing steel 5A.2 of TBDY2018. ....	30

Figure 2.14. The North Axis Frame of the Building Block-1.....	33
Figure 2.15. The Mid Axes Frames of the Building Block-1.....	33
Figure 2.16. The South Axis Frame of the Building Block-1.....	33
Figure 2.17. The East Axis Frame of the Building Block-1.....	34
Figure 2.18. The West Axis Frame of the Building Block-1.....	34
Figure 2.19. Finite element model of the Building Block-1.....	34
Figure 2.20. Conversion of the pushover curve into modal capacity curve.....	36
Figure 2.21. Pushover Curve X-Direction.....	37
Figure 2.22. Modal Capacity Curve X-Direction.....	37
Figure 2.23. Pushover Curve Y-Direction.....	38
Figure 2.24. Modal Capacity Curve Y-Direction.....	38
Figure 2.25. 5B.3 of TBDY 2018.....	39
Figure 3.1. Typical fluid damper and parts [33].....	43
Figure 3.2. Force-Displacement relation of linear and nonlinear viscous damper [17]....	43
Figure 3.3. Nonlinear and linear damper's velocity-force graphs [33].....	44
Figure 3.4. Representative sketch of a VE damper [34].....	45
Figure 3.5. Single Spring (a), Damper (b), Kelvin Model (c), Maxwell Model (d), a Generalized Model (e) [35].....	46
Figure 3.6. Typical force-displacement loop at 3 Hz [36].....	47

Figure 3.7. An example of diagonal bracing San Miguel Mall – Lima, Peru – New Build [33].....	48
Figure 3.8. Extender montage representation San Bernardino Justice Center – San Bernardino, CA – New Build [33].....	49
Figure 3.9. Finite element model of the Building Block-1.....	51
Figure 3.10. The West Axis Frame of the Building Block-1.....	51
Figure 3.11. The South Axis Frame of the Building Block-1.....	52
Figure 3.12. The North Axis Frame of the Building Block-1.....	52
Figure 3.13. Dimensions of the VE damper.....	55
Figure 3.14. Damper configuration along the shorter side of the Building Block-1. ....	56
Figure 3.15. Damper configuration along the longer side of the Building Block-1. ....	56
Figure 3.16. Damper configuration of the Building Block-1.....	57
Figure 3.17. Extender bars [33]. ....	58
Figure 3.18. Modelling of FVDs for linear and nonlinear analysis [40]. ....	58
Figure 4.1. Target spectrum, geometric mean spectrum and response spectrums of no-pulse like records... ..	62
Figure 4.2. Target spectrum, geometric mean spectrum and response spectrums of pulse like records... ..	63
Figure 5.1. Numbering of the North Axis Frame of the Building Block-1.....	66
Figure 5.2. Numbering of the Mid Axis Frame of the Building Block-1. ....	66
Figure 5.3. Numbering of the South Axis Frame of the Building Block-1.....	67

Figure 5.4. Numbering of the East Axis Frame of the Building Block-1.....	67
Figure 5.5. Numbering of the West Axis Frame of the Building Block-1.....	67
Figure 5.6. Imperial R2 maximum plastic rotation of columns.....	69
Figure 5.7. Imperial R3 maximum plastic rotation of columns.....	69
Figure 5.8. Superstitions R2 maximum plastic rotation of columns.....	70
Figure 5.9. Superstitions R3 maximum plastic rotation of columns.....	70
Figure 5.10. Manjil R2 maximum plastic rotation of columns.....	71
Figure 5.11. Manjil R3 maximum plastic rotation of columns.....	71
Figure 5.12. Landers R2 maximum plastic rotation of columns.....	72
Figure 5.13. Landers R3 maximum plastic rotation of columns.....	72
Figure 5.14. Tottori R2 maximum plastic rotation of columns. ....	73
Figure 5.15. Tottori R3 maximum plastic rotation of columns. ....	73
Figure 5.16. Morgan R2 maximum plastic rotation of columns.....	74
Figure 5.17. Morgan R3 maximum plastic rotation of columns.....	74
Figure 5.18. Chi-Chi R2 maximum plastic rotation of columns.....	75
Figure 5.19. Chi-Chi R3 maximum plastic rotation of columns.....	75
Figure 5.20. Parkfield R2 maximum plastic rotation of columns.....	76
Figure 5.21. Parkfield R3 Maximum Plastic Rotation of Columns.....	76
Figure 5.22. Darfield R2 maximum plastic rotation of columns. ....	77
Figure 5.23. Darfield R3 maximum plastic rotation of columns. ....	77

Figure 5.24. Duzce R2 maximum plastic rotation of columns. ....	78
Figure 5.25. Duzce R3 maximum plastic rotation of columns. ....	78
Figure 5.26. Geometric mean of R2 maximum plastic rotations of No-Pulse like records. .....	79
Figure 5.27. Geometric mean of R3 maximum plastic rotations of No-Pulse like records.....	79
Figure 5.28. Geometric mean of R2 maximum plastic rotations of Pulse like records. ....	80
Figure 5.29. Geometric mean of R3 maximum plastic rotations of Pulse like records. ....	80
Figure 5.30. Hysteresis behavior of link elements (Imperial Earthquake) [43].....	85
Figure 5.31. Hysteresis behavior of link elements (Superstitions Earthquake). ....	85
Figure 5.32. Hysteresis behavior of link elements (Manjil Earthquake). ....	86
Figure 5.33. Hysteresis behavior of link elements (Landers Earthquake). ....	86
Figure 5.34. Hysteresis behavior of link elements (Tottori Earthquake).....	87
Figure 5.35. Hysteresis behavior of link elements (Morgan Earthquake). ....	87
Figure 5.36. Hysteresis behavior of link elements (Chi-Chi Earthquake). ....	88
Figure 5.37. Hysteresis behavior of link elements (Parkfield Earthquake). ....	88
Figure 5.38. Hysteresis behavior of link elements (Darfield Earthquake).....	89
Figure 5.39. Hysteresis behavior of link elements (Duzce Earthquake).....	89
Figure 6.1. Velocity-Force graph of the Fluid Viscous Dampers having 0.3 nonlinearity coefficient and Velocity-Force graph of damping part of the Viscoelastic Dampers.....	95

Figure 6.2. Velocity-X time history (Morgan Earthquake). ..... 96

Figure 6.3. Velocity-Y Time History (Morgan Earthquake). ..... 96

Figure 6.4. Velocity-X Time History (Chi-Chi Earthquake). ..... 97

Figure 6.5. Velocity-Y Time History (Chi-Chi Earthquake). ..... 97

Figure 6.6. Velocity-X Time History (Parkfield Earthquake). ..... 98

Figure 6.7. Velocity-Y Time History (Parkfield Earthquake). ..... 98

## LIST OF TABLES

Table 2.1.	Local soil effect coefficient for the short period region [29].....	22
Table 2.2.	Local soil effect coefficient for the period of 1 second [29]. .....	22
Table 2.3.	Information on reinforcing steels 5A.1 TBDY 2018.....	30
Table 2.4.	Necessary parameters for section analyses of concrete on XTRACT [31]. ...	31
Table 2.5.	Necessary parameters for section analysis of S370 on XTRACT [31]. .....	31
Table 2.6a.	Comparison of sections' moment capacities for C16 and C12 (M2) .....	31
Table 2.6b.	Comparison of sections' moment capacities for C16 and C12 (M2) .....	32
Table 2.7a.	Comparison of sections' moment capacities for C16 and C12 (M3) .....	32
Table 2.7b.	Comparison of sections' moment capacities for C16 and C12 (M3) .....	32
Table 2.8.	Evaluation of beams.....	40
Table 2.9.	Evaluation of columns. ....	41
Table 3.1.	Shear strength of the members at the junction points.....	50
Table 3.2.	Properties of FVD 17120.....	53
Table 3.3.	Suggested C values of FVD having nonlinearity 0.3 for 250 KN rated force. .....	54
Table 3.4.	Properties of the extender bars.....	60
Table 4.1.	No-Pulse like earthquake records. ....	62
Table 4.2.	Pulse like earthquake records. ....	63

Table 5.1.	Modal periods of the Building Block-1 for each case. ....	81
Table 5.2a.	Peak spectral acceleration of No-Pulse like earthquake records. ....	81
Table 5.2b.	Peak spectral acceleration of No-Pulse like earthquake records. ....	81
Table 5.3a.	Peak spectral acceleration of Pulse like earthquake records.....	82
Table 5.3b.	Peak spectral acceleration of Pulse like earthquake records.....	82
Table 5.4.	Total number of plastic hinges for No-Pulse like earthquake records.....	82
Table 5.5.	Total number of plastic hinges for Pulse like earthquake records.....	82
Table 5.6.	Maximum link forces under No-Pulse like records (FVD). ....	83
Table 5.7.	Maximum link forces under Pulse like records (FVD).....	83
Table 5.8.	Maximum link forces under No-Pulse like records (VE).....	84
Table 5.9.	Maximum link forces under Pulse like records (VE). ....	84
Table 6.1.	Geometric mean of the ratios.....	93

## LIST OF SYMBOLS

$a_i$	Distance between the axes of longitudinal reinforcement
$A_s$	Longitudinal reinforcement area
$b_0$	Smaller section dimensions between the axes of stirrups that wrap core concrete
$c_d$	Damper coefficient
$d_{1,max}^{(X)}$	Modal displacement demand for the first mode
$d_{1,max}^{(X)}$	The largest modal displacement of single degree of freedom system
$E_s$	Elasticity of reinforcing steel
$F_1$	Local ground effect coefficient for period of 1 second
$f_c$	Compressive stress of confined concrete
$f_{c0}$	Compressive strength of unconfined concrete
$f_{cc}$	Compressive strength of confined concrete
$f_{ct}$	Tensile strength of concrete
$F_d$	Damping force
$f_{ex}$	Effective confinement strength – x direction
$f_{ey}$	Effective confinement strength – y direction
$F_s$	Local ground effect coefficient for short period
$f_s$	Strength of reinforcing steel
$f_{su}$	Ultimate strength of reinforcing steel
$f_{sy}$	Yielding strength of reinforcing steel
$f_{yw}$	Yield strength of transverse reinforcement
$G'$	Shear storage modulus of the viscoelastic material
$G''$	Shear loss modulus of the viscoelastic material
$h_0$	Larger section dimensions between the axes of stirrups that wrap core concrete
$k_d$	Stiffness coefficient
$K_d$	Axial flexibility of the fluid viscous damper
$k_e$	Confinement efficiency coefficient ratio
$K_e$	Stiffness of the extender bar

$P_k$	Snow load for calculation
$P_{k0}$	Snow load
$S_1$	Spectral acceleration coefficient for period of 1 second
$S_{ae}$	Spectral acceleration of horizontal elastic design spectrum
$S_{D1}$	Design spectral acceleration coefficient for period of 1 second
$S_{de}(T_1)$	Elastic design spectral displacement
$S_{di}(T_1)$	Nonlinear spectral displacement corresponding to the first natural vibration period $T_1$ of the carrier system
$S_{DS}$	Design spectral acceleration coefficient for short period
$S_s$	Short period spectral acceleration period
$T_A$	Corner period of horizontal design spectrum
$T_B$	Corner period of horizontal design spectrum
$T_L$	The period at the point of transition to constant displacement region
$U_{NX1,max}^{(X)}$	Displacement demand (target displacement) at the top of the building
$V_c$	Concrete contribution
$V_w$	Shear reinforcement contribution
$A$	Total shear area of the viscoelastic material
$C$	Damping constant
$F$	Damping force
$kN$	Kilonewton
$M_2$	Moment about Axis-2
$M_3$	Moment about Axis-3
$MPa$	Megapascal
$R_2$	Rotation about Axis-2
$R_3$	Rotation about Axis-3
$s$	Spacing between the axes of stirrups in the longitudinal direction
$t$	Thickness of the viscoelastic material
$V$	Velocity between the ends of the damper
$w$	Loading frequency
$\varepsilon_s^{(CP)}$	Limit strain value at collapse prevention level
$\theta_p^{(LD)}$	Plastic rotation limit value for limited damage region

$\theta_P^{(CD)}$	Plastic rotation limit value for significant damage region
$\theta_P^{(CP)}$	Plastic rotation limit value for collapse prevention region
$\epsilon_c$	Compressive unit deformation
$\epsilon_s$	Strain of reinforcing steel
$\epsilon_{sh}$	Strain of reinforcing steel (beginning of strain hardening region)
$\epsilon_{su}$	Ultimate strain of reinforcing steel
$\epsilon_{su}$	Strain at maximum stress in transverse reinforcing steel
$\epsilon_{sy}$	Yielding strain of reinforcing Steel
$\rho_x$	Volumetric ratio of transverse reinforcements – x direction
$\rho_y$	Volumetric ratio of transverse reinforcements – y direction
$\alpha$	Damping exponent ( $\alpha=1$ Linear FVD)

## LIST OF ABBREVIATIONS

2D	Two Dimensional
3D	Three Dimensional
ADAS	Added Damping and Stiffness Device
ASCE	American Society of Civil Engineers
BRB	Buckling Restraint Brace
CSD	Center of Supplemental Devices
DBE	Design Based Earthquake
DBYBHY	Deprem Bölgelerinde Yapılacak Binalar Hakkında Yönetmelik
DMRSF	Ductile Moment Resisting Space Frame
DOF	Degree of Freedom
EDB	Energy Dissipation Brace
FEM	Finite Element Model
FOE	Frequently Occurred Earthquake
FVD	Fluid Viscous Damper
GM	Generalized Model
HVAC	Heating, Ventilation and Airconditioning
HYD	Metallic Yielding Hysteretic Device
KM	Kelvin Model
LSA	Linear Static Analysis
LSP	Linear Static Procedure
MOE	Maximum Considered Earthquake
MOP	Multi Objective Optimization Process
MRF	Moment Resisting Frame
MW	Maxwell Model
NEHRP	National Earthquake Hazards Reduction Program
NLTHA	Nonlinear Time History Analysis
NSP	Nonlinear Static Procedure
NVD	Nonlinear Viscous Damper
PEER	The Pacific Earthquake Engineering Research Center
PGA	Peak Ground Acceleration

PI	Performance Index
P-Spectra	Performance Spectra Method
PVID	Parallel Layout Viscous Inerter Damper
RBS	Reduced Beam Section
RD	Peak Deformation Response
RSA	Response Spectrum Analysis
RTHS	Real-Time Hybrid Simulation Method
SDF	Single Degree of Freedom
SMA	Shape Memory Alloys
SOP	Single Objective Optimization Process
SRB	Supplemental Recentering Brace
TADAS	Triangular-Plate Added Damping and Stiffness devices
TBDY	Türkiye Bina Deprem Yönetmeliği
TDTH	Türkiye Deprem Tehlike Haritası
TR	Total Force Transmitted to the Structure
VE	Viscoelastic Damper
VID	Viscous Inerter Damper

# 1. INTRODUCTION

## 1.1. Overview

Engineers have investigated the behavior of structures throughout the last decades. These investigations improved our understanding of structures under specific excitations. Excitations structures generally faced with are earthquakes, blasts, and wind-induced oscillations. Under different excitation types, the behavior of specific type structures such as high-rise, mid-rise, industrial buildings, nuclear structures or bridges was analyzed, and design codes were constructed accordingly. As time progresses, design codes are being improved, and new buildings can resist the excitations more effectively. On the other hand, there is a significant number of old structures designed according to old regulations, and as it is stated before, regulations are being improved constantly, and therefore sufficiency of old structures is suspicious. In that case, dampers are an efficient tool used to eliminate the negative effect of severe excitations on the bearing capacity of the structures. There are four different types of passive dampers in the industry that are commonly used for the seismic protection of structures. These are viscous fluid dampers, solid viscoelastic dampers, friction dampers, and metallic dampers.

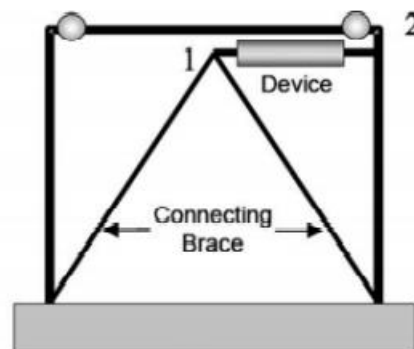


Figure 1.1. Working principle of passive control devices [1].

The structure shown in figure 1.1 has two DOFs. The lateral displacement of the top of the connecting brace is numbered as one, and the lateral displacement of the top of the frame is numbered as 2. The mechanical principle of these devices is mainly formulized

based on the relative displacement and/or velocity of point1 and point2. These devices are activated because of the relative displacement and/or velocity of point1 and 2, and therefore such devices are designated as passive control devices requiring no power to activate and operate. Because of that reason, passive control devices are uncontrollable and hence impossible to control forces or the behavior of the device during the excitation [2].

Passive energy dissipation devices are classified, generally, into three groups. Fluid viscous dampers and solid viscoelastic dampers are rate-dependent or velocity-dependent devices. Friction dampers and metallic dampers are considered as rate-independent or displacement-dependent devices. The mechanical and hysterical behavior of these dampers is crucial for modeling and assessing the dampers' effects on seismic response.

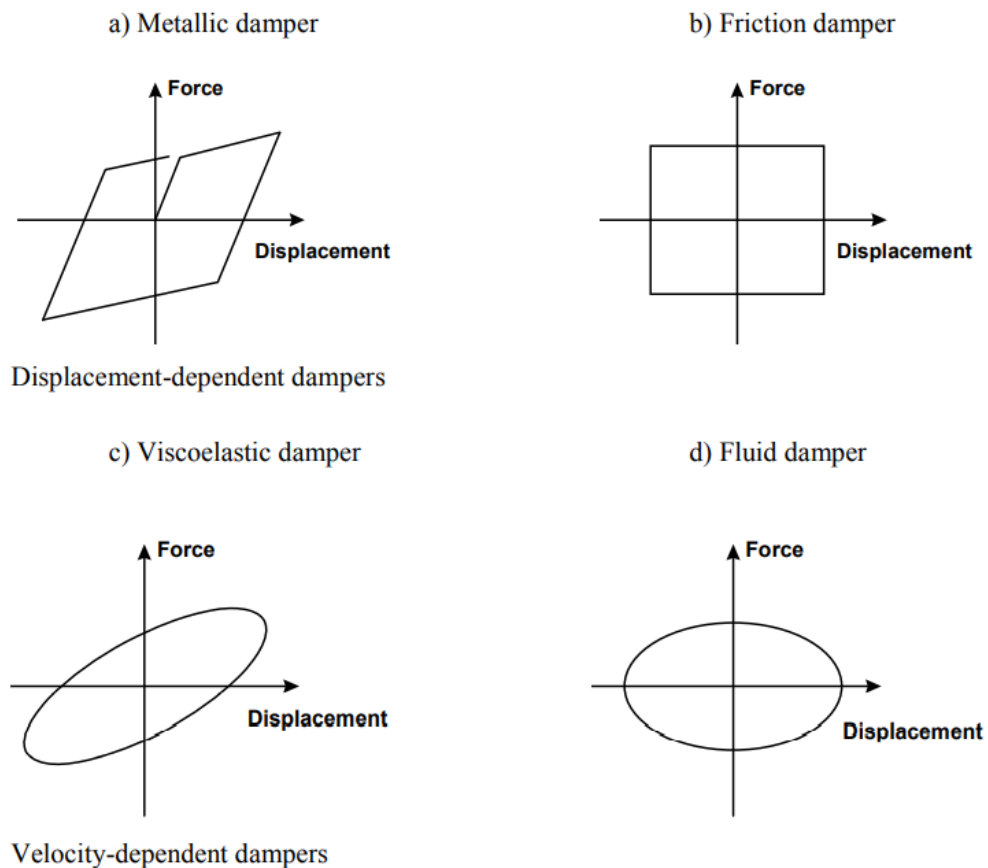


Figure 1.2. Force-Displacement graph of dampers [2].

Passive control devices are being widely used and are becoming more and more popular. One of the recent applications of fluid dampers is Torre Mayor Tower, Mexico City, Mexico. The structure is 57-story steel and reinforced concrete tower. The building Patient Tower, Seattle, was constructed originally as a concrete shear wall building and then retrofitted with friction dampers. The structure is a 14-story tower. For the retrofitting process of LAPD Recruit Training Center, Los Angeles viscoelastic dampers were used. The LAPD Center was constructed as four-storey steel building having sizeable open interior spaces. Under these conditions, the structure was considered a seismically deficient structure due to its low levels of inherent damping, and therefore retrofitting was required. For the construction of Kaiser Santa Clara Medical Center, Santa Clara, Calif., BRBs (Buckling Restrained Braces) were used. The structure is a steel-framed building with a 327-bed hospital having 120 BRB devices [1].



Figure 1.3. Torre Mayor Tower [1].



Figure 1.4. LAPD Recruit Training Center [1].

## 1.2. Literature Review

Symans *et al.* [1] presented the critical topics such as fundamental principles of energy dissipation systems, mechanical behavior and mathematical modeling of passive energy dissipation devices, advantages and disadvantages of these devices, development of guidelines and design philosophy for analysis and design, and recent applications of passive energy dissipation systems. Commonly used devices were categorized into four groups: viscous fluid dampers, solid viscoelastic dampers, friction dampers, and metallic dampers. Metallic yielding devices are considered as rate-independent because the resisting forces in the devices are only a function of relative displacement across the devices. However, viscous fluid dampers are considered rate-dependent because the device's resisting force is dependent on the relative velocity across the device. The elastic period of the structure change with metallic yielding devices but not with fluid viscous dampers. This change in period may be responsible for increased base shear in the structure. On the other hand, viscoelastic dampers are both displacement and velocity-dependent. Lastly, friction dampers dissipate energy via sliding friction across the interface between two solid bodies.

In the paper by Akcelyan *et al.* [3], several key findings about using linear and nonlinear analysis procedures for the seismic evaluation of steel frame buildings were published. In the analyses, steel frame building with supplemental damping devices and, in particular, buckling-restrained braces (BRBs) and nonlinear viscous dampers (NVDs) was used. At the end of the analyses, it is shown that 2D and 3D analyses give similar results in predicting the dynamic behavior of steel frame buildings regardless of the damper type. Moreover, considering the axial flexibility of the NVDs in the analytical model substantially improves the overall numerical predictions. Lastly, from the experiments and analyses, it is also understood that the effective damping ratio recommended by ASCE 41-13 for linear static analysis (LSA) for evaluating frame buildings with BRBs or NVDs may not be conservative enough.

Dong *et al.* [4] evaluated the response of Moment Resisting Frames (MRFs), and during the experiments, Real-Time Hybrid Simulation Method (RTHS) was used. Reduced strength MRFs were designed with added damping to achieve better seismic performance. The strength of MRFs is 100%, 75%, and 60%, respectively. The aim of the reduced beam sections is to limit the bending moment at the beam-column interface. During the testing process, the same structure was used with different seismic weights to reflect the reduced beam section effect on the structure. During the tests, FOE (Frequently Occurred Earthquake), DBE (Design Based Earthquake) and MCE (Maximum Considered Earthquake) types of earthquakes were applied to the structure. In conclusion, under MCE and 1.4MCE ground motions, the D60V structure demonstrated better performance with respect to conventional MRF structure (D100V structure without dampers). Much of the energy dissipated through nonlinear viscous dampers, and RBS beam-column connections showed excellent performance during the tests.

Lin and Chopra [5] investigated the earthquake responses of a single degree of freedom system with a nonlinear fluid viscous damper. The effectiveness of the FVDs on response was investigated based on the dampers' supplemental damping ratio and nonlinearity because these two parameters are dimensionless and independent. Parametrization of nonlinear FVDs is hard to achieve because of the nonlinear governing equations, and therefore a system with nonlinear FVDs is replaced with an equivalent linear system, and the equivalent linear system is constructed based on equating the energy dissipation in the

two systems. The dynamic response of the system was evaluated by two critical parameters peak deformation response (RD) and total force transmitted to the foundation (TR). Earthquake response of SDF was evaluated based on response quantities. Investigation showed that the influence of the damper nonlinearity on the acceleration, velocity and deformation of the system is very limited. However, damper nonlinearity affects the damper force significantly. Especially in the velocity-sensitive spectral region, the damper nonlinearity has no influence and small influence in acceleration and displacement sensitive regions. This observation led to a practical design application that is the prediction of system response with nonlinear FVDs by analyzing the equivalent linear viscous system.

Singh *et al.* [6] presented a method to find the amount of damping for reaching the desired level of response reduction. Viscos and viscoelastic dampers were used as a source of extra damping. An effort was also given to optimally distribute these devices to achieve the best performance. The gradient-based optimization approach was used for the purpose of finding optimal distribution of the damping devices. In the application, 24-storey building structure was used, and the objective was to reach the maximum reduction in performance functions. The response reduction target is set to reduce the drift by 40 percent for 24-storey building structure with damping devices. During the optimization process, along with sensitivity analysis, it was observed that the distribution of the devices is highly dependent on structural and ground motion characteristics. In the 24-storey structure building case, devices were mainly placed in the upper stories, but this result is unique for the investigated structure. For a different structure with different characteristics, the optimization process would lead to placing the devices more in lower stories.

It is known that buildings with an asymmetric plan are open to taking more earthquake-induced damage than symmetric-plan buildings. Chopra and Lin [7] investigated how the plane-wise distribution of FVDs affects the behavior of one-storey, linear elastic, and asymmetric plan systems. The system used in the investigation is symmetric about the x and y-axis in terms of mass distribution. On the other hand, stiffness properties are unsymmetric about the y axis, and therefore one side of the system is relatively stiffer. RSA (response spectrum analyses) for classically damped systems was extended to determine the peak deformation of non-classically damped systems. Extended RSA for non-classically damped systems gives accurate predictions for peak deformation. Also, it was shown that the

unsymmetric distribution of dampers is more effective in reducing the response than the symmetric distribution. According to the study, it is also essential to place the dampers farther away from the CSD to increase the effectiveness of the devices in reducing the response.

Singh *et al.* [8] tried to utilize the frequency-dependent and independent dampers in a structure to reach the desired performance level under earthquake excitation. For the optimization process, genetic algorithm was used. The advantage of the genetic algorithm is that it can be used for any type of performance function. Primarily used for the performance functions that are not differentiable and whose gradient changes drastically. On the other hand, the disadvantage of the genetic algorithm is having high computational effort. The optimization process was conducted for two buildings with three types of dampers to illustrate the application of the algorithm. The first building is a shear-beam model of a 24-storey building, whereas the second building is 6-storey torsional system. The viscous dampers exhibit pure viscous behavior for low frequency of deformation. However, as the frequency increases, the damper also exhibits restoring behavior. Besides classical viscous dampers, viscoelastic damper and frequency-dependent Maxwell model types of dampers were used.

Cardone *et al.* [9] considered the two different types of braces to evaluate the effectiveness of bracing systems for a reinforced concrete frame. The first bracing system depends on the hysteric behavior of steel elements, while the other relies on the superelastic properties of shape memory alloys (SMA). These bracing systems increase the stiffness of the structure as well as the energy dissipation capacity. These systems can reduce the deformation of elements effectively. However, due to the increase in stiffness, the structure may experience more base shear, and hence foundation costs may increase. The SMA-based device exhibits significant re-centering capacity, which means restoring the undeformed shape of the structure even if yielding of the structural members occurs extensively. Experiments were conducted based on two strategies. For the structure with steel-based energy dissipation braces (EDB's), limiting the ductility demand in members and the residual displacement of the structure were aimed. For the structure with Supplemental Recentering Braces (SRB's), no residual displacement was aimed at the end of the earthquake. Nine different groups of tests were arranged with or without EDBs and SRBs.

The shaking test results showed that the test structure with SRBs could return its initial position with negligible residual displacement. Lastly, it was understood that the advantages of SRBs over EDBs are mainly economic and architectural aspects.

Rama Raju *et al.* [10] evaluated the effectiveness of different bracing mechanisms for a 20-storey benchmark building with linear viscous fluid dampers. Chevron Brace, Upper Toggle, and Scissors Jack mechanisms are bracing mechanisms used in the analyses. It was observed that the optimal location for dampers is the first few storeys from the ground, and using damping beyond 30% leads to a small increase in performance level and therefore is not economically feasible. In the study, the linear time history analysis with modal superposition for a 20-storey building was conducted. The link elements were used for defining linear dampers, and the same effective stiffness and damping values were used for each mechanism. Performance indicators were determined as inter-storey drift, base shear and maximum floor acceleration. The analysis results showed that the most efficient mechanism is the toggle brace mechanism, and the second-best configuration is the scissor jack mechanism.

The study by Pan *et al.* [11] proposed a demand-based optimal design method for a single degree of freedom system with PVID (Parallel Layout Viscous Inerter Damper). The Viscous Inerter Damper mainly consists of an inerter, a viscous element, and a support spring. A parametric study was conducted to comprehend the dynamic response of an oscillator when the parameters of natural frequency, damping ratio and mass ratio were changed within given ranges. The analysis results concluded that optimization of a PVID-equipped oscillator for vibration mitigation without additional constraint conditions is meaningless from the viewpoint of optimization. The additional constraint was specified as a new parameter that considers the total cost of the dampers because a lower response is always accompanied by a higher cost, and therefore optimization process needs to find a balance point between cost and response reduction. By using MOP (Multi Objective Optimization Problem), the optimal design would be achieved by considering the damper force and displacement as objectives while defining the constraints as mass ratio, damping ratio and stiffness. However, in the study, the  $\epsilon$ -constraint approach was adopted by treating the second objective as an additional constraint, and therefore MOP turns into a SOP with an additional constraint. For the optimization process, the PVID's force was chosen as the

objective function and displacement of the PVID's was defined as the additional constraint. In the end, some design examples with their performance were presented.

Tubaldi [12] analyzed the dynamic behavior of the two adjacent buildings of different heights connected to each other at the top of the shortest one by viscous/viscoelastic dampers. The buildings were defined as two linear elastic shear beams of different heights. The complex model analysis method was used to investigate the dynamic behavior of the coupled system. Firstly, the equation of motion for the system undergoing damped free vibration was constructed, and the characteristics parameters that control the response were determined. Later, the weak form and reduced-order model of the system was built. Finally, two case studies with viscous dampers were analyzed. In the paper, it was indicated that the linear elastic shear beam model might not be suitable for the realistic structures, and therefore model can be developed when needed.

Patel *et al.* [13] investigated the behavior of two identical adjacent two-degree of freedom systems connected to each other by viscous damper under harmonic and stationary white-noise base excitation. Past studies showed that if the frequencies of the connected structures are well separated, passive dampers are more effective. Reducing the system's relative displacement or absolute acceleration is considered control objective. From the analysis results under harmonic, white-noise and real earthquake motions, some conclusions were drawn. Firstly, it was observed that for a specific structure under given excitation, there exists an optimum damping coefficient of the damper for the minimum response. Moreover, optimum parameters of the damper are not influenced much by the damping of the connected structures, and therefore for the optimum damper properties, a closed-form expression of the undamped system can be used. It was also obtained from the analysis that the dampers become more effective in reducing the responses for the structures with stiffer lower storey compared to upper storey and having uniform masses at each story. Finally, from the real earthquake base excitation analyses, it was concluded that the response of the system is sensitive to the frequency content of the earthquake.

In the work of Mazza *et al.* [14], attention was given to HYDs (Metallic Yielding Hysteretic Devices), and hysteric behavior of these devices is independent of temperature and velocity of motion. The advantages of these devices are being manufactured from

traditional materials, requiring little maintenance, and having a low cost for energy dissipation. The application of the passive control devices to existing structures is always more difficult than to new structures because the application of control devices to existing structures requires properly knowing the current system properties. In the investigation, nonlinear static analysis was conducted to obtain the vulnerability level of the structure. Later, optimal HYDs damper properties were selected, and nonlinear dynamic responses of the braced and unbraced structure were compared. The test structure is a three-storey reinforced concrete school building. At the end of the investigation, it is concluded that the determination of the equivalent viscous damping is the key step for the reliability of the design.

In the paper by Mazza *et al.* [15], a design procedure for steel braces equipped with metallic yielding damper and viscoelastic damper to reach the desired performance level was put forward. The primary structure used for the investigation was a six-storey reinforced concrete plane frame representing a medium-rise symmetric framed building. By using different damped bracing properties, nonlinear dynamic analyses were conducted, and responses were obtained for unbraced and damped brace frames, and results were compared. Furthermore, VE damper was modeled as a six-element generalized model (GM), which is a combination of the Kelvin and Maxwell Model. By using GM, viscoelastic materials can be modeled better depending on the frequency. At the end of the paper design procedure for hysteretic and viscoelastic dampers was explained.

Del Gobbo *et al.* [16] used 4-, 8- and 16-storey buildings retrofitted with linear fluid viscous dampers to evaluate the seismic performance of retrofitted buildings. The paper is the first to analyze optimal damping by considering repair costs. At the end of the analyses, several tendencies related to damping ratio-repair cost were identified. First, it was shown that repair costs are reduced as the total damping increases. Furthermore, the SLS costs showed more reductions at a lower level of damping than the ULS costs. Importantly, it was stated that repair costs could be further decreased if acceleration-sensitive nonstructural components such as HVAC equipment were placed on an upper floor from the base floor.

Lin *et al.* [17] have presented a displacement-based design methodology for seismic retrofit of an existing structure. For the methodology, nonlinear viscous dampers were used,

and an equivalent linear system approach was adopted. Based on the equivalent linear system design chart was constructed for seismic retrofit using nonlinear viscous dampers. For the analyses, an artificial input motion with PGA of 0.9 g was used. The paper only considers the first mode effect eliminating the effect of higher modes from the response because it is known from previous investigations that nonlinear viscous dampers are able to reduce the effect of higher modes from the response. According to the author, the effects of higher modes should be considered for future studies, especially for high-rise buildings.

In the paper by Jankowski *et al.* [18], the system of two adjacent three-storey buildings with different dynamic properties connected by link elements such as link, dashpot, or viscoelastic was investigated. The structures were connected at each storey level. The left building is lighter and more flexible, while the right one is heavier and stiffer. According to analysis results, additional link elements are very beneficial for the lighter and more flexible structure, while a stiffer one was not influenced much by link elements. Larger stiffness and damping values for the link elements led to the highest decrease in response, and structures vibrated in-phase. This case indicates the fully connected structures. The authors also indicated that the reason for structural pounding is the difference in the natural periods of the building. As the mass and stiffness matrixes of the structures differ from each other's much, they vibrate out of phase, increasing the probability of structural pounding.

From 1986 to 1991, seven different passive control devices were investigated at the Earthquake Engineering Research Center of California at Berkeley, and in the paper by Aiken *et al.* [19], these investigations were summarized. Different types of devices were described, and results of shaking table experiments along with analytical works were presented. Friction dampers constituted four of the studied systems, and ADAS, viscoelastic and Nickel-Titanium alloy shape memory devices are the three other systems investigated. For the large-scale earthquake simulator studies, Sumitomo Friction and 3M Viscoelastic Dampers, Pall Friction Devices, ADAS elements and Friction Devices for Steel MRF were used. The mechanical characteristics of the viscoelastic dampers led to elliptical hysteretic loops, while the friction damper showed extremely regular and repeatable behavior. For the small-scale earthquake simulator studies, Fluor Daniel energy dissipating devices and Niti Shape Memory Alloy dampers were used. Niti Shape Memory Alloy dampers were identified as useful tools for no permanent deformations.

Tsai *et al.* [20] presented the results of experimental results of triangular-plate added damping and stiffness devices (TADAS). Experimental results showed that TADAS can sustain large number of yielding hysteresis without any stiffness and strength degradation. ADAS devices made of X-shaped steel plates have been found to be very sensitive to the bolts' tightness, and therefore stiffness obtained is generally much less than predicted stiffness. In that aspect, TADAS are more useful than ADAS. In the paper, stress concentration due to the shape of the steel plates was indicated as the primary constraint for selecting shapes because for a specific shape of steel plates, stress concentrations occur, and the performance of the ADAS reduces. X-shaped and triangular-shaped steel plates can deform well into the plastic range without curvature concentration. After the investigation of the mechanical behavior of TADAS, by using the pseudo-dynamic testing procedure for a two-story steel building, the effectiveness of the TADAS was further analyzed. Experimental and analytical results showed general agreement for the TADAS device.

Whittaker *et al.* [21] investigated the hysteretic performance of steel plate ADAS elements by conducting sub-assembly experiments. Moreover, a three-storey ductile moment-resisting space frame (DMRSF) retrofitted with ADAS was used for earthquake simulator testing to study the effect of ADAS elements on response parameters. The shape of the steel plates in designing ADAS elements was identified as the main concern in the article because some shapes, such as rectangle steel plates, cause stress concentrations while some of them, such as X-shape steel plates, lead to uniform stress distribution, which is more advantageous than concentrated stresses. The main advantages of using ADAS elements are increasing strength, stiffness, and energy dissipation capacity. The most important mechanical characteristics of the ADAS element that affect the response are elastic stiffness, yield strength and yield displacement. The test structure (three-storey DMRSF) was subjected to several earthquake records. The structure with ADAS elements showed two major improvements compared to the bare frame. Firstly, the increase in elastic stiffness decreased the inter-storey drifts. Secondly, due to the yielding of ADAS elements, energy dissipated, and hence inter-storey drifts were reduced.

Chang *et al.* [22] have conducted experimental and analytical investigations about viscoelastic dampers. Three-story and nine-story steel frame structures were used for the experimental studies using shaking tables. Test results showed that, although the viscoelastic

dampers effectively reduce the seismic response, efficient design requires considering essential factors such as environmental (operational) temperature and excitation frequency. Although the increase in temperature decreases the effectiveness of viscoelastic material, they were able to reduce the seismic response considerably at all temperatures. An increase in temperature softens the viscoelastic material and eventually loses its strength and efficiency. That is the main reason behind the temperature effect. At the end of the article, the modal strain energy method using linearly equivalent viscous damping theory to predict the seismic response of VE damped structure was introduced.

Ramirez *et al.* [23] investigated the effect of supplemental damping to structure on elastic and inelastic responses. Nonlinear time history analysis was used for the purpose, and earthquake records compatible with the 2000 NEHRP spectrum were chosen. Because passive control devices are not part of a gravity-load resisting system, they can easily be replaced after earthquakes in case of taking damage. Some of the simplifications and limits for buildings with damping structures stated in the 2000 NEHRP Provision analysis methods were summarized, and the 2000 NEHRP provisions tried to be improved and verified by the authors. In that context, the paper is considered the first of two, presenting the development and verification. The paper suggested modifying the 5 % damped response spectrum for higher damping effects listed in the 2000 NEHRP Provisions.

The paper by Martinez-Romero *et al.* [24] describes the retrofitting processes using damping devices for three buildings in Mexico City. Studied three buildings are Izizaga #38-40, Cardiology Hospital Building and The Reforma #476 Building. The intention of the author in writing this paper is only to share his experiences with other colleagues. For all three buildings, ADAS-type supplemental devices were used, and an overall increase in performance was obtained. In the paper, some other serious problems common in existing structures were shared. One of them is hidden defects of the construction, such as improper anchorage of reinforcing columns or shear-wall bars of the previous retrofit into the existing building. The other problems can be summarized as insufficient strength of building materials, unrecorded and undocumented changes and modifications, changed dimensions of structural members, and impediments and difficulties in reaching the specific locations where the retrofitting work must take place.

Ramirez *et al.* [25], in the article, evaluated the accuracy of the simplified methods in predicting the peak displacement, velocity and acceleration responses of a single degree of freedom system. These simplified methods can be found within the 2000 NEHRP Provisions. By using SDOF system, the effects of higher modes on response automatically were eliminated. It was stated that the simplified methods of 2000 NEHRP Provisions can estimate the peak acceleration and peak displacement velocity very accurately. On the other hand, the differences in the velocity were as large as 50% for large effective periods while as large as 100% for short effective periods, and therefore further investigations were made to enhance the predicting peak velocities using simplified methods. Sadek et al. (1999) and Pekcan et al. (1999) proposed a new methodology for predicting relative velocity. They stated that relative velocities can be better estimated by multiplying pseudo-velocity with a correction factor. In the study of Sadek and Pekcan, the way to determine correction factors was explained as the exact displacement times the natural angular frequency of the system. With the help of more earthquake records, correction factors found by Sadek and Pekcan were further improved, and results close to exact values were obtained. Comparison of the results showed that using correction factors of Sadek and Pekcan reduced the scattering of the predictions, and further improvement of the correction factors led to more reduction in the scattering of results meaning that getting extremely close to exact relative velocity values.

Whittaker *et al.* [26] published the procedure for calculating the higher mode damping ratios, effective damping and period for buildings having yielding, viscoelastic, linear viscous and nonlinear viscous type of supplemental damping extensions. The authors described these devices as a tool for dissipation of earthquake-induced energy into the damping devices, and therefore the gravity-load resisting system of the structure would be exposed to less energy and deformation causing the less repair cost and business interpretation. Three analysis methods were presented for the design of passive control devices. These methodologies are response spectrum analysis, linear response history analysis and nonlinear response history analysis.

### 1.3. Objective

In this study, performance of an existing industrial building located in Malatya, Yeşilyurt, was investigated, and retrofitting process using fluid viscous dampers and viscoelastic dampers was considered. The industrial building is Kızılay Malatya Barınma Sistemleri Factory, and the building experienced severe earthquakes and fire. Recently, the structure experienced the Sivrice Earthquake with Mw 6.78 on the 22nd of January, 2020. The structure is very close to the East Anatolian Fault, and therefore the effect of near-fault excitations on the response of structure was also analyzed. Moreover, it is also known that near-fault excitations can be very harmful to structures because such excitations may have pulse-like characteristics. In the case of close matching of pulse period and structures fundamental period, such excitations lead to much more demands on structures compared to no-pulse like excitations, and therefore the performance of the structure with and without dampers was also investigated under pulse-like excitations.

Before the study of retrofitting process using fluid viscous dampers and viscoelastic dampers, some other retrofitting methodologies were considered, and analyses were conducted by other engineers. In that context, retrofitting with steel jacketing and retrofitting with shear walls were considered, and results showed that these methodologies are not feasible in the aspects of economics and performance.

In this study, a retrofitting methodology, which is passive control devices, was chosen as a new tool for bringing the structure to the desired performance level. Plastic deformations of members were determined as the performance index (PI), and plastic deformations were compared for the damped frames and bare frame under earthquake excitations having different characteristics. For that purpose, Nonlinear Time History Analyses (NLTHA) were conducted with ten different earthquakes for the bare frame, damped with FVD frame and damped with VE frame. Five of these excitations were chosen as no-pulse-like records, and the rest were chosen as pulse-like records. In addition, the performance and effectiveness of dampers were evaluated by comparing the plastic deformation demands on members under seismic loadings. Finally, the feasibility of retrofitting with FVD or VE was answered as well as comparing the performance of FVDs and VEs under no-pulse-like excitations and pulse-like excitations separately.

## 1.4. Scope

Chapter 1 is the introduction part of the thesis. Firstly, general information about seismic retrofitting with passive control devices is introduced, and the literature review is presented. Then, the objective of the thesis is briefly explained.

In chapter 2, general information related to the structure and seismicity of the region is presented. Then, Finite Element Modelling of the structure is explained with necessary information. Required mechanical parameters (section analyses) for defining hinges and conducting nonlinear analyses are given in that section. Finally, Nonlinear Static Analysis (Pushover Analysis) is explained, and the performance level of the bare frame is evaluated.

In chapter 3, after the evaluation of the performance level of the existing building, a new methodology using passive control devices, fluid viscous damper and viscoelastic damper, for retrofitting process is introduced, and necessary information for understanding the behavior of FVD and VE and their effects on response are briefly explained. Then, the effect of the structure's deficiency on determining appropriate damper mechanical properties is introduced, and placements and modeling of dampers are explained.

In chapter 4, the selection of earthquake records according to the purpose indicated in section 1.3 is shown, and the characteristics of selected earthquake records are summarized.

In chapter 5, determinants of selecting substantial members for the evaluation and presentation are explained, and plastic deformation amounts obtained from the Nonlinear Time History Analyses for the selected members are presented.

In chapter 6, significant observations obtained from the results are summarized, and candidate explanations for important conclusions emerging from the analysis results are presented.

In chapter 7, summary of the results, conclusions, and comments on future studies are presented.

## **2. THE STRUCTURE AND NONLINEAR STATIC ANALYSIS (NSA)**

### **2.1. General Information**

The building, Kızılay Malatya Barınma Sistemleri Factory, is located in Malatya, Yeşilyurt. The structure was being used for industrial purposes, and now it is unserviceable due to having significant damages. The structure experienced severe earthquakes and fire. These damages occurred on gravity-load carrying systems of the structure, and therefore usage of the building without retrofitting endangers people's life seriously. Besides these damages, the structure was constructed in 1989 and hence approximately 33 years old. The static report of the structure is unreachable, and therefore site and survey investigations, geometrical measurements, observations regarding damages, and examinations based on measurements were performed by related firms. Moreover, concrete, reinforcement, and steel samples were taken and examined by the related firms at the laboratory. These investigations and measurements were carried out for the previous retrofitting studies. Previous retrofitting studies using steel jacketing and addition of shear walls were not able to reach the desired level of performance while keeping the retrofitting cost within reasonable and feasible limits. In our study, a new method, passive control devices, for retrofitting the factory is investigated by making use of the information and reports prepared by the related firms for previous retrofitting studies.



Figure 2.1. General view of the structure.

The width and length of the structure are 144 m and 314.2 m, respectively. Although the structure seems as a one-piece, it consists of three different building blocks connected to each other by joints. Due to being exposed to earthquakes and fire, joint connections lost their function, and therefore the structure should be evaluated as three different independent building blocks. In our investigation, the first building block was used for retrofitting using passive control devices FVD and VE. The first building block involves the first 29.7 meters along the length of the structure. The building investigated in this study is designated as the Building Block-1.



Figure 2.2. Side view of the structure.



Figure 2.3. Front view of the structure.

## 2.2. Seismicity of the Region

The factory is located in Malatya, Yeşilyurt. The latitude and longitude of the factory are  $38.31861^\circ$  and  $38.136139^\circ$ , respectively. The location of the structure is very close to the East Anatolian Fault, and therefore near-fault effect with velocity pulses was also considered as well as far-fault effect. The seismicity map of Turkey and seismicity of the region Malatya, Yeşilyurt, can be found below.

## TÜRKİYE DEPREM TEHLİKE HARİTASI

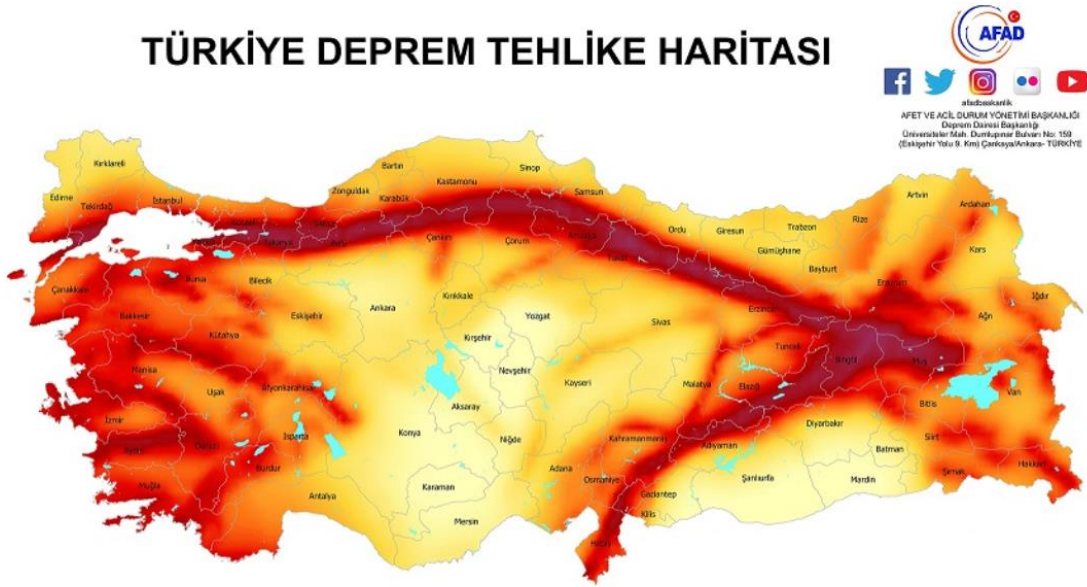


Figure 2.4. Seismicity map of Turkey [27].

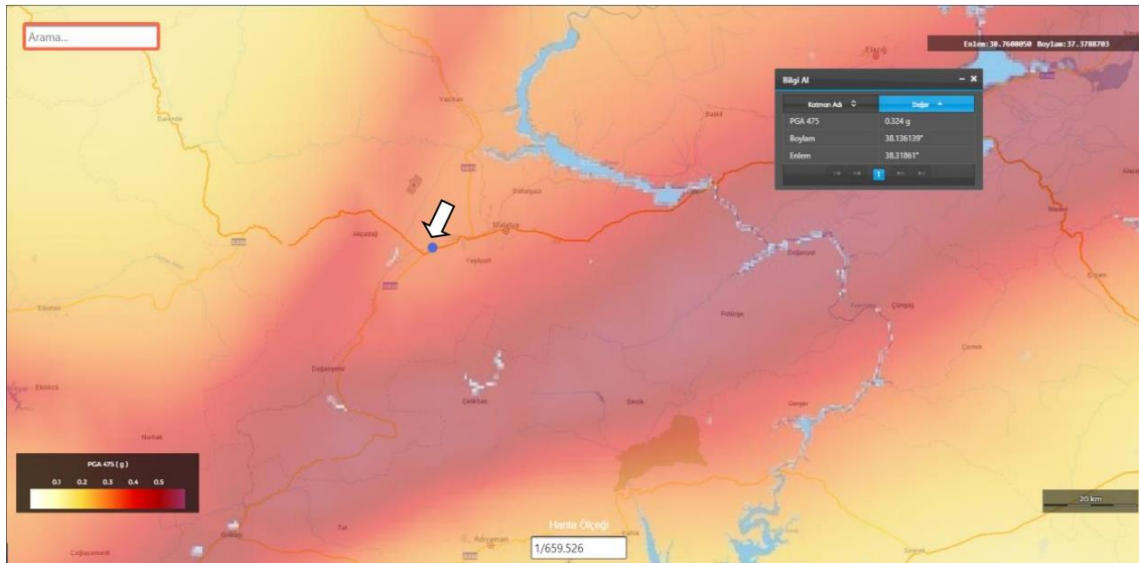


Figure 2.5. Seismicity of the region [28].

The design spectrum of the region compatible with TBDY 2018 [29] for DD2 earthquake ground motion level was constructed. DD2 earthquake ground motion level stands for seismic excitations having a 10% probability of exceeding the spectral magnitudes in 50 years and corresponding recurrence period of 475 years. This earthquake ground motion is also known as standard design earthquake ground motion. The soil class of the site was determined as class ZC based on the site investigations.

The structure has one story having 10 m in height. Short period spectral acceleration period ( $S_s$ ) and spectral acceleration coefficient for the period of 1 second ( $S_1$ ) for the coordinates having latitude and longitude as  $38.31861^\circ$  and  $38.136139^\circ$  respectively with soil class ZC can be obtained from TDTH AFAD web site [28] as  $S_s = 0.775$  and  $S_1 = 0.218$ . Map spectral acceleration coefficients  $S_s$  and  $S_1$  are converted to design spectral acceleration coefficients as

$$S_{DS} = S_s F_s, \quad (2.1)$$

$$S_{D1} = S_1 F_1, \quad (2.2)$$

where  $F_s$  and  $F_1$  stands for the local ground effect coefficients, and are obtained by using table 2.1 and table 2.2 of TBDY 2018.

Table 2.1. Local soil effect coefficient for the short period region [29].

Local Soil Class	Local Soil Effect Coefficient for the Short Period Region $F_s$					
	$S_s \leq 0.25$	$S_s = 0.50$	$S_s = 0.75$	$S_s = 1.00$	$S_s = 1.25$	$S_s \geq 1.50$
ZA	0.8	0.8	0.8	0.8	0.8	0.8
ZB	0.9	0.9	0.9	0.9	0.9	0.9
ZC	1.3	1.3	1.2	1.2	1.2	1.2
ZD	1.6	1.4	1.2	1.1	1.0	1.0
ZE	2.4	1.7	1.3	1.1	0.9	0.8
ZF	Site-Specific Soil Behavior Analysis Will Be Made					

Table 2.2. Local soil effect coefficient for the period of 1 second [29].

Local Soil Class	Local Soil Effect Coefficient for the Period of 1.0 s $F_1$					
	$S_1 \leq 0.10$	$S_1 = 0.20$	$S_1 = 0.30$	$S_1 = 0.40$	$S_1 = 0.50$	$S_1 \geq 0.60$
ZA	0.8	0.8	0.8	0.8	0.8	0.8
ZB	0.8	0.8	0.8	0.8	0.8	0.8
ZC	1.5	1.5	1.5	1.5	1.5	1.4
ZD	2.4	2.2	2.0	1.9	1.8	1.7
ZE	4.2	3.3	2.8	2.4	2.2	2.0
ZF	Site-Specific Soil Behavior Analysis Will Be Made					

$F_s$  and  $F_1$  are determined as  $F_s = 1.2$  and  $F_1 = 1.5$  from the tables 2.1 and 2.2 of TBDY 2018, and thereafter spectral acceleration coefficients are calculated as  $S_{DS} = 0.93$  and  $S_{D1} = 0.327$ .

Corner periods of horizontal design spectrum accordingly to TBDY 2018 are calculated as

$$T_A = 0.2 \frac{S_{D1}}{S_{DS}}, \quad (2.3)$$

$$T_B = \frac{S_{D1}}{S_{DS}}. \quad (2.4)$$

Corner periods of horizontal design spectrum, then, are calculated as  $T_A = 0.07$  second and  $T_B = 0.352$  second. The period at the point of transition to constant displacement region ( $T_L$ ) is given in the TBDY 2018 as  $T_L = 6$  second. After all the necessary constants are obtained, horizontal elastic design spectrum is constructed accordingly to TBDY 2018 as follows.

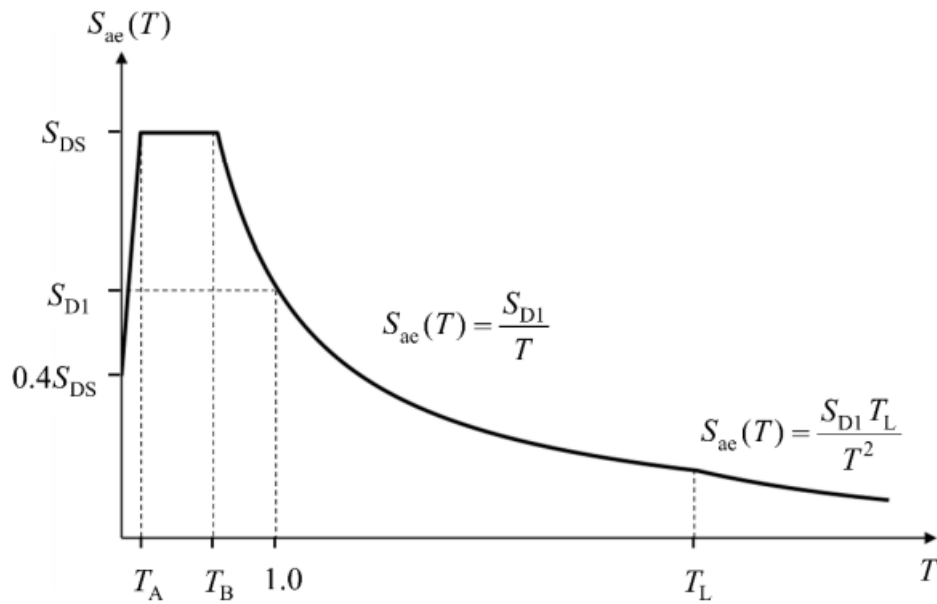


Figure 2.6. Horizontal elastic design spectrum TBDY 2018 [29].

The horizontal elastic design spectrum for the region having latitude =  $38.31861^\circ$  and longitude =  $38.136139^\circ$  for the soil class ZC is constructed and drawn as follows.

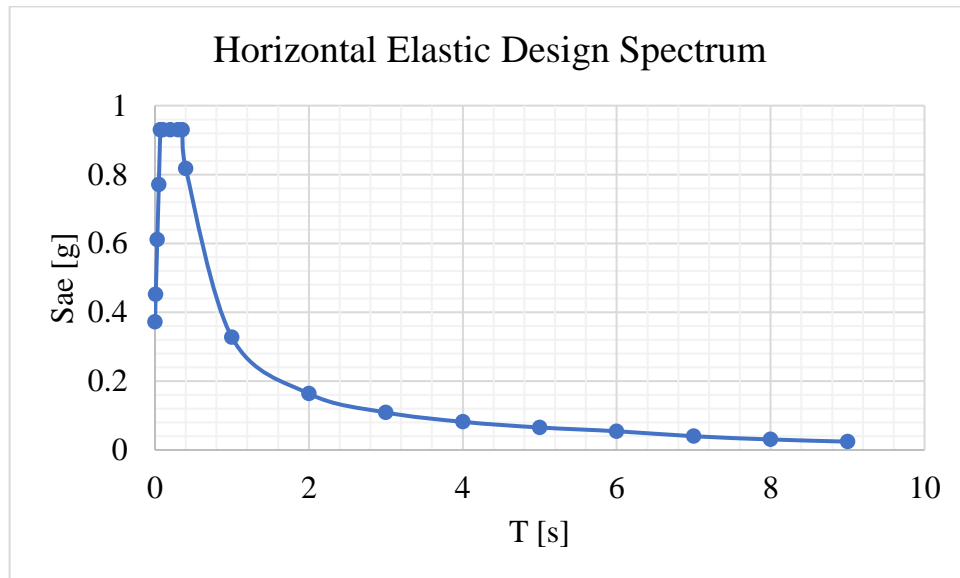


Figure 2.7. Horizontal elastic design spectrum of the region.

## 2.3. Finite Element Model

### 2.3.1. Material Properties and Section Analysis

According to the test results obtained from the concrete and reinforcement samples, the compressive strength of concrete is 16 MPa, the yield strength of longitudinal reinforcing steel is 370 MPa, and the yield strength of transverse reinforcement (stirrup) steel is 180 MPa globally. However, the compressive strength of concrete was taken as 12 MPa for the analytical analysis because samples were taken from the undamaged part of the columns and beams therefore compressive strength of 16MPa does not consider the overall strength of the members. Due to the having global damage, concrete compressive strength was taken as 12 MPa for each concrete section.



Figure 2.8. Column fire damage.



Figure 2.9. Column damage.



Figure 2.10. View from the inside of the factory building.

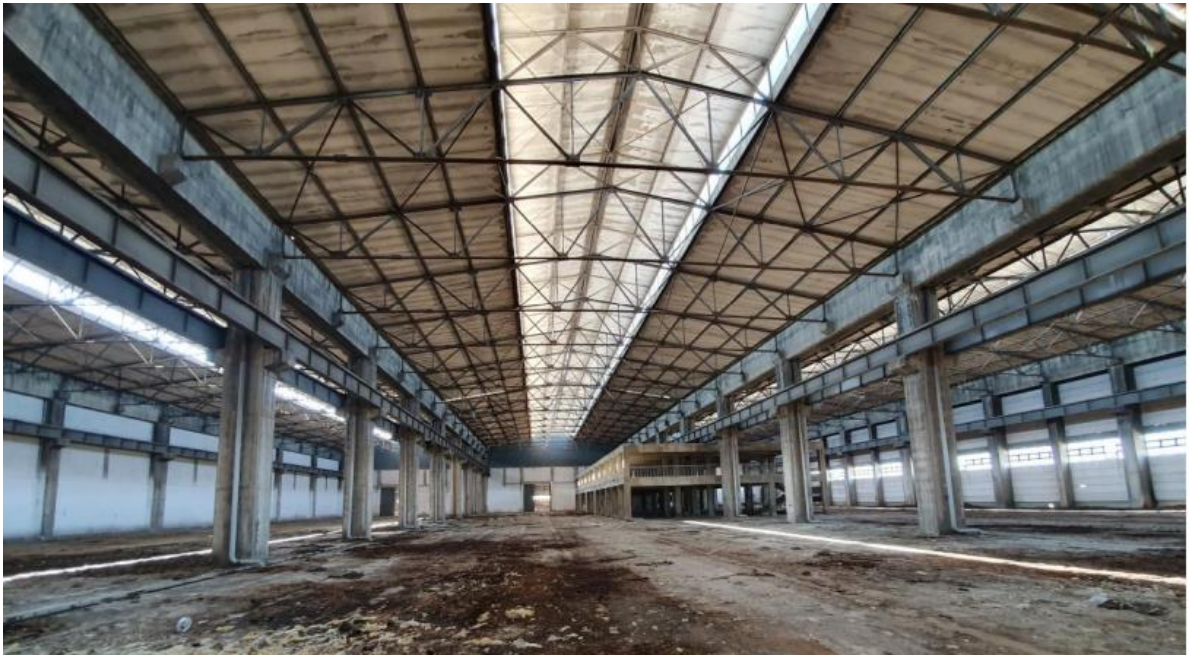


Figure 2.11. Another view from the inside of the factory building.

Stress-strain relation of confined and unconfined concrete for evaluation with nonlinear methods, accordingly to TBDY 2018 EK5.A, were adopted in this study and stress-strain relations are as follows for confined and unconfined concrete.

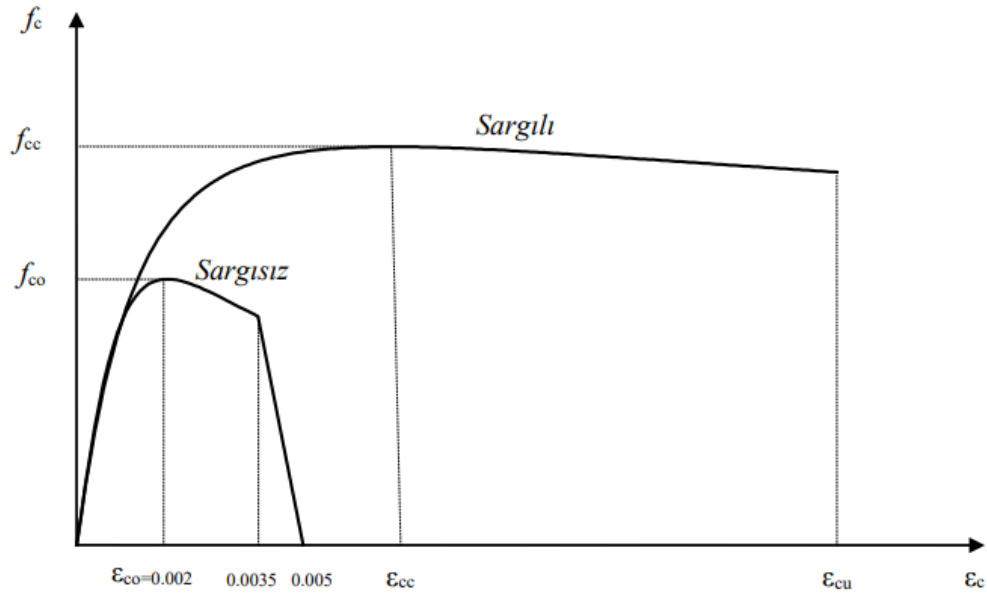


Figure 2.12. Stress-Strain Relation of confined and unconfined concrete 5A.1 of TBDY 2018.

Mathematical representation of stress-strain relation for confined and unconfined concrete according to TBDY 2018 is as

$$f_c = \frac{f_{cc}x^r}{r-1+x^r}, \quad (2.5)$$

$$f_{cc} = \lambda_c f_{c0}, \quad (2.6)$$

$$\lambda_c = 2.254 \sqrt{1 + 7.94 \frac{f_e}{f_{c0}} - 2 \frac{f_e}{f_{c0}} - 1.254}, \quad (2.7)$$

$$f_{ex} = k_e \rho_x f_{yw} \quad ; \quad f_{ey} = k_e \rho_y f_{yw}, \quad (2.8)$$

$$k_e = \left(1 - \frac{\sum a_i^2}{6b_0h_0}\right) \left(1 - \frac{s}{2b_0}\right) \left(1 - \frac{s}{2h_0}\right) \left(1 - \frac{A_s}{b_0h_0}\right)^{-1}, \quad (2.9)$$

where

$$x = \frac{\varepsilon_c}{\varepsilon_{cc}}, \quad (2.10)$$

$$\varepsilon_{cc} = \varepsilon_{c0} (1 + 5(\lambda_c - 1)), \quad (2.11)$$

$$\varepsilon_{c0} \cong 0.002, \quad (2.12)$$

$$r = \frac{E_c}{E_c - E_{sec}}, \quad (2.13)$$

$$E_c \cong 5000\sqrt{f_{c0}} \quad [\text{MPa}], \quad (2.14)$$

$$E_{\text{sec}} = \frac{f_{cc}}{\varepsilon_{cc}}, \quad (2.15)$$

and

$f_c$  = Compressive stress of confined concrete,

$f_{cc}$  = Compressive strength of confined concrete,

$f_{c0}$  = Compressive strength of unconfined concrete,

$f_{ex}$  = Effective confinement strength – x direction,

$f_{ey}$  = Effective confinement strength – y direction,

$f_{yw}$  = Yield strength of transverse reinforcement,

$\varepsilon_c$  = Compressive unit deformation,

$\rho_x$  = Volumetric ratio of transverse reinforcements – x direction,

$\rho_y$  = Volumetric ratio of transverse reinforcements – y direction,

$k_e$  = Confinement efficiency coefficient ratio,

$a_i$  = Distance between the axes of longitudinal reinforcements around the section,

$b_0$  = Smaller section dimensions between the axes of stirrups,

$h_0$  = Larger section dimensions between the axes of stirrups,

$s$  = Spacing between the axes of stirrups in the longitudinal direction,

$A_s$  = Longitudinal reinforcement area.

According to DBYBHY 2007 [30], the maximum compressive strain  $\varepsilon_{cu}$  is calculated as

$$\varepsilon_{cu} = 0.004 + \frac{1.4\rho_s f_{yw} \varepsilon_{su}}{f_{cc}}, \quad (2.16)$$

where

$$\rho_s = \rho_x + \rho_y, \quad (2.17)$$

and  $\varepsilon_{su}$  = strain at maximum stress in transverse reinforcing steel.

Stress-strain relation of reinforcing steel for evaluation with nonlinear methods, accordingly to TBDY 2018 EK5.A, were adopted in this study and stress-strain relations are as follows for reinforcing steel.

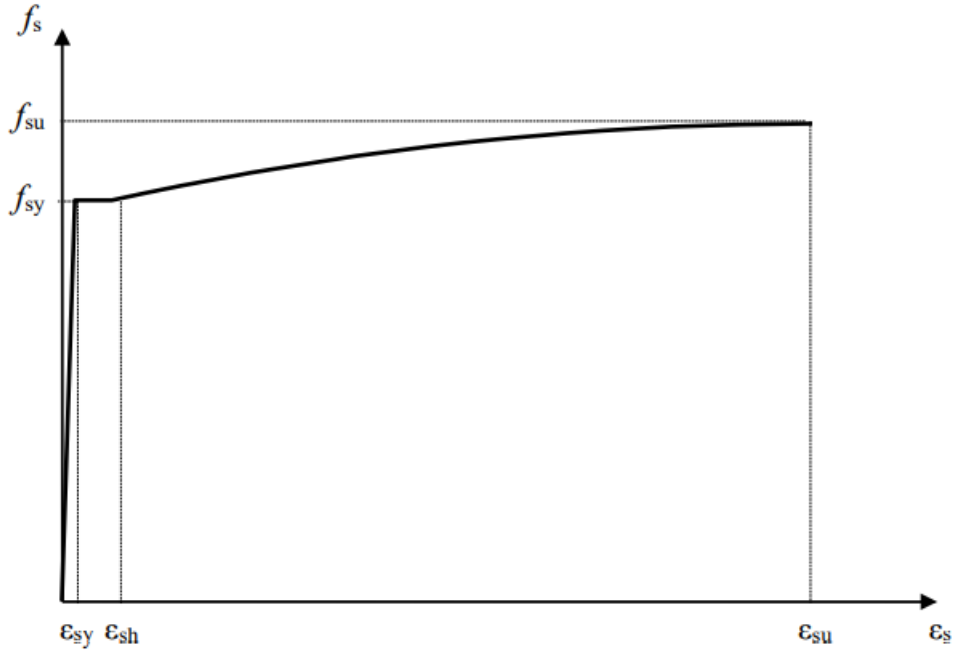


Figure 2.13. Stress-Strain relation of reinforcing steel 5A.2 of TBDY2018.

Mathematical representation of stress-strain relation of reinforcing steel according to TBDY 2018 is as

$$f_s = E_s \varepsilon_s \quad (\varepsilon_s \leq \varepsilon_{sy}), \quad (2.18)$$

$$f_s = f_{sy} \quad (\varepsilon_{sy} < \varepsilon_s \leq \varepsilon_{sh}), \quad (2.19)$$

$$f_s = f_{su} - (f_{su} - f_{sy}) \frac{(\varepsilon_{su} - \varepsilon_s)^2}{(\varepsilon_{su} - \varepsilon_{sh})^2} \quad (\varepsilon_{sh} < \varepsilon_s \leq \varepsilon_{su}), \quad (2.20)$$

where modulus of elasticity of reinforcing steel is  $2 * 10^5 \text{ MPa}$ .

Table 2.3. Information on reinforcing steels 5A.1 TBDY 2018.

Grade	$f_{sy}$ (MPa)	$\varepsilon_{sy}$	$\varepsilon_{sh}$	$\varepsilon_{su}$	$f_{su} / f_{sy}$
S220	220	0.0011	0.011	0.12	1.20
S420	420	0.0021	0.008	0.08	1.15 - 1.35
B420C	420	0.0021	0.008	0.08	1.15 - 1.35
B500C	500	0.0025	0.008	0.08	1.15 - 1.35

Commercial software XTRACT was used for section analyses. The material behaviors are accepted according to section 2.3.1, and sections were analyzed. P-M2-M3 interaction diagrams of columns for 0-degree, 45-degree and 90-degree loadings and M3-K diagrams of beams were constructed.

Table 2.4. Necessary parameters for section analyses of concrete on XTRACT [31].

Section	$f_{co}$ [MPa]	$f_{cc}$ [MPa]	$E_c$ [MPa]	$E_{sec}$ [MPa]	$\epsilon_{cc}$	$\epsilon_{cu}$
C120X90	12	12.28	17320.51	5494.43	0.00224	0.00713
C120X70	12	12.24	17320.51	5565.39	0.00220	0.00775
C120X50	12	12.02	17320.51	5963.48	0.00202	0.00905
C100X50	12	12.19	17320.51	5649.98	0.00216	0.00928
B130X100	12	12.26	17320.51	5528.24	0.00222	0.00682
B60X50	12	12.52	17320.51	5149.94	0.00243	0.01040

Table 2.5. Necessary parameters for section analysis of S370 on XTRACT [31].

Material	$f_{sy}$ [MPa]	$\epsilon_{sy}$	$\epsilon_{sh}$	$\epsilon_{su}$	$f_{su} / f_{sy}$	$f_{su}$ [MPa]
S370	370	0.00185	0.006275	0.09	1.25	462.5

Ultimate moment and yielding moment for each section were calculated by taking the compressive strength of concrete as 12 MPa and 16 MPa separately to show the effect of compressive strength on the moment capacity of the sections. The results are summarized in tables 2.6. and 2.7. It is known that the effect of steel strength is more influential on the moment capacity of sections than the effect of concrete strength. Since the sections' steel reinforcement design is the same, change in the moment capacity of sections calculated by taking the compressive strength of concrete as 12MPa and 16 MPa is not much. However, concrete strength directly influences the shear strength of sections, and therefore it is crucial for the shear capacity of sections.

Table 2.6a. Comparison of sections' moment capacities for C16 and C12 (M2).

M2	C120X90		C120X70		C120X50	
	C16	C12	C16	C12	C16	C12
Yield Moment [kN.m]	1683	1647	995.9	977.4	485.4	475.5
Ultimate Moment [kN.m]	1819	1769	1110	1070	523.9	517.6

Table 2.6b. Comparison of sections' moment capacities for C16 and C12 (M2).

	<b>C100X50</b>		<b>B130X100</b>		<b>B60X50</b>	
<b>M2</b>	<b>C16</b>	<b>C12</b>	<b>C16</b>	<b>C12</b>	<b>C16</b>	<b>C12</b>
Yield Moment [kN.m]	413.9	405.6	1175	1131	206.4	202.9
Ultimate Moment [kN.m]	446.8	441	1221	1172	232.7	229.9

Table 2.7a. Comparison of sections' moment capacities for C16 and C12 (M3).

	<b>C120X90</b>		<b>C120X70</b>		<b>C120X50</b>	
<b>M3</b>	<b>C16</b>	<b>C12</b>	<b>C16</b>	<b>C12</b>	<b>C16</b>	<b>C12</b>
Yield Moment [kN.m]	2250	2196	1715	1670	1179	1143
Ultimate Moment [kN.m]	2437	2356	1837	1775	1237	1189

Table 2.7b. Comparison of sections' moment capacities for C16 and C12 (M3).

	<b>C100X50</b>		<b>B130X100</b>		<b>B60X50</b>	
<b>M3</b>	<b>C16</b>	<b>C12</b>	<b>C16</b>	<b>C12</b>	<b>C16</b>	<b>C12</b>
Yield Moment [kN.m]	842.8	818.2	1724	1719	169.6	165.8
Ultimate Moment [kN.m]	900.4	855.7	2011	2005	180.9	179.2

### 2.3.2. SAP2000 Model of the Structure

The Building Block-1 has seven main axes along the shorter dimension of the Building Block-1 and two main axes along the longer dimension of Building Block-1. Seven main axes along the shorter dimension of Building Block-1 consist of three unique axes because the middle five axes of the Building Block-1 are the same. Same sections are designated with the same color.

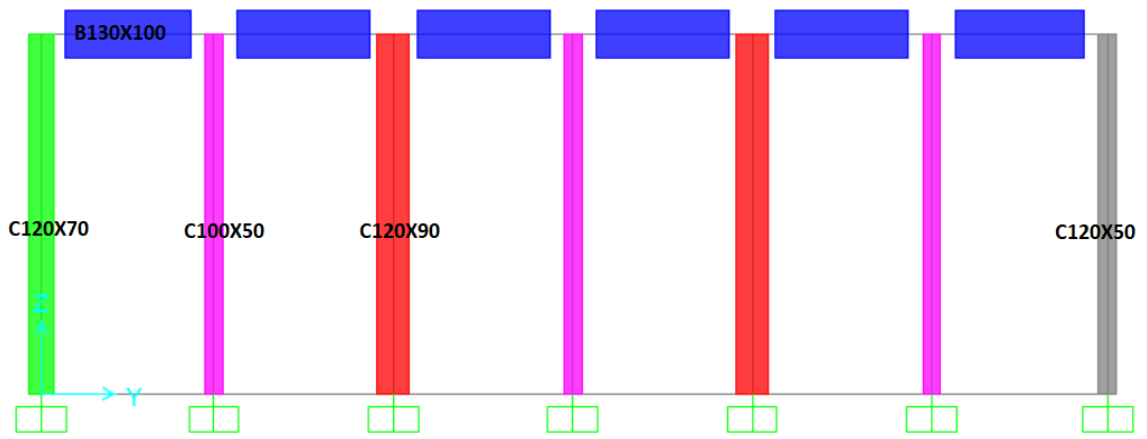


Figure 2.14. The North Axis Frame of the Building Block-1.

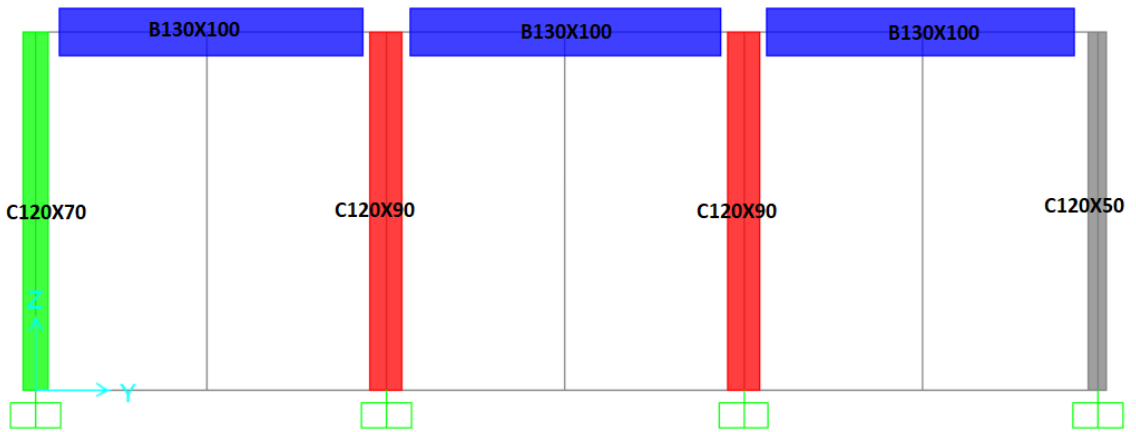


Figure 2.15. The Mid Axes Frames of the Building Block-1.

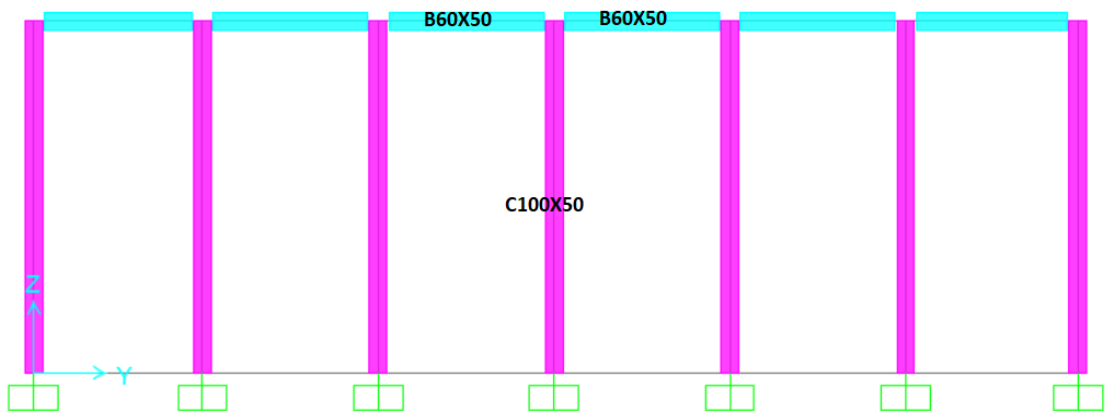


Figure 2.16. The South Axis Frame of the Building Block-1.

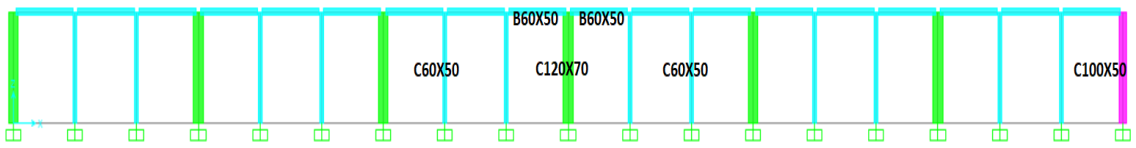


Figure 2.17. The East Axis Frame of the Building Block-1.

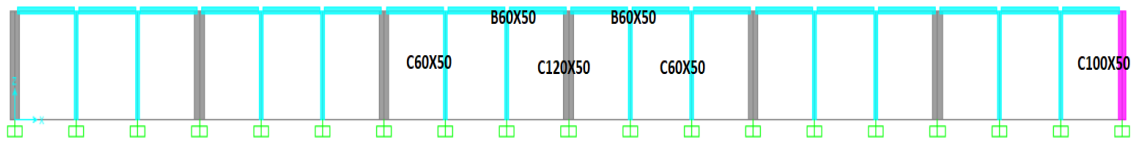


Figure 2.18. The West Axis Frame of the Building Block-1.

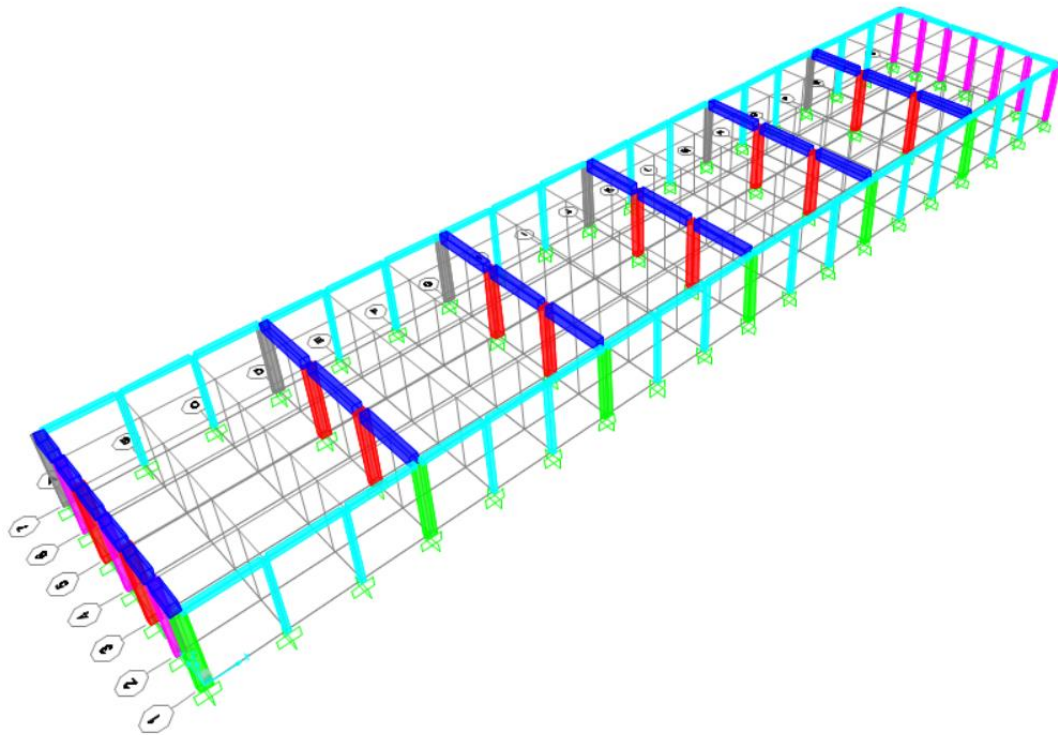


Figure 2.19. Finite element model of the Building Block-1.

### 2.3.3. Loads

The steel roof members were not modeled explicitly, but their effect on the response was considered by assigning rigid diaphragms along the X and Y directions and distributing total weight of the roof members to the beams uniformly. Besides the dead load of roof members, snow load was calculated according to TS 498 [32] and applied to the structure as a live load. Yeşilyurt, Malatya is located in snow zone III and altitude of Yeşilyurt, Malatya, is 998 meters.

Inclination angle of the roof is  $10^\circ$ , and therefore  $P_k = P_{ko}$  where  $P_k$  is the value that is used for calculating the snow load.  $P_k$  value was calculated according to TS 498 as

$$P_k = 1.35 \frac{\text{kN}}{\text{m}^2}. \quad (2.21)$$

The contributions of the dead load of roof members and snow load to mass were considered within the modeling.

### 2.3.4. Plastic Hinges

Plastic hinges for nonlinear analyses were constructed based on the elastic-perfectly plastic hinge model. Beam and column sections C120X90, C120X70, C120X50, C100X50, C60X50, B130X100 and B60X50 are doubly symmetric about M2 and M3 axes. For the beam frame sections, deformation-controlled Moment-M3 hinges were constructed and assigned. On the other hand, for the column sections, deformation-controlled P-M2-M3 interaction diagrams were constructed for 0-degree, 45-degree, and 90-degree loadings and assigned.

## 2.4. Evaluation of the Existing Structure (NSA)

Firstly, displacement-controlled Nonlinear Static Analyses were conducted for X and Y directions until an arbitrary large displacement, and pushover curves were obtained for the Building Block-1. Then, pushover curves were converted into the modal capacity curves according to TBDY 2018 as follows.

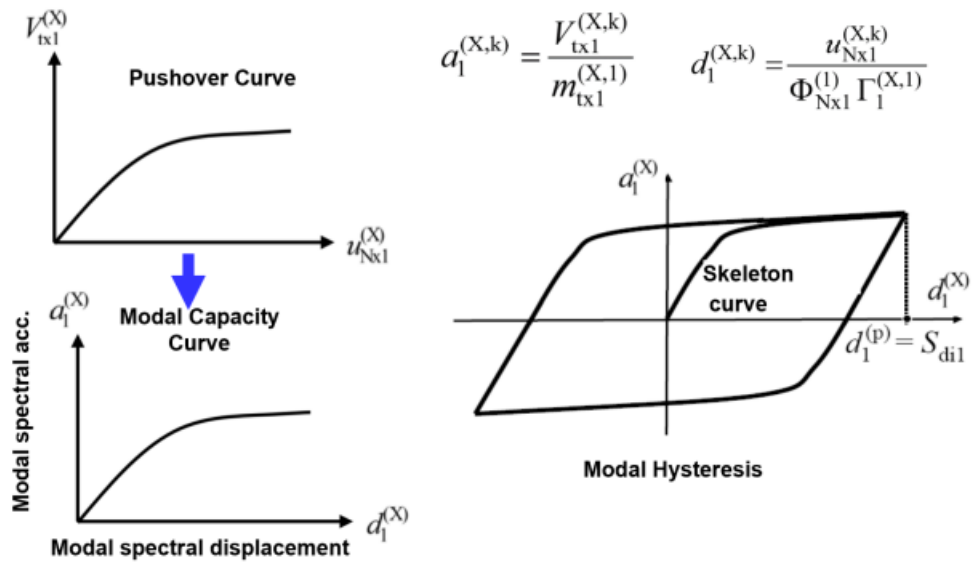


Figure 2.20. Conversion of the pushover curve into modal capacity curve.

Pushover and modal capacity curves for the Building Block-1 for X and Y directions are presented below.

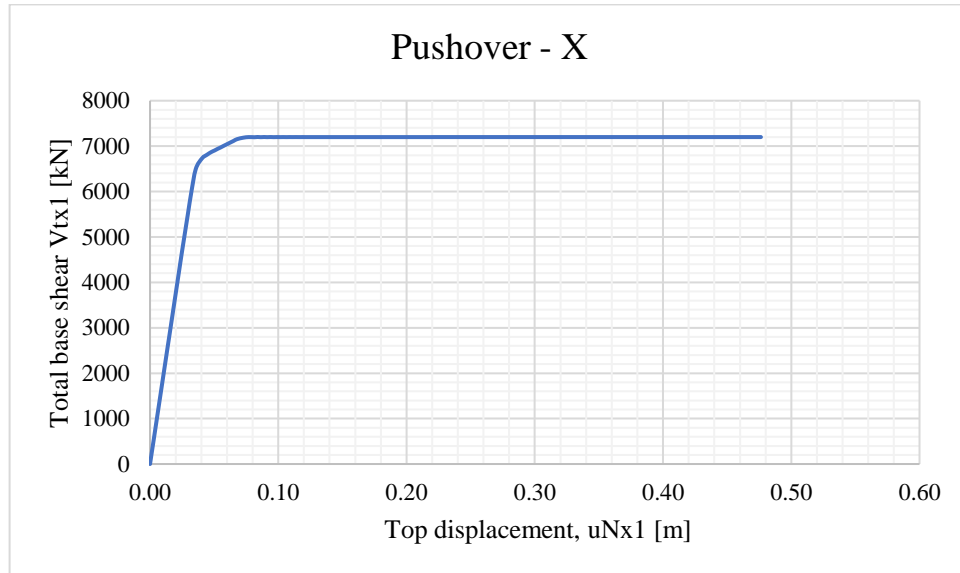


Figure 2.21. Pushover Curve X-Direction.

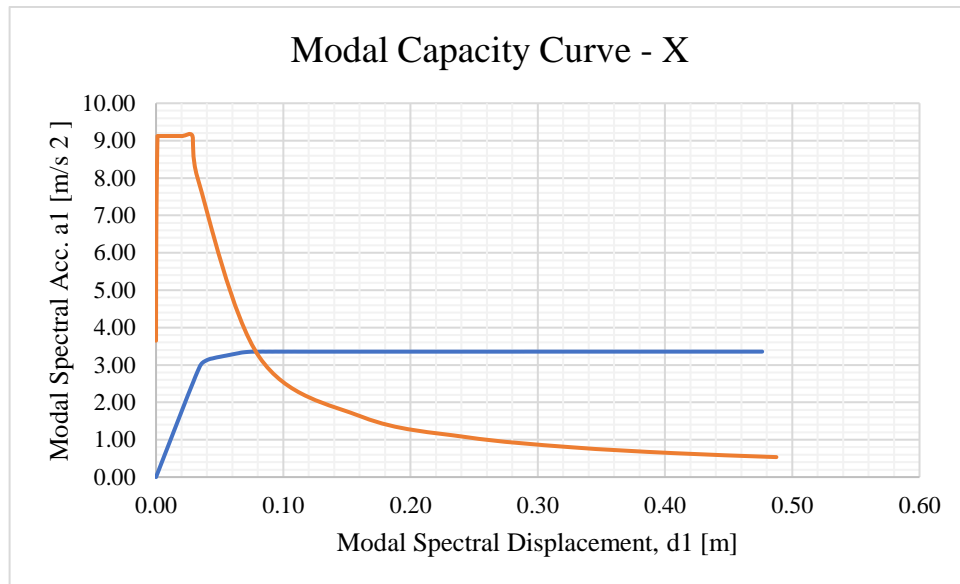


Figure 2.22. Modal Capacity Curve X-Direction.

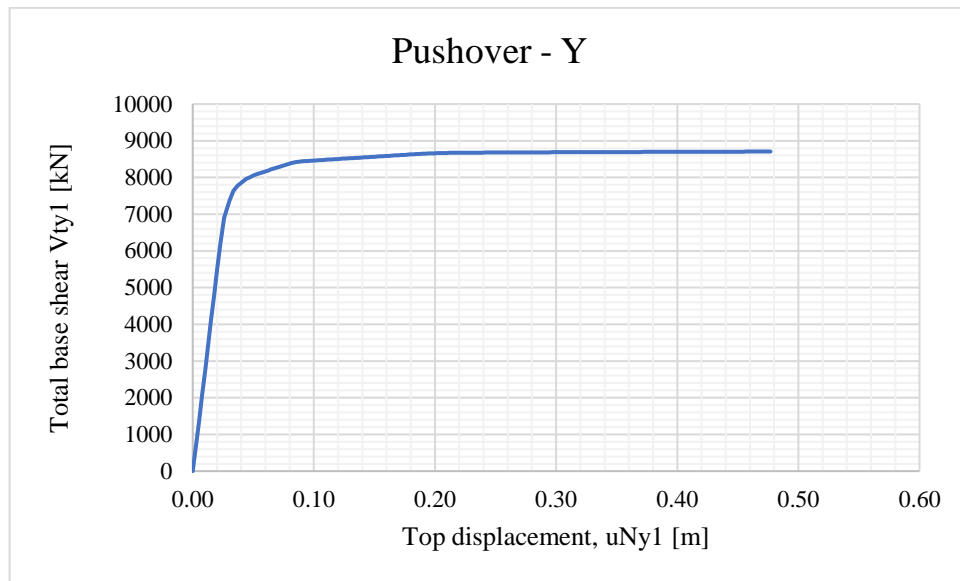


Figure 2.23. Pushover Curve Y-Direction.

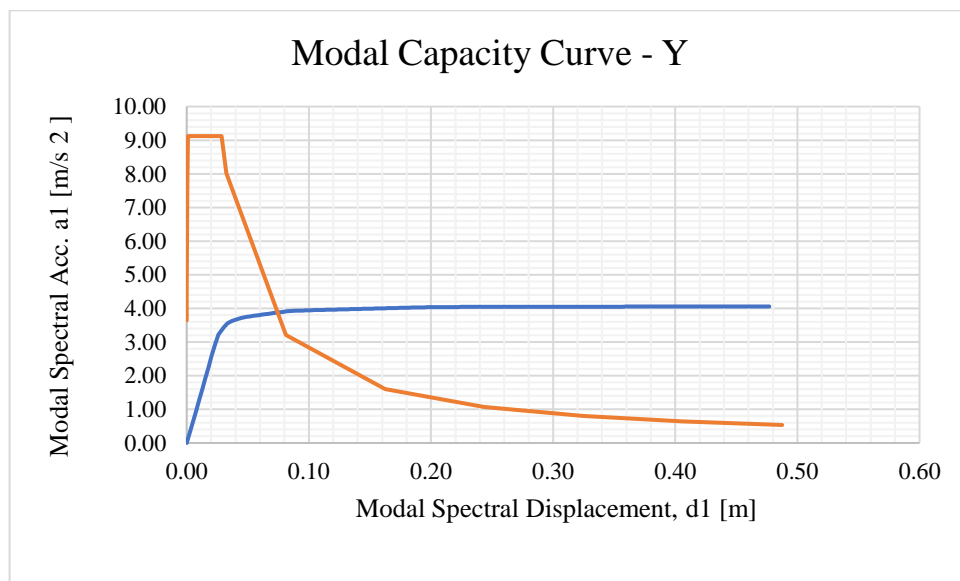


Figure 2.24. Modal Capacity Curve Y-Direction.

Then, modal displacement demands were obtained for the Building Block-1 having modal periods  $T_x = 0.79s$  and  $T_y = 0.65s$ . The corner periods  $T_A$  and  $T_B$  of the horizontal design spectrum are 0.07s and 0.352s respectively. The period at the point of transition to constant displacement region ( $T_L$ ) is given in the TBDY 2018 as  $T_L = 6$  second. The structure is evaluated as flexible in both directions since  $T_x = 0.79s$  and  $T_y = 0.65s$  values are bigger than  $T_B=0.352s$ , and therefore equal displacement rule is valid in determining the modal displacement demand.

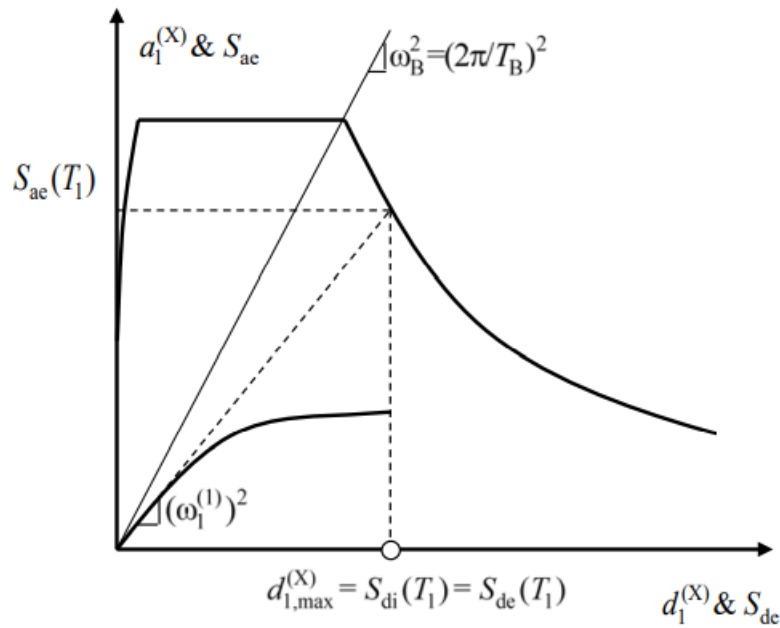


Figure 2.25. 5B.3 of TBDY 2018.

Modal displacement demands are calculated for the flexible systems as

$$S_{di}(T_1) = C_r S_{de}(T_1), \quad (2.22)$$

$$C_r = 1, \quad (2.23)$$

$$S_{de}(T) = \frac{T^2}{4\pi^2} g S_{ae}(T), \quad (2.24)$$

$$S_{di}(T_1) = S_{de}(T_1) \text{ (Equal Displacement Rule)}, \quad (2.25)$$

$$d_{1,max}^{(X)} = S_{di}(T_1), \quad (2.26)$$

where

$S_{de}(T_1)$  = Elastic Design Spectral Displacement,

$S_{di}(T_1)$  = Nonlinear spectral displacement corresponding to the first natural vibration period  $T_1$  of the carrier system,

$d_{1,max}^{(X)}$  = The largest modal displacement of single degree of freedom system.

Based on the formulations, nonlinear spectral displacements and the largest modal displacements for X and Y directions are calculated as

$$d_{1,max}^{(X)} = S_{di}(T_X = 0.79s) = 0.06433 \text{ m}, \quad (2.27)$$

$$d_{1,max}^{(Y)} = S_{di}(T_Y = 0.65s) = 0.05318 \text{ m}. \quad (2.28)$$

Then, the largest modal displacements (modal displacement demands) are converted into displacement demands (target displacements) according to TBDY 2018 as

$$d_1^{(X,k)} = \frac{U_{NX1}^{(X,k)}}{\Phi_{NX1}^{(1)} \Gamma_1^{(X,1)}}, \quad (2.29)$$

where

$d_{1,\max}^{(X)}$  = Modal displacement demand for the first mode,

$U_{NX1,\max}^{(X)}$  = Displacement Demand (Target Displacement) at the top of the building.

The structure has one story, and rigid diaphragms were assigned at the top of the structure in the X and Y directions therefore the structure has only one mode in each direction. Because of these reasons, responses of the structure in both directions are purely governed by one mode, and mass participation for each mode is one indicating that all the mass is participated in the X and Y direction responses. When the back conversions are performed for each direction, displacement demands are obtained as equal to modal displacement demands as

$$U_{NX1,\max}^{(X)} = d_{1,\max}^{(X)} = S_{di}(T_X = 0.79s) = 0.06433 \text{ m}, \quad (2.30)$$

$$U_{NY1,\max}^{(Y)} = d_{1,\max}^{(Y)} = S_{di}(T_Y = 0.65s) = 0.05318 \text{ m}. \quad (2.31)$$

Then, displacement-controlled Nonlinear Static Analysis were conducted for the X and Y directions until the target displacements  $U_{NX1,\max}^{(X)}$  and  $U_{NY1,\max}^{(Y)}$ , and pushover curves were obtained again for the Building Block-1. At the end of the NSA, maximum plastic rotation demands were obtained at target displacement.

When the plastic rotation demands are compared to plastic rotation limits, all the plastic rotation demands are within the visible damage region. Summary of the result can be found for beams and columns below.

Table 2.8. Evaluation of beams.

# of Beam	Visible Damage Level Beams		Beam Damage Percentage	
	Pushover-X	Pushover-Y	Pushover-X	Pushover-Y
63	24	6	38.10	9.52

Table 2.9. Evaluation of columns.

<b>Base Shear [kN]</b>		<b>Total Shear Force Carried by the Vertical Structural Members Within the Visible Damage Region [kN]</b>		<b>Total Damaged Columns Shear Force / Total Column Shear Force [Percentage]</b>	
Pushover-X	Pushover-Y	Pushover-X	Pushover-Y	Pushover-X	Pushover-Y
7079.52	8039.10	6238.37	7407.52	88.12	92.14

The Building Block-1 is at the Collapse Prevention Level. The building possesses a risk of life safety and therefore should be rehabilitated.

### **3. PASSIVE CONTROL DEVICES AS A RETROFITTING METHODOLOGY**

In chapter 2, it was shown that the structure is at the collapse prevention level for both directions, and hence performance of the Building Block-1 should be improved. The methodology, passive control devices, was adopted in this study aiming to improve the performance of the structure. Fluid Viscous Dampers and Viscoelastic Dampers were used for that purpose.

#### **3.1. Theory and Mechanics of Fluid Viscous Dampers**

Fluid Viscous Dampers (FVDs) are rate-dependent damping devices used in many different fields such as building, machinery, and vehicle industry. They can be classified as the most frequently used damping devices because their mechanical behavior has been well investigated and understood for decades. Although the mechanical behavior of other passive damping devices is well understood, their interactions with other structure components and effects on cumulative response are harder to comprehend and model than FVDs. On the other hand, FVDs can be easily modeled and installed, and analytical model of a system with FVDs gives very similar results to experiments. There are numerous studies in literatures related to modeling FVDs, and therefore reliable and qualitative information can be found easily. Using FVD leads to substantial stress reduction and minimizes the structure's dimensions, and causes less structural cost. Because FVDs are rate-dependent devices, they also make the structures velocity-sensitive. FVDs do not contribute to the elasticity of the structures and do not carry any static loads. They only work when they move and provide a resisting force to the structures [33].

A FVD has a small number of critical design parts and its components are shown in figure 3.1. Figure 3.1 shows the Damper in its mid-stroke position. The primary pressure chamber (Cylinder), as well as the volumes on both sides of the Piston Head, is totally filled with fluid. The fluid on either side of the Piston Head is driven through orifices in the Piston Head and produces resisting force as it travels [33].

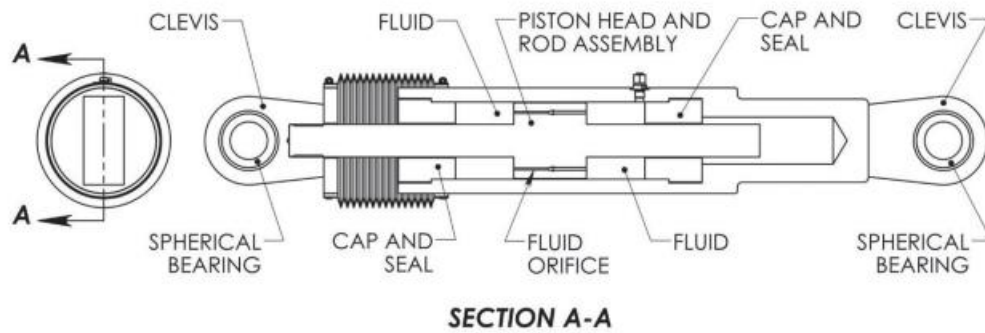


Figure 3.1. Typical fluid damper and parts [33].

The resisting force produced by the viscous damper is calculated by the constitutive equation as

$$F = CV^\alpha, \quad (3.1)$$

where

$F$  = Damping Force,

$C$  = Damping Constant,

$V$  = Relative Velocity Between the Ends of the Damper,

$\alpha$  = Damping Exponent ( $\alpha=1$  Linear FVD).

Force-displacement relation of linear and nonlinear viscous damper are demonstrated in figure 3.2.

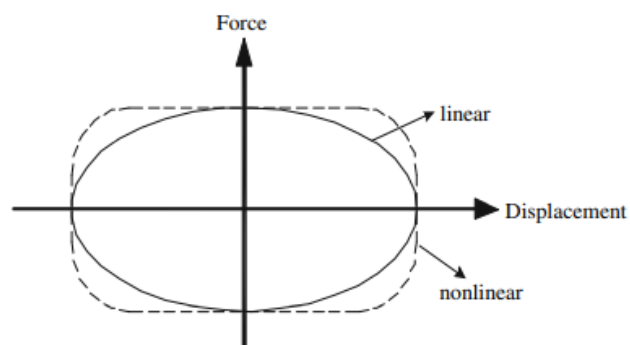


Figure 3.2. Force-displacement relation of linear and nonlinear viscous damper [17].

$\alpha$  determines the nonlinearity of the damper and can be arranged between 0.2 and 2.0 depending on the application type.  $\alpha = 1$  is used for defining linear fluid viscous dampers. For the current building designs with seismic inputs,  $\alpha$ , is generally set within the range of 0.3 to 0.5 [33]. Under the seismic excitation, dampers' working velocities are smaller than unity (1 m/s), and therefore nonlinearity of the dampers should be set to a value smaller than 1 in order to take advantage of the nonlinearity. Figure 3.3 shows that nonlinear FVD having  $\alpha=0.3$  resist more force than linear FVD under working velocities smaller than 1 m/s. It is also obvious that as the nonlinearity increases (smaller  $\alpha$  values), the effectiveness of dampers increases under working velocities smaller than 1m/s. However, as we keep increasing the nonlinearity beyond 0.3 ( $\alpha$  smaller than 0.3), the gain we get by reducing  $\alpha$  would approach zero. On the other hand, the applicability of the nonlinearity having  $\alpha$  smaller than 0.3 or 0.2 would be unfeasible. Therefore, a damping exponent around 0.3 often provides an optimal solution for response reduction, but different values of  $\alpha$  can be used for specific purposes. The C value, damping constant, can be easily arranged by the manufacturers, and therefore desired performance level can be reached easily by changing the C and  $\alpha$  values relatedly.

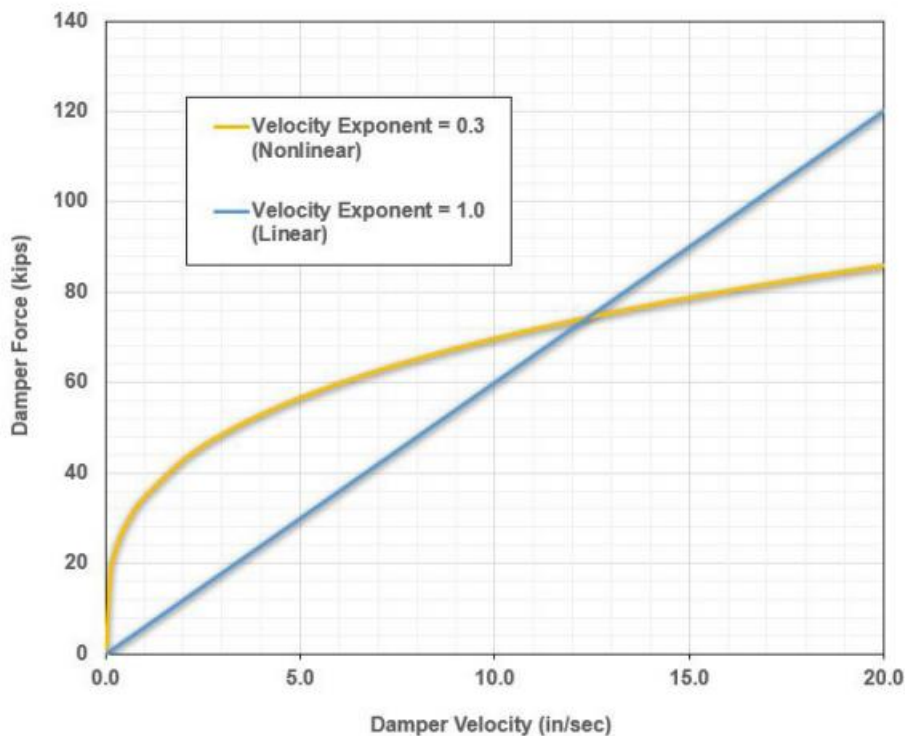


Figure 3.3. Nonlinear and linear damper's velocity-force graphs [33].

### 3.2. Theory and Mechanics of Viscoelastic Dampers

ViscoElastic (VE) dampers are another kind of passive energy dissipation device often employed in the industries of building, machinery and aerospace for vibration control. Low maintenance and production costs are the main advantages of viscoelastic dampers. They are easily implemented into the structure and renewed after base or wind excitations in case of having damage. VE dampers provide additional stiffness to the structures as well as damping, and therefore they are very effective kind of tools in improving the performance level of structures having low stiffness. They are also used for decreasing the torsional irregularity of the structures having low and high stiffness story sections. VE dampers are made up of viscoelastic layers that are linked together with steel plates. Through hysteretic shear deformation of viscoelastic materials, VE dampers diffuse vibrational energy and minimize structural responses.

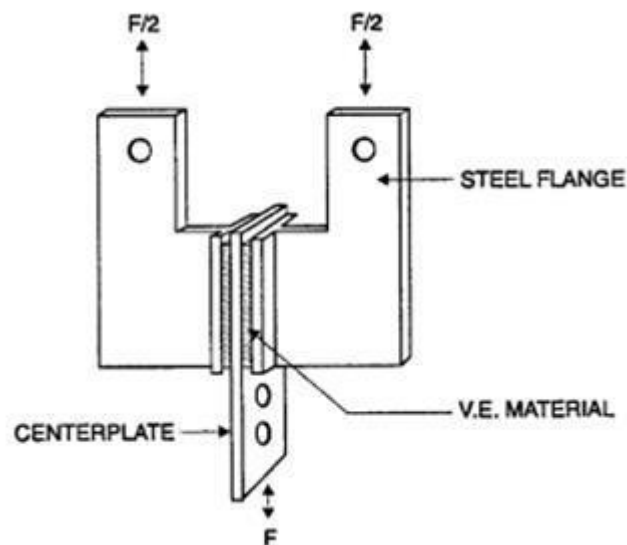


Figure 3.4. Representative sketch of a VE damper [34].

Viscoelastic dampers compose of viscoelastic materials, and the mechanical behavior of the dampers is governed by the mechanical behavior of viscoelastic material used in the viscoelastic damper. The Kelvin Model (KM), Maxwell Model (MW) and Generalized Models (GM) are used for modeling the behavior of viscoelastic dampers. The models are governed by different combinations of link elements representing the different behavioral characteristics of viscoelastic materials, such as damping and stiffness. Therefore, the

dynamic properties of the viscoelastic materials are the main determinates of the behavior of viscoelastic dampers. The deficiency of relatively simpler models KM (Kelvin Model) and MW (Maxwell Model) is considering the mechanical properties of viscoelastic dampers based on individual frequencies. However, viscoelastic materials are frequency and temperature dependent, and Generalized Models can be adopted by considering the change in working frequency and temperature for advanced studies. The previous studies showed that the energy dissipation capacity of the viscoelastic dampers decreases as temperature increases. Nevertheless, they effectively reduce the seismic response at all temperature levels [22]. In our investigation, the response of the structure in each direction is completely dominated by a single mode, and fundamental frequencies of vibrational modes in each direction after the implementation of viscoelastic dampers (provide additional stiffness to the structure) come very close to each other. Therefore, Kelvin Model (linear spring and dash-pot in parallel) was adopted in this study. Because of the stated reason above and having an almost constant working temperature, Kelvin Model gives very accurate results for the Building Block-1.

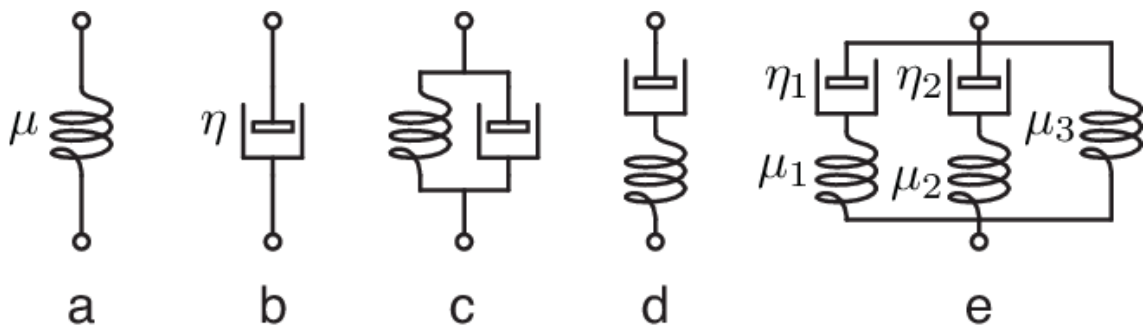


Figure 3.5. Single Spring (a), Damper (b), Kelvin Model (c), Maxwell Model (d), a Generalized Model (e) [35].

The mathematical model of a Kelvin Model VE damper is constructed by considering the effect of the viscous part (provides damping) and elastic part (provides stiffness) of the viscoelastic material separately and combining them in parallel. The governing equation of a Kelvin Model VE damper in the time domain is as

$$F_d(t) = k_d x(t) + c_d \dot{x}(t), \quad (3.2)$$

where

$F_d$  = Damping Force,

$k_d$  = Stiffness Coefficient,

$c_d$  = Damper Coefficient.

$k_d$  and  $c_d$  values are obtained from viscoelastic material properties and will be discussed in the next section.

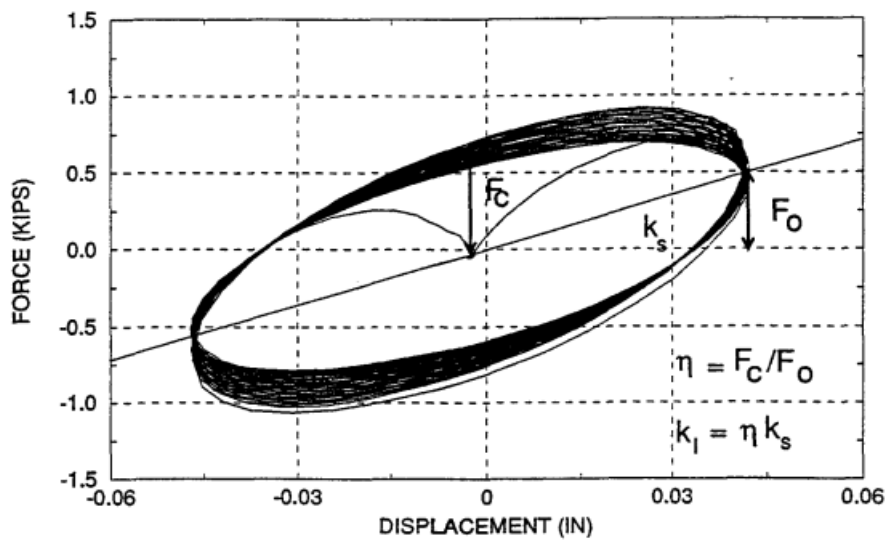


Figure 3.6. Typical force-displacement loop at 3 Hz [36].

### 3.3. Selection of Dampers' Mechanical Properties (Shear Constraint)

Experimental studies revealed that concrete having compressive strength of 16 MPa was used globally during the construction process. However, due to the damage on the structural members, the compressive strength of the frame sections was taken as 12 MPa for the analytical study. Dampers were placed diagonally by using extender bars because of the structure height. The height of the Building Block-1 is 10 meters, and therefore long extender bars were required. The buckling criteria for the extender bars were investigated and will be explained in the next section.



Figure 3.7. An example of diagonal bracing San Miguel Mall – Lima, Peru – New Build [33].



Figure 3.8. Extender montage representation San Bernardino Justice Center – San Bernardino, CA – New Build [33].

As it can be seen from the figures 3.7 and 3.8, diagonally placed dampers create a hysteretic force on the beam-column connection parts under seismic excitation. The damper force during the excitation is transmitted to the beam and columns at the joint and creates additional demands. The shear strength of the concrete sections is more critical than the axial strength, and therefore damper capacity should be determined based on the shear strength of the members at joints. In our study, this is an extremely important constraint because the compressive strength of the concrete is 12 MPa, and therefore shear strength of the sections is very low.

Shear strength of the concrete sections under gravitational loads were calculated according to TS500 [37] Chapter 8 as

$$V_r = V_w + V_c, \quad (3.3)$$

$$V_c = 0.52 f_{ct} b_w d \Psi, \quad (3.4)$$

$$V_w = \frac{A_{sw}}{s} f_{yw} d, \quad (3.5)$$

$$\Psi = 1 + 0.3 \frac{N_d}{A_c} \quad N_d = - (\text{tension}), \quad (3.6)$$

$$\Psi = 1 + 0.07 \frac{N_d}{A_c} \quad N_d = + (\text{compression}), \quad (3.7)$$

where

$V_w$  = Shear Reinforcement Contribution,

$V_c$  = Concrete Contribution,

$f_{ct}$  = Tensile Strength of Concrete.

The effect of axial loads on shear strength is almost zero. The Building Block-1 is a one-story factory having gravitational loads in terms of dead load of the roof and snow load considered as live load leading to very low axial demands on the column members, and therefore shear strength of the same sections having different axial loads are almost same. Shear strength of the frame sections at the junction points is given in table 3.1 together with compressive strength. It can be seen from table 3.1 that the shear strength of the concrete sections is much more critical than axial strength.

Table 3.1. Shear strength of the members at the junction points.

Direction	Section	Cross-Section	Total Shear Strength [kN]	Axial Strength [kN]
X	Beam	60X50	359	3600
X	Column	60X50	364	3600
Y	Beam	130x100	1102	15600
Y	Beam	60X50	359	3600
Y	Column	120x90	1038	12960
Y	Column	100x50	606	6000

The frame sections summarized in table 3.1 are the potential column and beam sections for damper mounting located at the outmost axes of the Building Block-1. Outmost axes of the Building Block-1 were determined as the potential damper mounting locations not to reduce the factory's interior usage area.

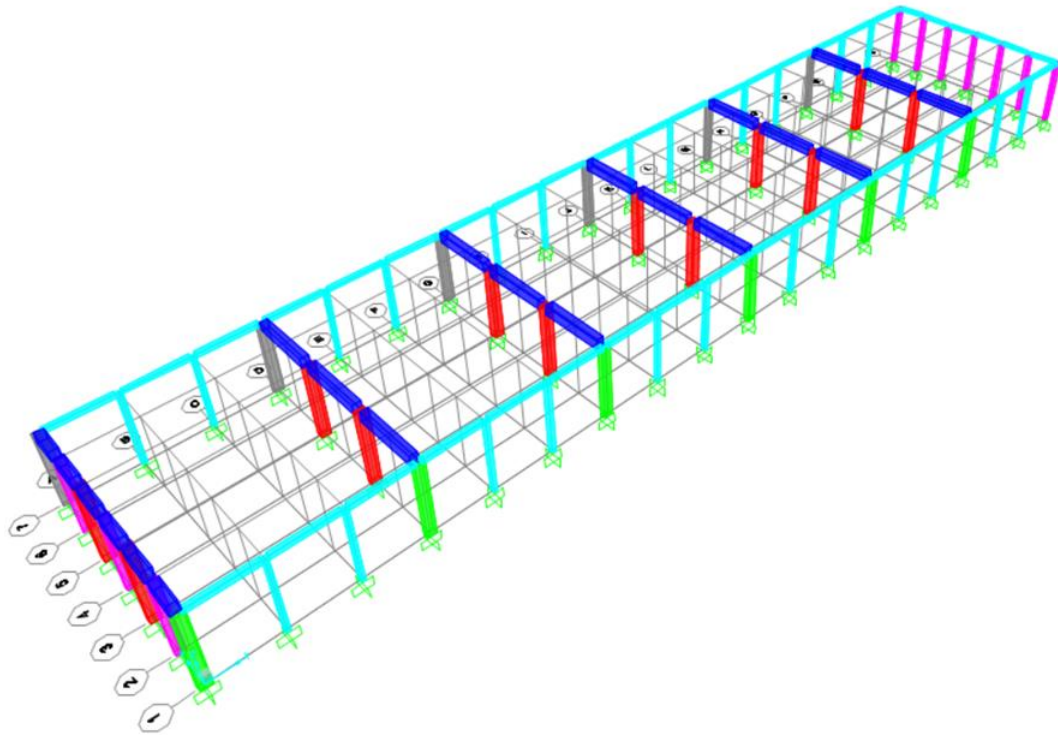


Figure 3.9. Finite element model of the Building Block-1.

Sections 60X50 are designated with aqua blue, and beam 60X50 section has the lowest shear strength with 359 KN. On the other hand, column 60X50 sections have shear strength 365 KN which is very close to the beam 60X50 sections. Since the yellow marked areas shown in figure 3.10 are used for loading and unloading production materials, dampers will not be placed in these regions, and therefore it is certain that at each potential junction point for damper mounting along the longer dimensions of Building Block-1, section 60X50 having approximately 360 KN shear strength will take place.

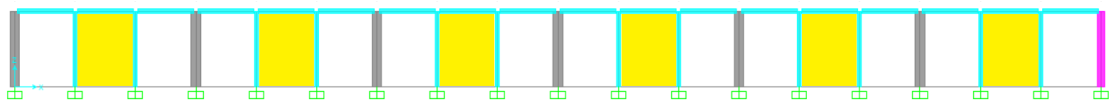


Figure 3.10. The West Axis Frame of the Building Block-1.

At each potential junction point for damper mounting along the south axis of the Building Block-1, section 60X50 having approximately 360 KN shear strength will also take place.

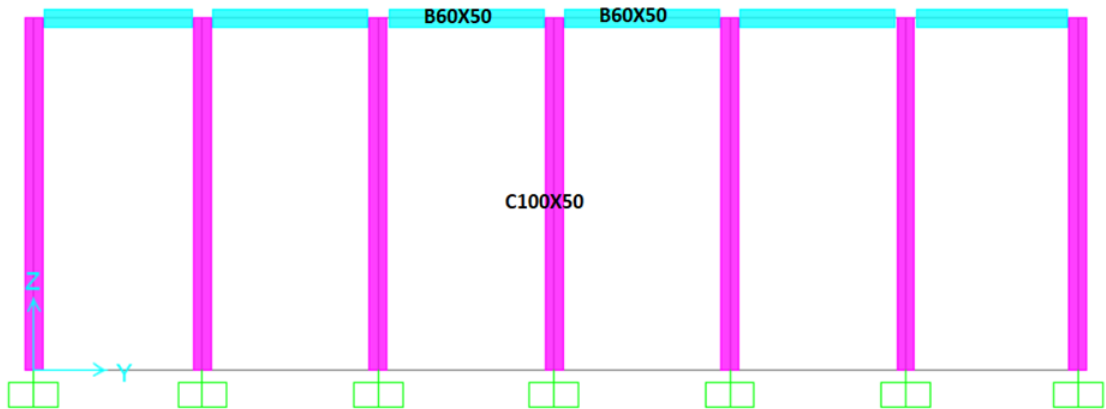


Figure 3.11. The South Axis Frame of the Building Block-1.

Although there is no 60X50 frame section along the north axis of the Building Block-1, the dampers along the north axis should be designed associated with the north axis because placing the dampers symmetrically and uniformly along each direction of the structure is substantial in order not to enhance torsional irregularity of the structure.

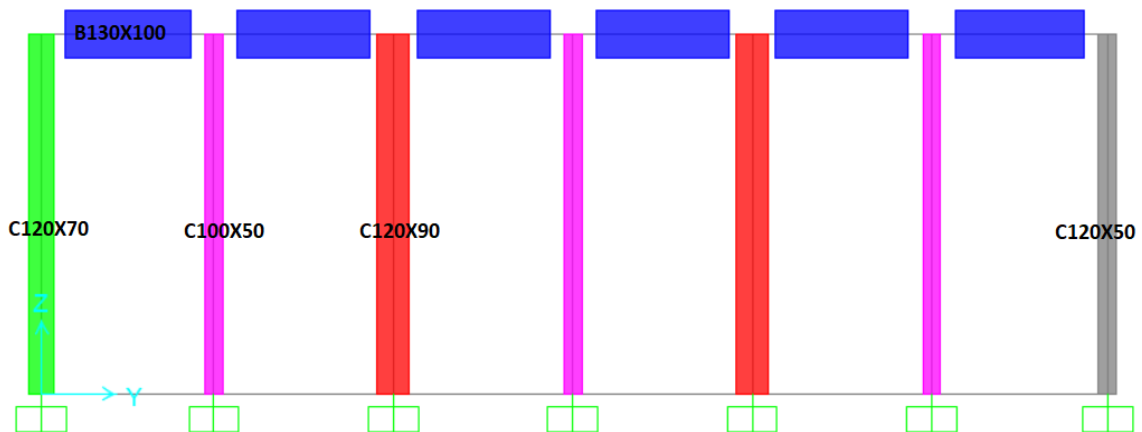


Figure 3.12. The North Axis Frame of the Building Block-1.

By considering all the aforementioned points, maximum damper force for each side of the structure is controlled by the shear capacity of the 60X50 sections.

Maximum damper capacity was determined based on the contributions of earthquake loads, gravitational loads, and maximum damper force to shear demand on horizontal and vertical members so that sum of each contribution will not pass the shear capacity of the sections 60X50. In accordance with this purpose, earthquake loads calculated by the equivalent static earthquake load method (TBDY 2018 Chapter 4.7), gravitational loads, and maximum damper force at the joints in the direction of extender bars were applied to the structure statically. This analysis was conducted separately for each orthogonal direction of the structure, and the maximum damper force that the horizontal and vertical members at junctions can resist was determined by the trial-and-error method by changing the applied maximum damper force and checking the shear demands on critical members. Due to the symmetry and simplicity of the structure (having one mode in each direction), considering the load contributions statically gives reasonable estimations. At the end of the analyses, the maximum damper force that the structure can safely resist was determined as 250 KN.

For the retrofitting with fluid viscous dampers, the product catalog of commercial firm Taylor Devices [33] was benefitted, and FVD model number 17120 having rated force 250 KN was chosen. The nonlinearity of the FVD was determined as 0.3. In addition, the elastic flexibility of the damping devices' fluid column and connecting mechanisms is designated as  $K_d$ .

Table 3.2. Properties of FVD 17120.

<b>Taylor Device Model Number</b>	<b>Rated Force [kN]</b>	<b>Mid Stroke Length [mm]</b>	<b>Kd [kN/m]</b>
17120	250	787.00	109454.24

The rated force on the FVDs is calculated by the constitute equation  $F = C * V^\alpha$ . C value of the dampers is arranged by the manufacturer so that the maximum force that occurs on the dampers will not exceed the rated force stated in the catalog for a specific device. However, in order to arrange the damping constant properly, the maximum relative velocity at the ends of the dampers must be estimated. If C values are set to small values, the capacity of the damper is not used efficiently. If C values are set to very large values, then the maximum rated force exceeds the limit, and failure occurs because dampers are designed so

that their parts can withstand to maximum rated force specified in the product catalog. Because of these reasons, C value is determined by estimating the maximum relative velocity at the ends of the dampers under working conditions. Suggested C values can be found in the Product Catalog of Taylor Device. In our study, C value of the FVD having nonlinearity 0.3 was determined as  $425 \frac{\text{kN}\cdot\text{s}}{\text{m}}$ .

Table 3.3. Suggested C values of FVD having nonlinearity 0.3 for 250 KN rated force.

<b>Suggested C Values in kN - (Sec/m) where <math>F=C*(V)^{0.3}</math></b>			
<b>Max vel = 0.127 m/s</b>	<b>Max vel = 0.254 m/s</b>	<b>Max vel = 0.381 m/s</b>	<b>Max vel = 0.508 m/s</b>
454.60	369.20	326.90	299.90

On the other hand, stiffness and damping coefficients of the viscoelastic dampers are determined based on the shear storage modulus and shear loss modulus of the viscoelastic material and its dimensions. Viscoelastic material that was used in the study by R.F. Lobo *et al.* [36] is made use of as the material of the viscoelastic damper in this study. Stiffness and damping coefficients of Kelvin Model Viscoelastic Dampers are calculated according to Abbas H. and Kelly J.M. [38] as

$$k_d = \frac{G'A}{t}, \quad (3.8)$$

$$c_d = \frac{G''A}{wt}, \quad (3.9)$$

where

A = Total Shear Area of the Viscoelastic Material,

G' = Shear Storage Modulus of the Viscoelastic Material,

G'' = Shear Loss Modulus of the Viscoelastic Material,

w = Loading Frequency,

t = Thickness of the Viscoelastic Material.

Shear storage modulus and shear loss modulus of the viscoelastic material, under working conditions, are 1682.32 KPa and 2102.9 KPa, respectively, according to Lobo *et al.* [36]. Dimensions of the viscoelastic materials were chosen so that the maximum damper force during an earthquake compatible with the design spectrum will not exceed 250 kN which is the maximum damper force that structural members at joints can carry. Sketches of the VE damper are given below [39].

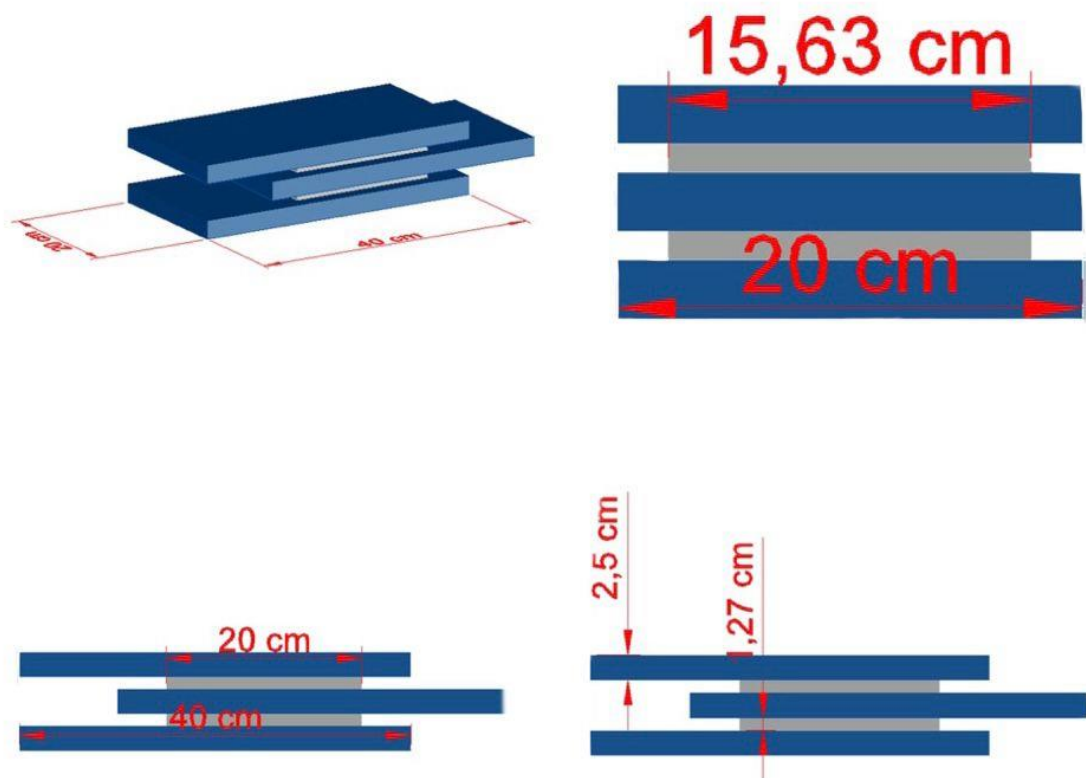


Figure 3.13. Dimensions of the VE damper.

Stiffness and damping coefficients of the Kelvin Model (KM) viscoelastic damper having dimensions given in figure 3.13 were calculated according to Abbas and Kelly [38], respectively, as  $8279.14 \frac{\text{kN}}{\text{m}}$  and  $1098.06 \frac{\text{kN}\cdot\text{s}}{\text{m}}$ .



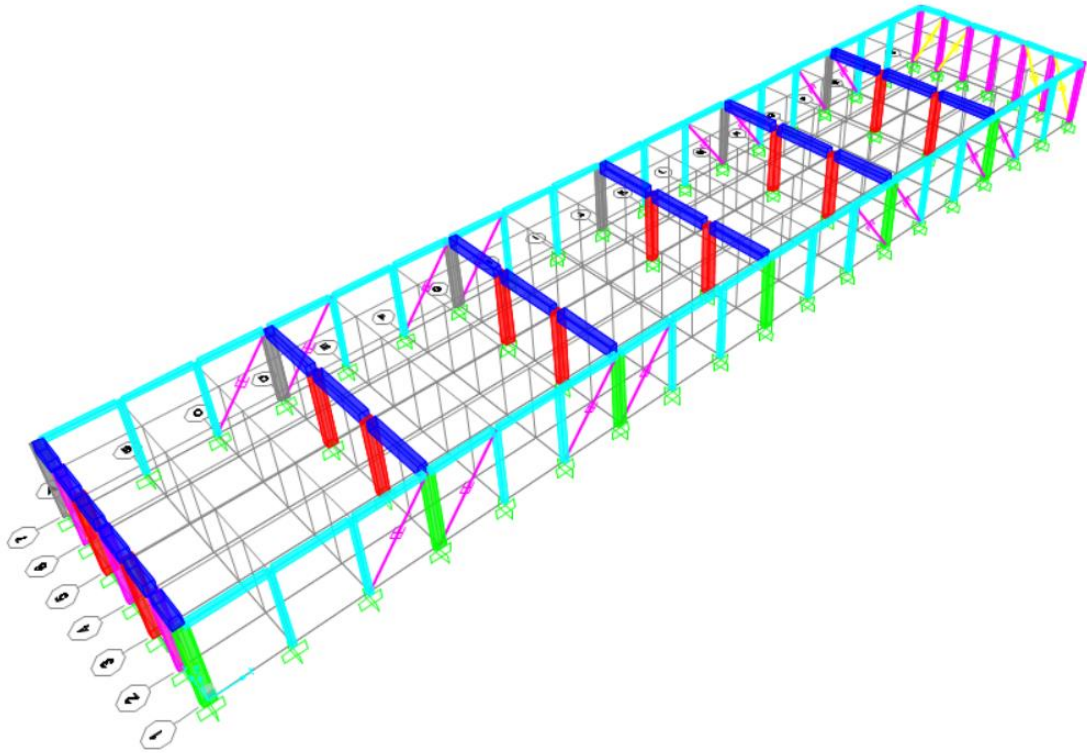


Figure 3.16. Damper configuration of the Building Block-1.

As it can be seen from the figures 3.14., 3.15. and 3.16., dampers were placed diagonally, and diagonal distances are 12.81m and 11.18m, respectively, for the longer side and shorter of the Building Block-1. However, the length of the dampers (both FVD and VE) is approximately 0.8 m, and therefore extender bars were required having length of 12 m and 10.4 m, respectively, for the longer and shorter sides. An example from Taylor Device Manual is shared below aiming to help visualizing the mounting scheme and effects of extender bars.



Figure 3.17. Extender bars [33].

Effects of the extender bars on the response of the structure were regarded implicitly by calculating the stiffness value of the diagonal link elements considering the axial flexibility of the damper ( $K_d$ ) and stiffness of the extender bar ( $K_e$ ) together. For the different analysis cases, FVDs are modeled differently. Damping and stiffness contributions of fluid viscous dampers are modeled in series for nonlinear analysis cases and parallel for linear analysis cases. This configuration is shown in figure 3.18.

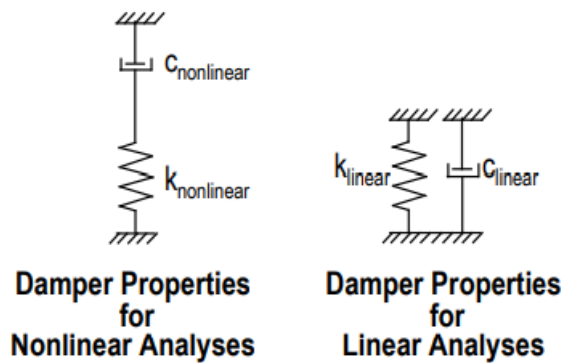


Figure 3.18. Modelling of FVDs for linear and nonlinear analysis [40].

For the pure damping behavior, stiffness value of the link elements is set to a very large number for nonlinear analyses and zero for linear analyses. In this study, nonlinear analysis method was used, and axial flexibility of the fluid viscous dampers was considered as well as the stiffness of the extender bars. As stated, stiffness of the extender bars was considered implicitly by embedding their stiffness contribution to the stiffness of the link element in modeling as

$$\frac{1}{K} = \frac{1}{K_d} + \frac{1}{K_e}, \quad (3.10)$$

$$K_e = \frac{AE}{L}, \quad (3.11)$$

where

$K$  = Stiffness Value of the Exponential Damper Link Element for Nonlinear Analysis

Case,

$K_d$  = Axial Flexibility of the Fluid Viscous Damper,

$K_e$  = Stiffness of the Extender Bar.

On the other hand, viscoelastic dampers were modeled as a link element according to Kelvin Model. Extender bars were also required for mounting the viscoelastic dampers. In order to calculate the stiffness of the extender bars, dimensions must be determined. The maximum damper force was calculated as 250 KN and explained in Section 3.3. The extender bars must resist the maximum damper load axially, and therefore, based on the boundary conditions, critical buckling loads were calculated, and dimensions of the extender bars were determined. The critical buckling load of the extender bar sections must be bigger than 250 KN. On the other hand, dampers are more effective for flexible structures, and therefore dimensions of the extender bars should be kept as small as possible while having critical buckling load bigger than 250 KN. The boundary condition of the connection mechanism is pinned-free. The section of the extender bars was determined as a square section having a side length of 0.2m.

Table 3.4. Properties of the extender bars.

	<b>Extenders</b>	
	<b>Extender 1 (Longer)</b>	<b>Extender 2 (Shorter)</b>
<b>Extender Material</b>	S420 Steel	S420 Steel
<b>Extender Crossection [m]</b>	0.2 x 0.2	0.2 x 0.2
<b>E of steel [Pa]</b>	2E+11	2E+11
<b>Area of Extender [m<sup>2</sup>]</b>	0.04	0.04
<b>Pcr for Buckling (Pinned-Free) [kN]</b>	455.18	609.15
<b>Pcr for Yielding [kN]</b>	16800	16800

Finally, the link elements were modeled by considering the contribution of square extender bars having a side length of 0.2 m to the response.

## 4. SEISMIC LOADING

For the Nonlinear Time History Analyses, two different types of earthquake records compatible with the target spectrum of the region were used. The first type is no-pulse like records which contain no velocity pulse characteristics. The second type is pulse like records containing velocity pulse characteristics. The structure is very close to the East Anatolian Fault, and therefore near-fault effect having velocity pulse characteristics was considered in the analyses. Earthquakes having velocity pulse characteristics are extremely damaging since most of the energy in a pulse motion is concentrated in one or two cycles of the velocity-time series [41]. In the case of close matching of pulse period and structure period, the effect of the earthquake on the structure is magnified. In this study, plastic rotation demands on members of bare framed, FVD frame, and VE frame under no-pulse-like and pulse-like excitations were obtained separately by using Nonlinear Time History Analysis method, and the effectiveness of the dampers was evaluated. For each type of earthquake characteristic, five records were chosen from PEER Database [42] suitable for the region where the structure is placed. The fault type is strike-slip for the East Anatolian Fault. Average shear wave velocity in the upper 30 meters for local soil class ZC is between 360 m/s to 760 m/s according to TBDY 2018 table 16.1. The geometric mean was used for scaling in order to choose the best records compatible with the target spectrum. The target spectrum was constructed by simply multiplying the design spectrum of the region with 1.3 since earthquake records were applied to the structure simultaneously in the x and y directions. Moreover, scaling factors of the earthquakes were improved so that each earthquake record, together with the geometric mean of the record, should satisfy the condition stated in TBDY 2018 Section 2.5.2.1.b for the 3D analysis method. Based on these criteria, earthquake records were chosen and summarized in sections 4.1. and 4.2.

#### 4.1. No-Pulse Like Records

Characteristics of the no-pulse like records chosen for the Nonlinear Time History Analyses to evaluate the effectiveness of the passive control devices, FVDs and VEs, are given below together with the scaled response spectrums.

Table 4.1. No-Pulse like earthquake records.

Earthquake Name	Magnitude	Mechanism	Rjb (km)	Vs30 (m/sec)	Scale Factor
Imperial Valley-06	6.53	strike slip	15.19	471.53	1.557
Superstition Hills-02	6.54	strike slip	5.61	362.38	0.577
Manjil-Iran	7.37	strike slip	12.55	723.95	0.672
Landers	7.28	strike slip	26.95	367.84	2.453
Tottori_Japan	6.61	strike slip	9.1	616.55	1.792

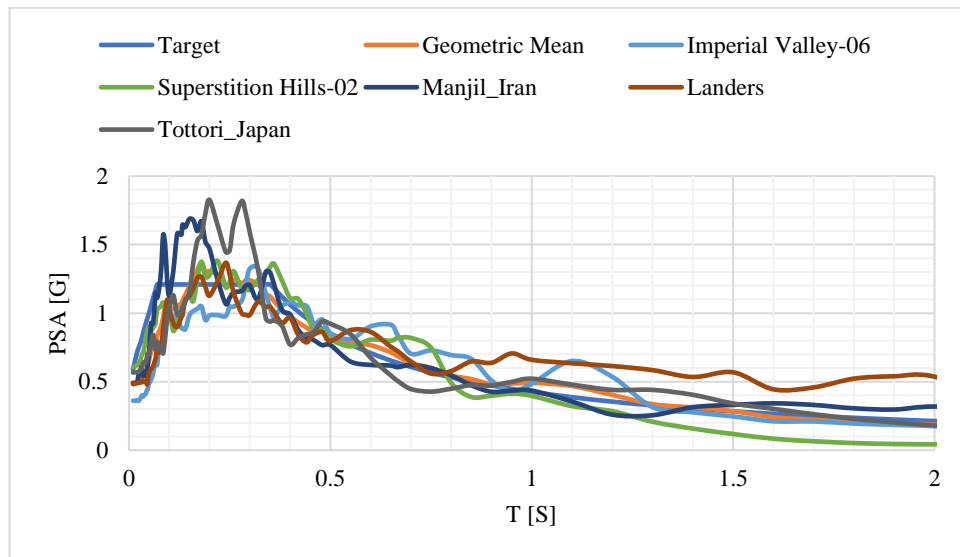


Figure 4.1. Target spectrum, geometric mean spectrum and response spectrums of no-pulse like records.

## 4.2. Pulse-Like Records

Characteristics of the pulse like records chosen for the Nonlinear Time History Analyses to evaluate the effectiveness of the passive control devices, FVDs and VEs, are given below together with the scaled response spectrums.

Table 4.2. Pulse like earthquake records.

Earthquake Name	Magnitude	Mechanism	Rjb (km)	Vs30 (m/sec)	Scale Factor
Morgan Hill	6.19	strike slip	9.85	663.31	1.17
Chi-Chi_ Taiwan-04	6.2	strike slip	6.02	553.43	0.80
Parkfield-02_ CA	6	strike slip	3.3	410.4	0.93
Darfield_ New Zealand	7	strike slip	25.21	649.67	1.56
Duzce_ Turkey	7.14	strike slip	2.65	690	1.11

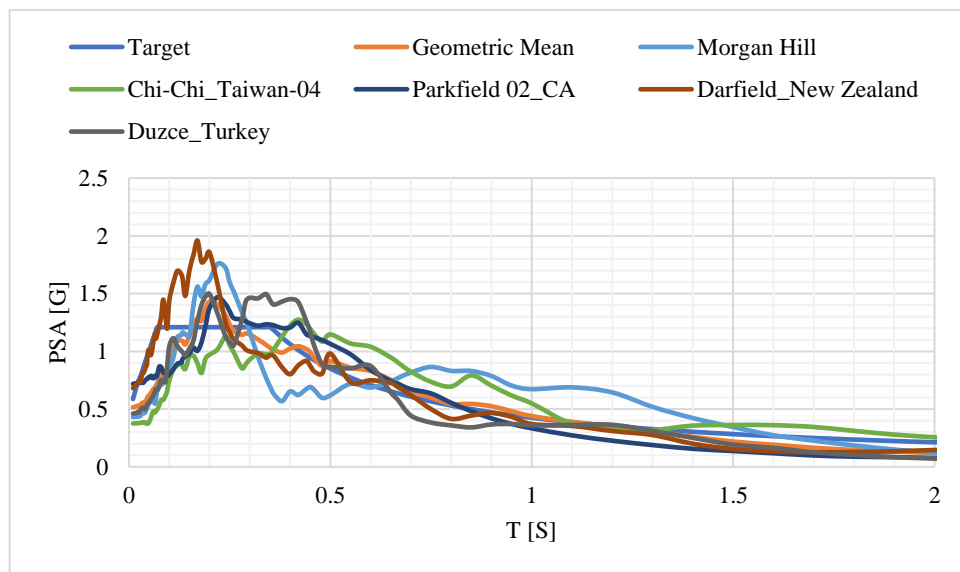


Figure 4.2. Target spectrum, geometric mean spectrum and response spectrums of pulse like records.

### **4.3. Nonlinear Time History Analysis (NLTHA)**

Nonlinear direct integration time history analyses were performed by using earthquake records given in sections 4.1 and 4.2. Nonlinear time histories continued at the end of the nonlinear static analysis. P-delta effects were considered, and viscous proportional damping was specified by period. The scaled earthquake records were simultaneously applied to the structure as acceleration load type in the X and Y directions. NLTHA was conducted separately for each case, bare frame - FVD frame - VE frame, and maximum plastic rotation demands on members were obtained for further evaluation.

## 5. NLTHA RESULTS

For the evaluation of the NLTHA results, maximum plastic rotation demands on the members were chosen as an assessment parameter. Plastic rotation demands were compared for the same member in different cases: the bare frame, FVD frame, and VE Frame. Most of the beam frame sections of the Building Block-1 have 100 cm X 130 cm dimensions, and therefore under each earthquake record, these beam elements did not get into the plastic region for the cases of bare frame, FVD Frame, and VE Frame. The rest of the beam elements having dimensions different and smaller than 100X130 could not provide adequate information for evaluation of the response, and therefore only column frame sections were used for evaluation purposes. The Building Block-1 has 58 column elements, but not all the column sections were used to demonstrate the plastic rotation demands. Critical columns were selected for the evaluation of the retrofitting processes. For the selected members, maximum plastic rotations occurred at H1 hinges for columns. Because of that, for the evaluation of the column's responses, only H1 hinges were used. Columns were selected based on the aiming to obtain more information with fewer data. Some columns showed almost the same behavior because of the symmetricity of the structure and rigid diaphragm in the X and Y directions, and therefore only one of these sections was selected for the bar chart. For the geometric means, members having plastic rotations for each case, bare-FVD-VE, were chosen to avoid losing information. Along the shorter dimension of the Building Block-1, maximum plastic rotation demands on the columns having frame numbers 8, 9, 12, 13, 14, 15, 16, 41, 42, 43, 44, 69, 70, 71, 72, 73, 74, and 75 will be presented on the bar charts. Along the longer dimension of the Building Block-1, maximum plastic rotation demands on the columns having frame numbers 82, 83, 87, 88, 92, 93, 94, 95, 99, 100, 104, and 105 will be presented on the bar charts.

Frame numbers 8,9,12,13,14,15, and 16 are located on the north axis of the Building Block-1.

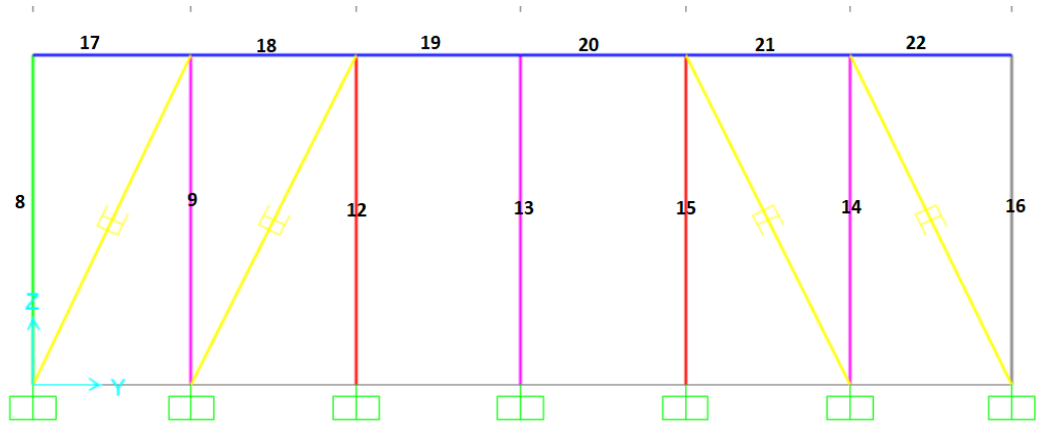


Figure 5.1. Numbering of the North Axis Frame of the Building Block-1.

Frame numbers 41,42,43, and 44 are located on the mid axis of the Building Block-1.

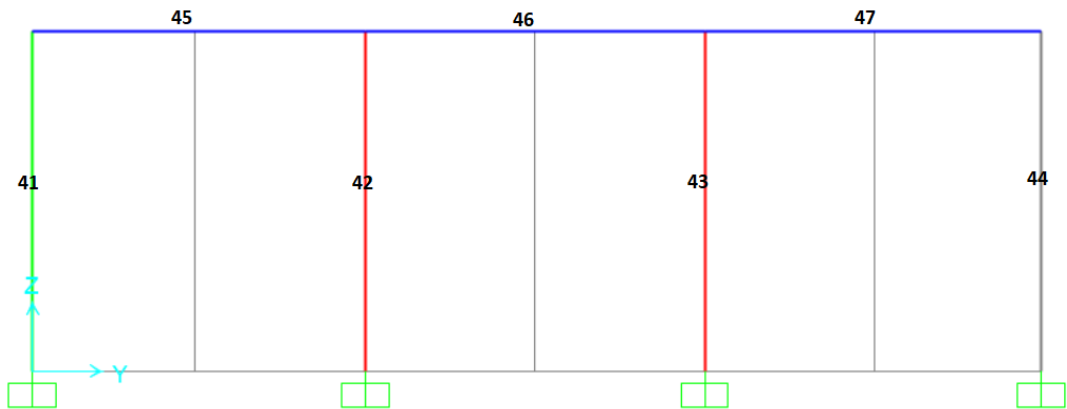


Figure 5.2. Numbering of the Mid Axis Frame of the Building Block-1.

Frame numbers 69,70,71,72,73,74, and 75 are located on the south axis of the Building Block-1.

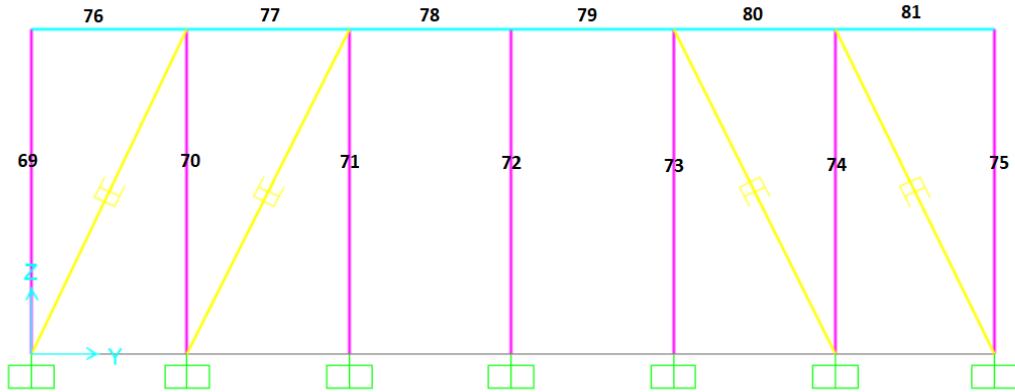


Figure 5.3. Numbering of the South Axis Frame of the Building Block-1.

Frame numbers 82, 83, 87, 88, 92, and 93 are located on the east axis of the Building Block-1.



Figure 5.4. Numbering of the East Axis Frame of the Building Block-1.

Frame numbers 94, 95, 99, 100, 104, and 105 are located on the west axis of the Building Block-1.



Figure 5.5. Numbering of the West Axis Frame of the Building Block-1.

Numbering of the frame are same for the cases of bare frame, FVD frame and VE frame.

### 5.1. Plastic Rotation Demands

Before passing the plastic rotation demand bar charts, necessary information for understanding and interpreting the results is shared below:

- In the X direction, the total number of dampers is 16 (along the longer dimension of the Building Block-1).
- When the structure is displaced in the X direction, R3 rotations occur on the columns.
- Displacement in the X direction causes R3 rotations, which are rotations about strong axis of the column members.
- In the Y direction, the total number of dampers is 8 (along the shorter dimension of the Building Block-1).
- When the structure is displaced in the Y direction, R2 rotations occur on the columns.
- Displacement in the Y direction causes R2 rotations, which are rotations about the weak axis of the column members.

5.1.1. No-Pulse Like Records' Bar Charts

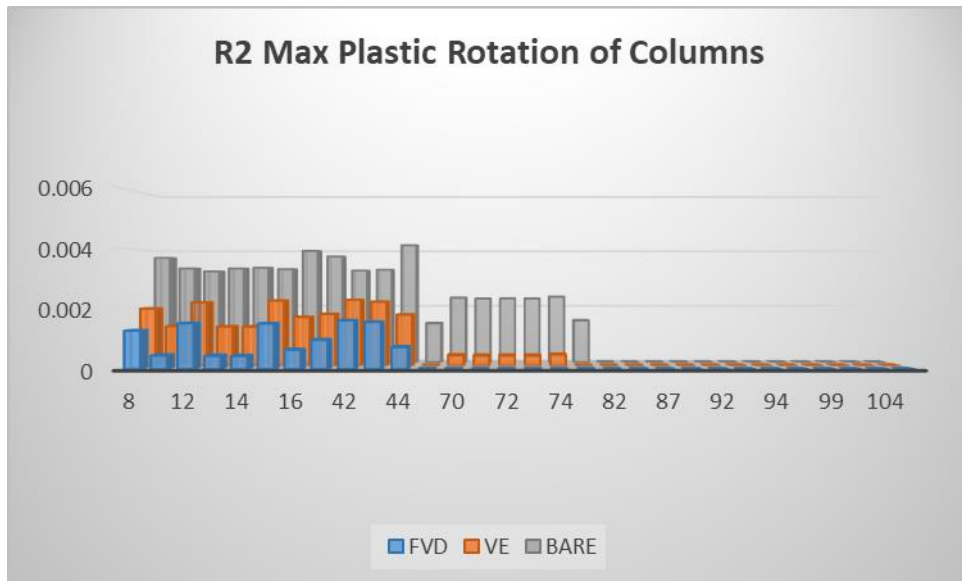


Figure 5.6. Imperial R2 maximum plastic rotation of columns.

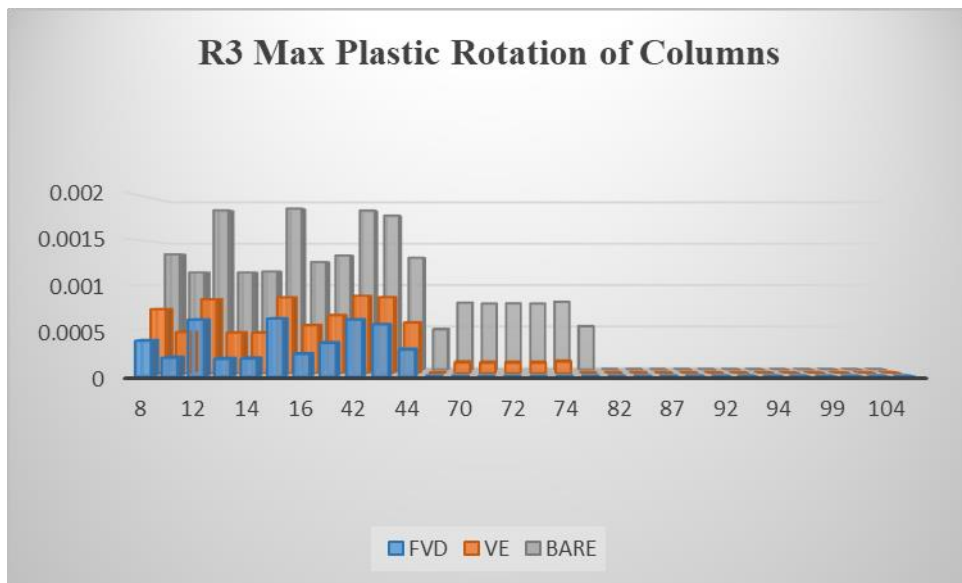


Figure 5.7. Imperial R3 maximum plastic rotation of columns.

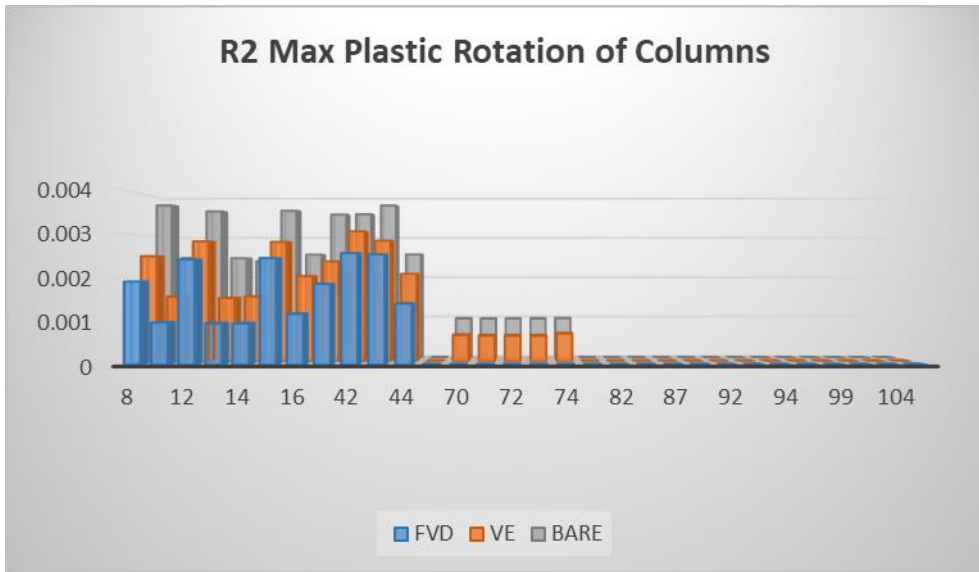


Figure 5.8. Superstitions R2 maximum plastic rotation of columns.

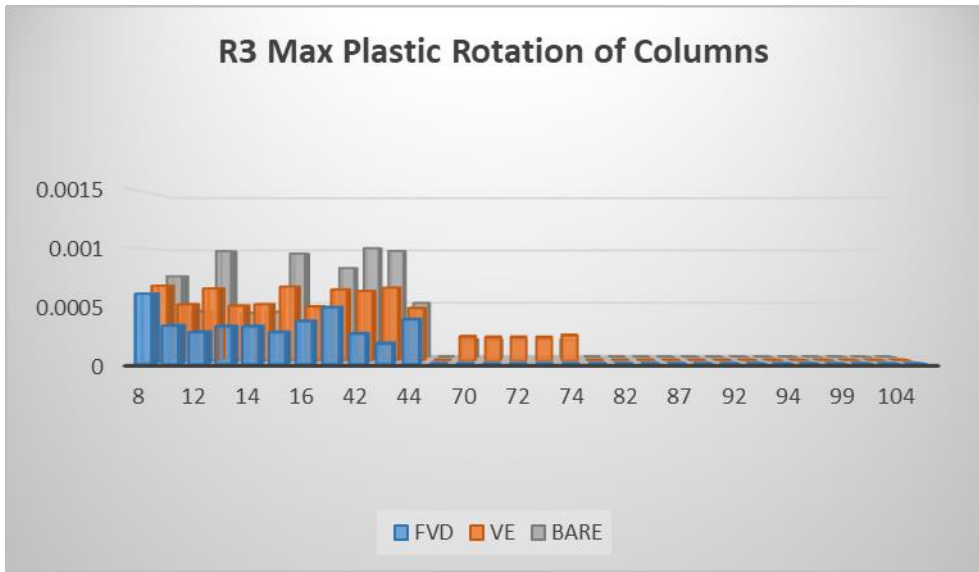


Figure 5.9. Superstitions R3 maximum plastic rotation of columns.

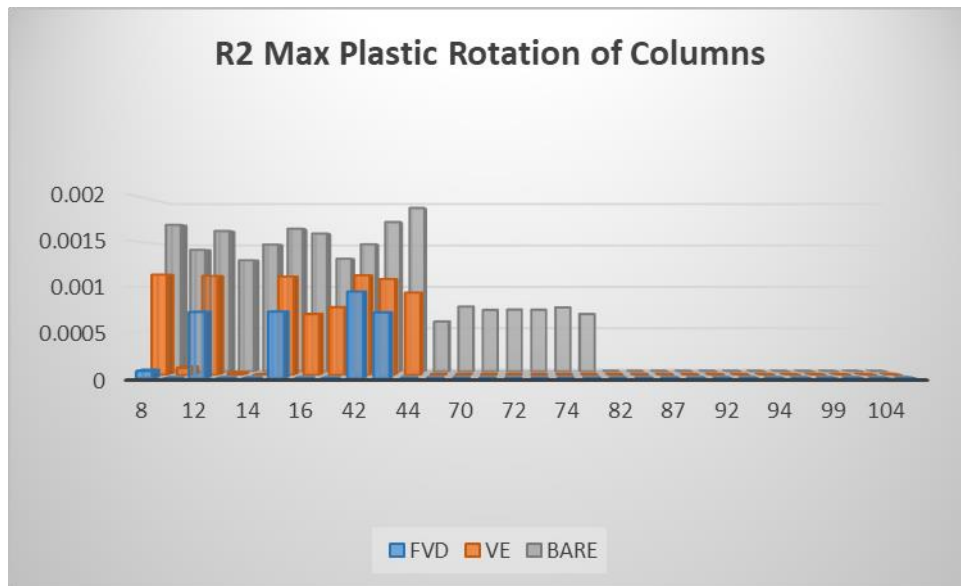


Figure 5.10. Manjil R2 maximum plastic rotation of columns.

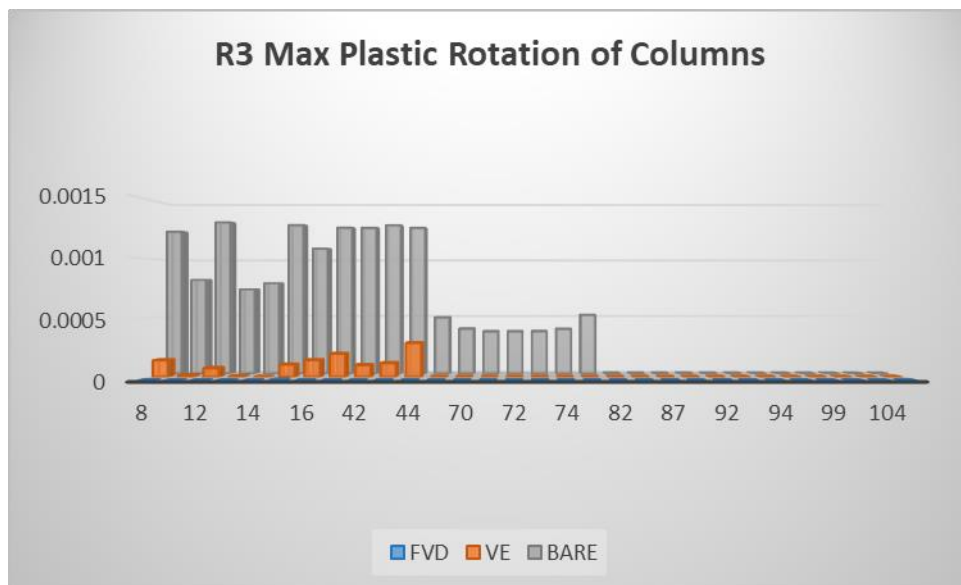


Figure 5.11. Manjil R3 maximum plastic rotation of columns.

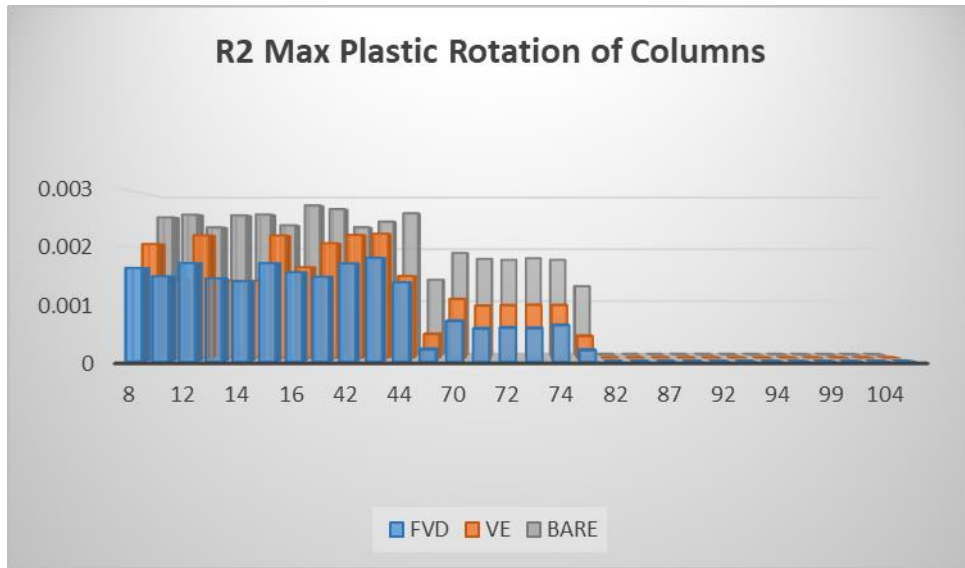


Figure 5.12. Landers R2 maximum plastic rotation of columns.

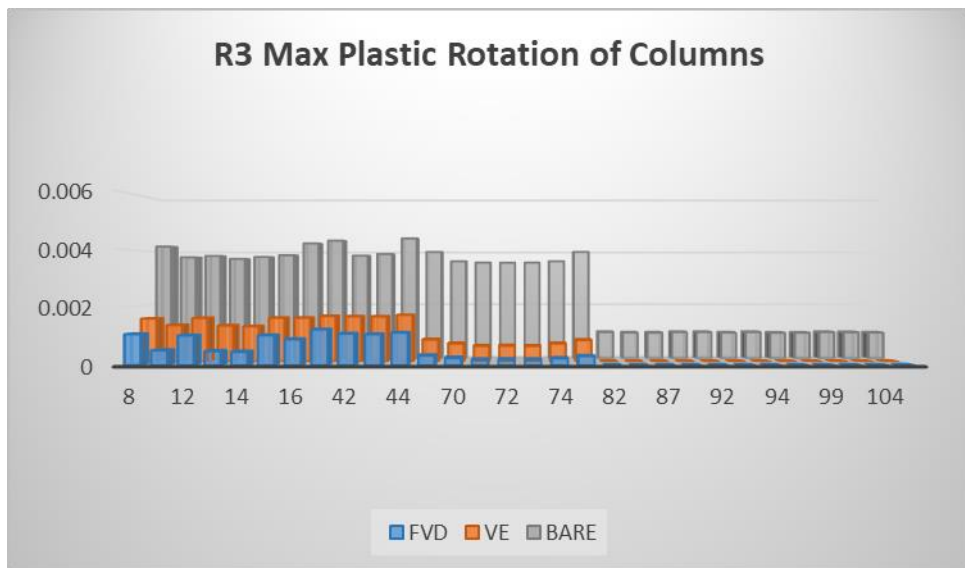


Figure 5.13. Landers R3 maximum plastic rotation of columns.

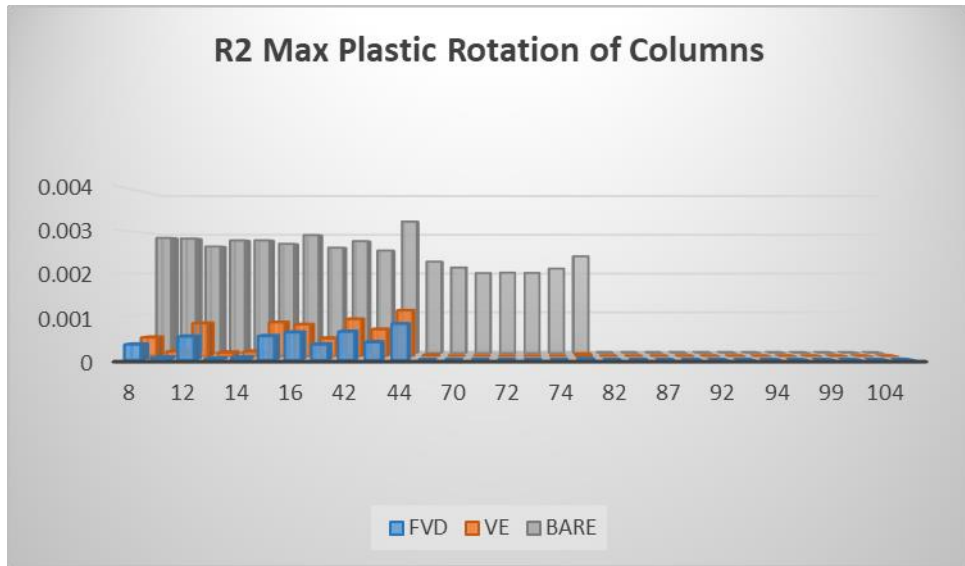


Figure 5.14. Tottori R2 maximum plastic rotation of columns.

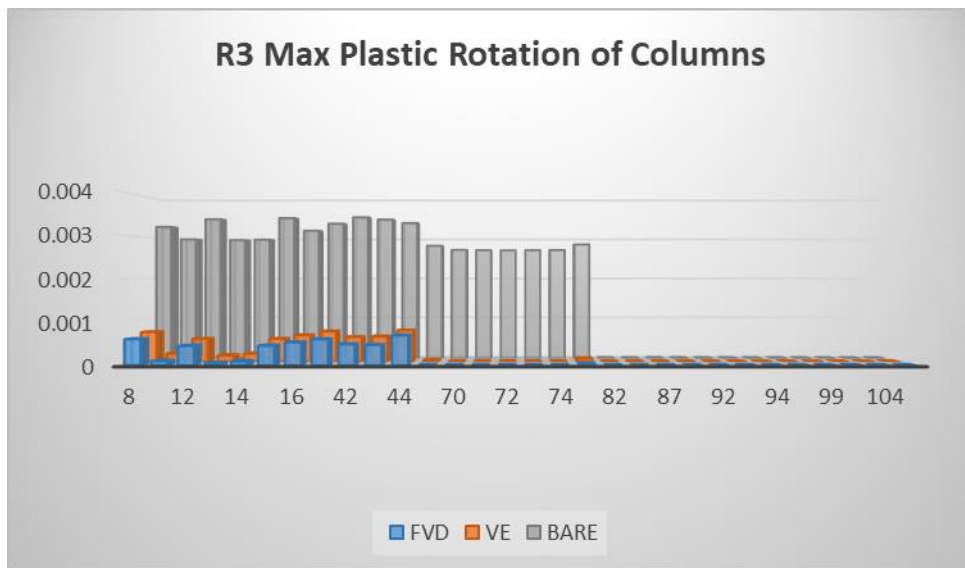


Figure 5.15. Tottori R3 maximum plastic rotation of columns.

5.1.2. Pulse-Like Records' Bar Charts

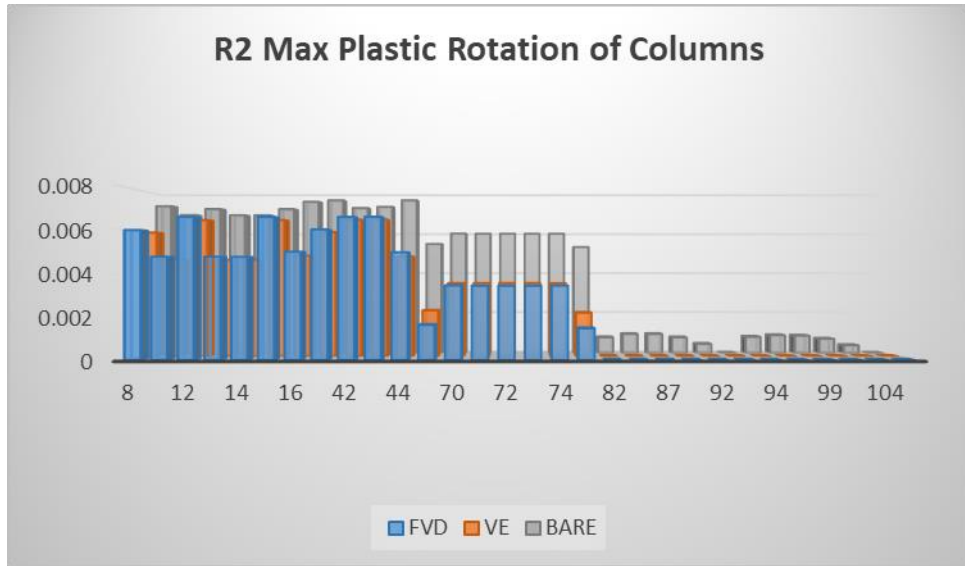


Figure 5.16. Morgan R2 maximum plastic rotation of columns.

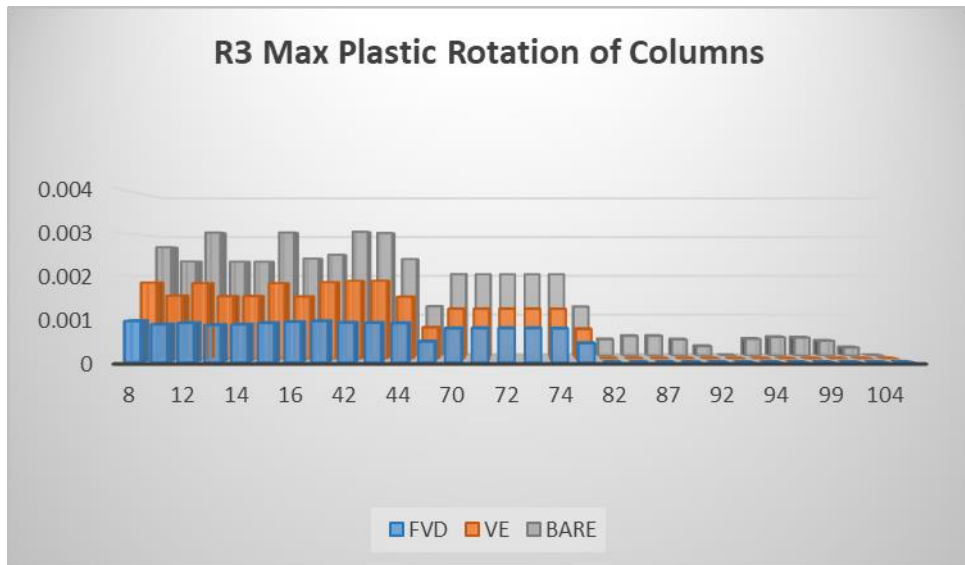


Figure 5.17. Morgan R3 maximum plastic rotation of columns.

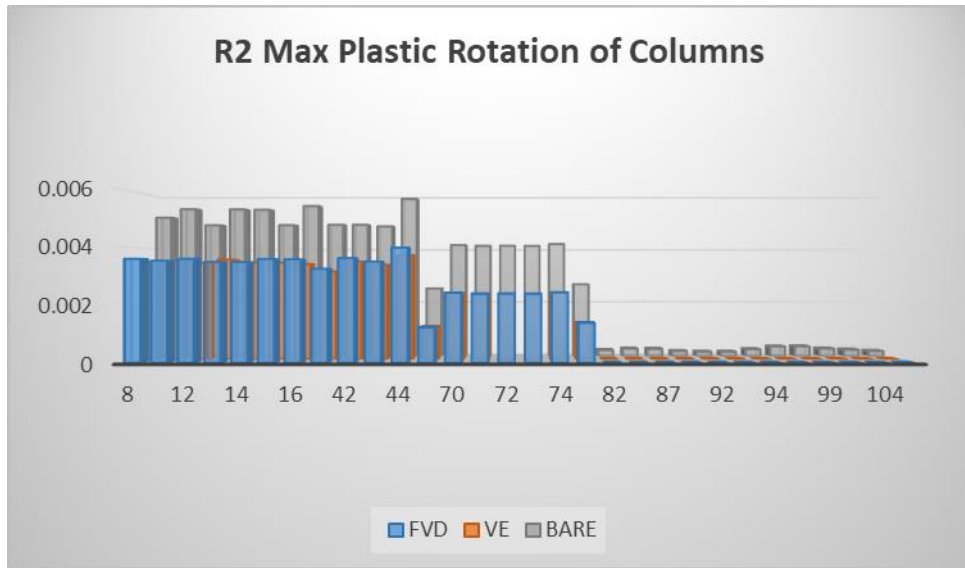


Figure 5.18. Chi-Chi R2 maximum plastic rotation of columns.

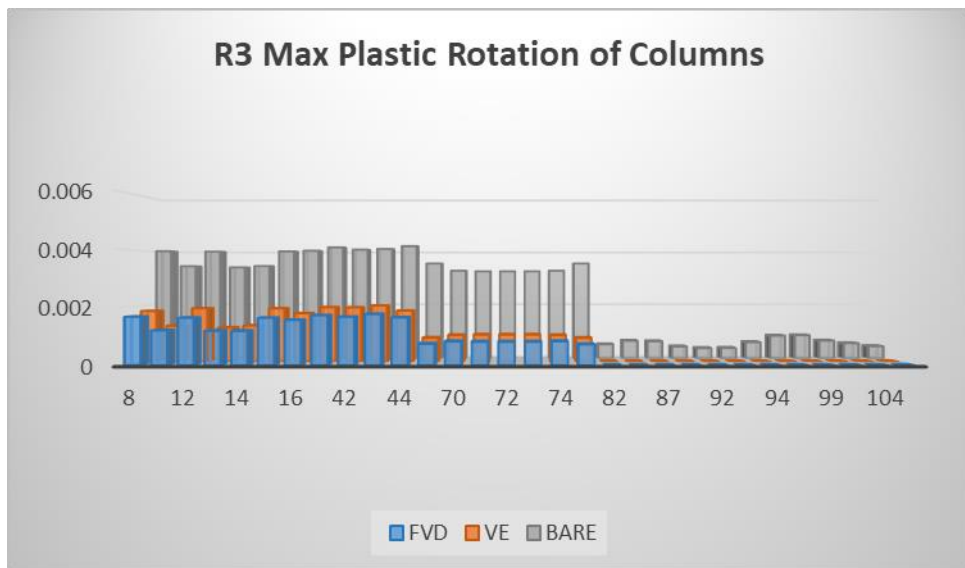


Figure 5.19. Chi-Chi R3 maximum plastic rotation of columns.

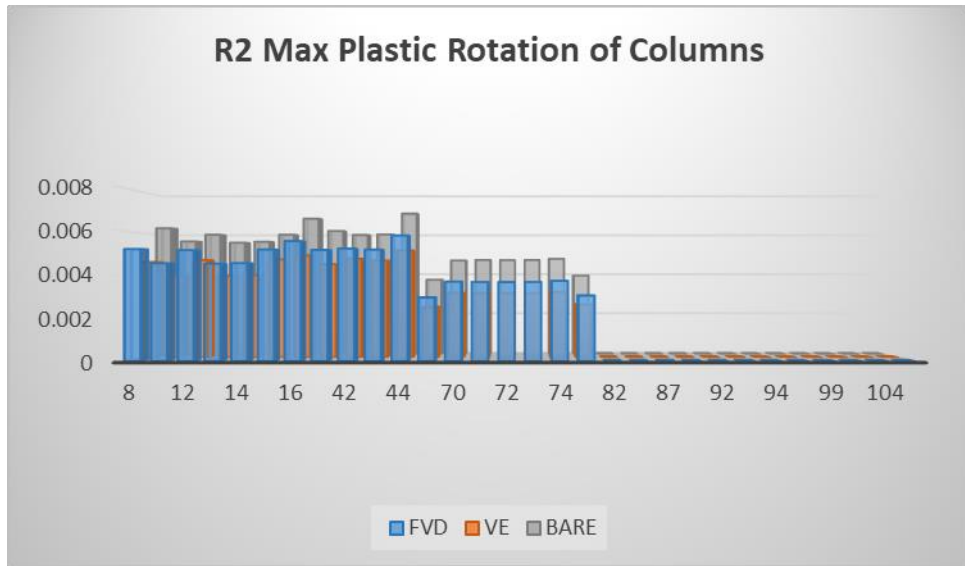


Figure 5.20. Parkfield R2 maximum plastic rotation of columns.

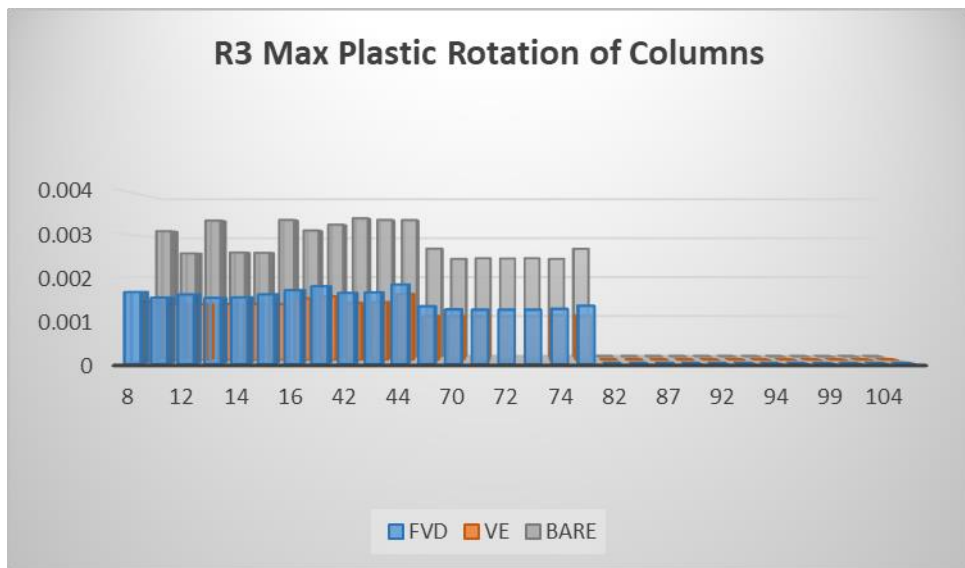


Figure 5.21. Parkfield R3 Maximum Plastic Rotation of Columns.

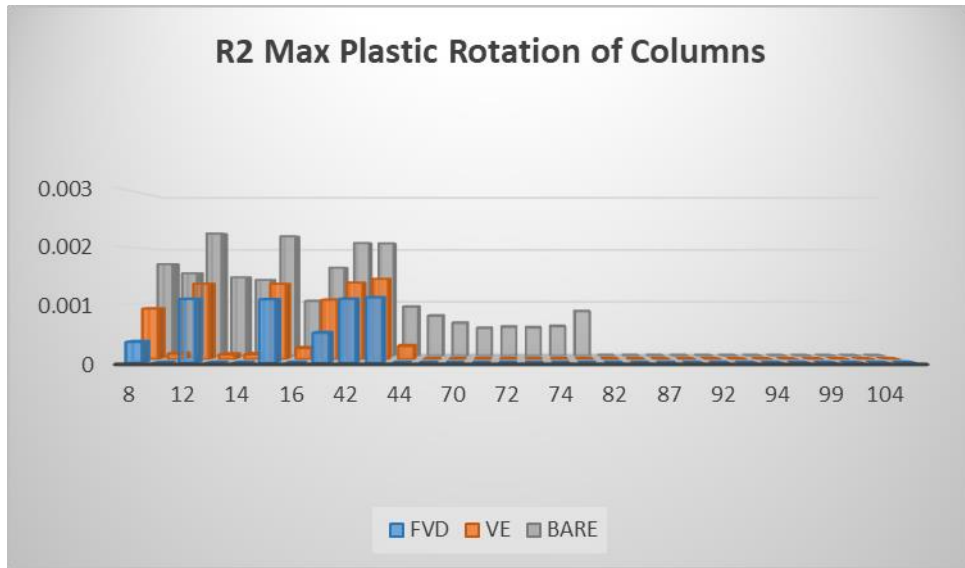


Figure 5.22. Darfield R2 maximum plastic rotation of columns.

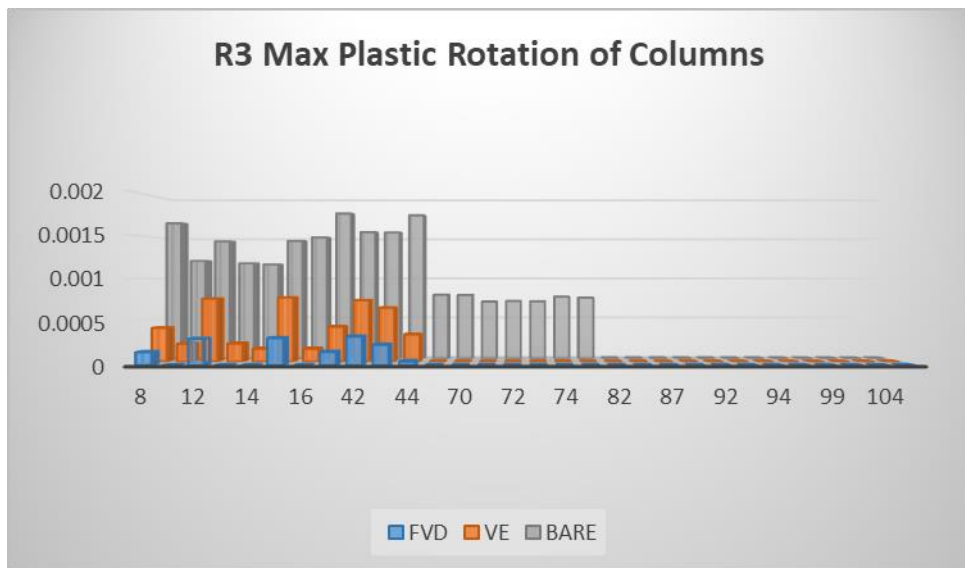


Figure 5.23. Darfield R3 maximum plastic rotation of columns.

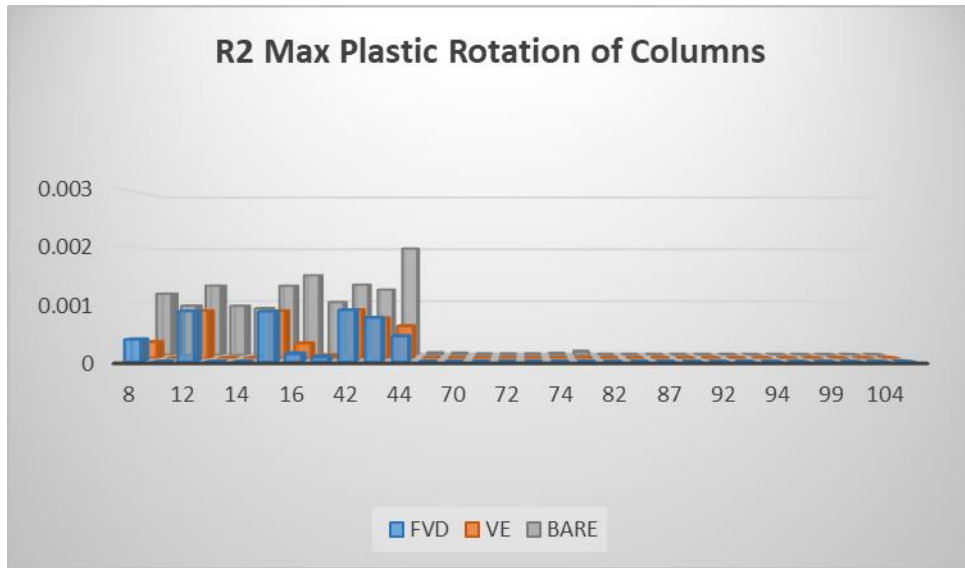


Figure 5.24. Duzce R2 maximum plastic rotation of columns.

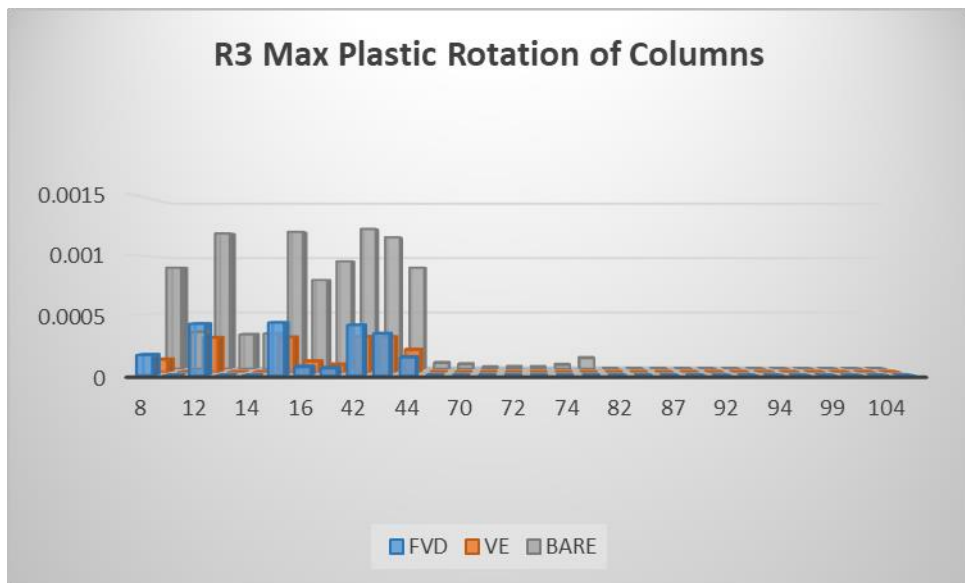


Figure 5.25. Duzce R3 maximum plastic rotation of columns.

### 5.1.3. Geometric Means

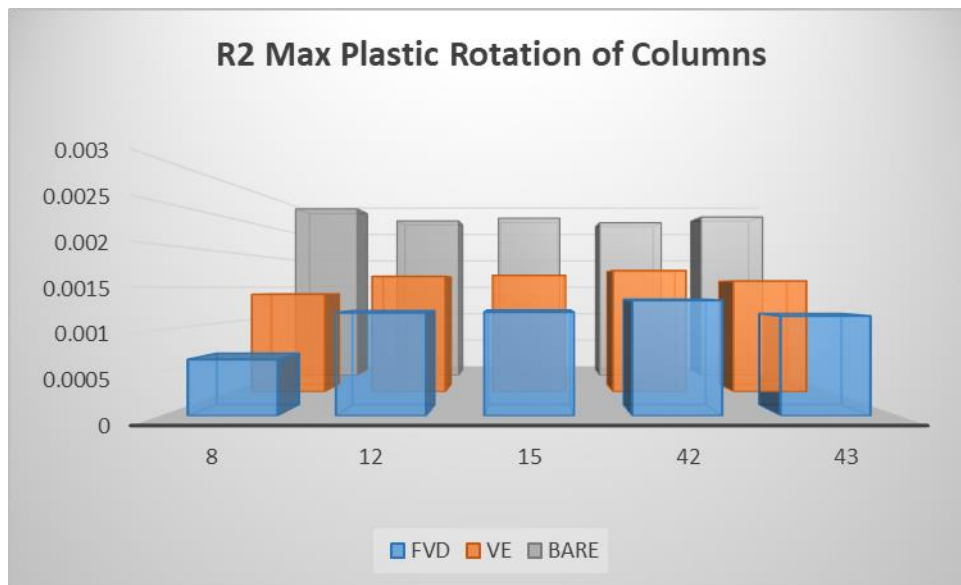


Figure 5.26. Geometric mean of R2 maximum plastic rotations of No-Pulse like records.

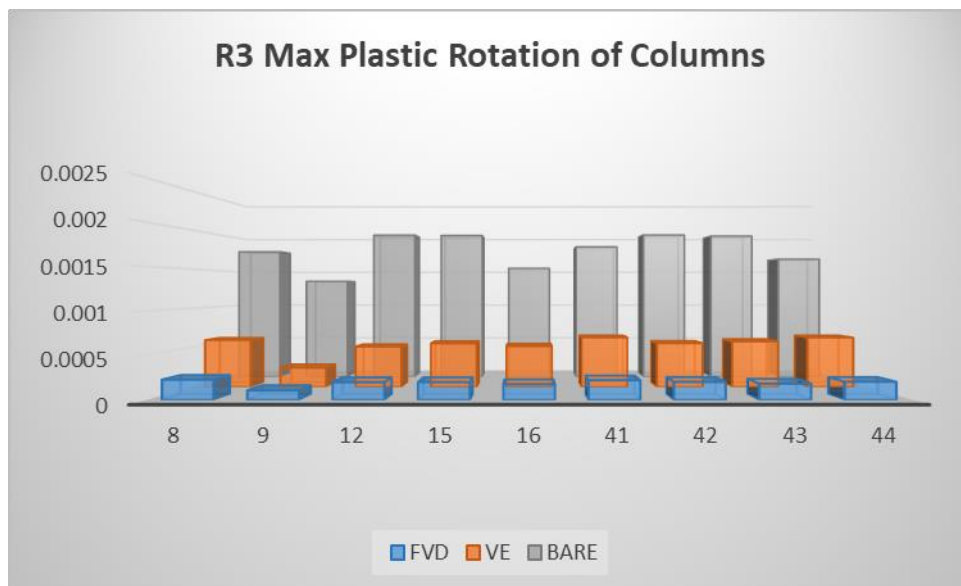


Figure 5.27. Geometric mean of R3 maximum plastic rotations of No-Pulse like records.

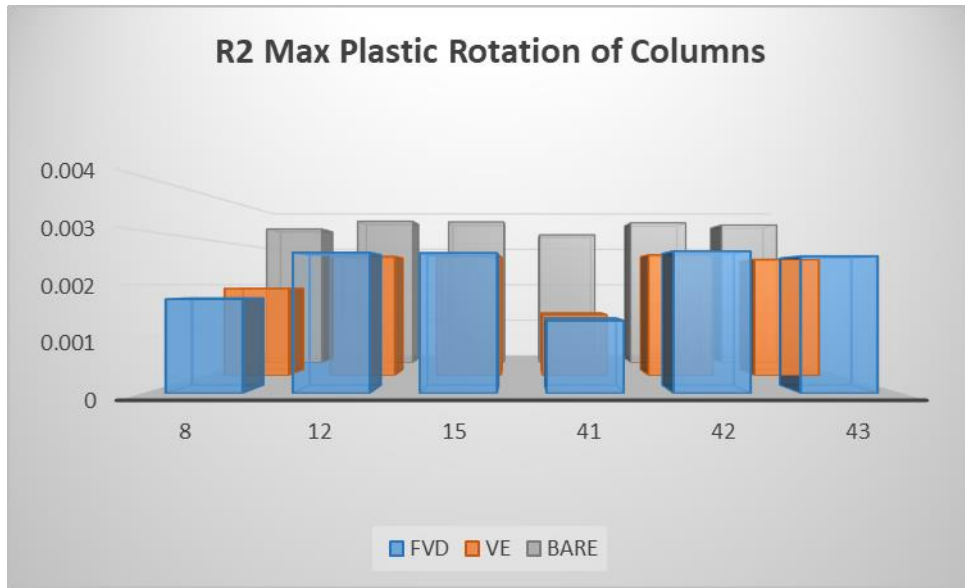


Figure 5.28. Geometric mean of R2 maximum plastic rotations of Pulse like records.

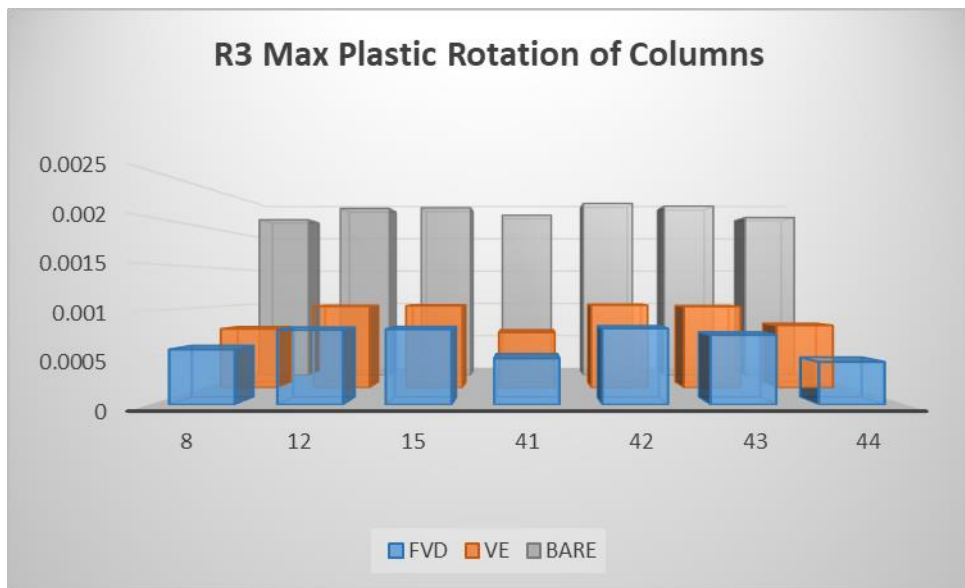


Figure 5.29. Geometric mean of R3 maximum plastic rotations of Pulse like records.

## 5.2. Change in the Modal Periods, Peak Spectral Accelerations and Total Number of Plastic Hinges

Dampers provide additional stiffness to the structure due to their components and extender bars used for mounting. These stiffness provider elements also alter the peak spectral acceleration value that structures experience under a specific earthquake due to the change in the modal periods. The change in the modal periods and corresponding changes in the spectral accelerations for each earthquake record are shared in tables 5.1., 5.2., and 5.3. Moreover, the change in the total number of plastic hinges is given in tables 5.4. and 5.5.

Table 5.1. Modal periods of the Building Block-1 for each case.

	<b>Tx [s]</b>	<b>Ty [s]</b>
<b>Bare Frame</b>	0.79	0.65
<b>FVD Frame</b>	0.39	0.53
<b>VE Frame</b>	0.70	0.64

Table 5.2a. Peak spectral acceleration of No-Pulse like earthquake records.

	<b>Imperial</b>		<b>Superstition</b>		<b>Manjil</b>	
	<b>pSa X [g]</b>	<b>pSa Y [g]</b>	<b>pSa X [g]</b>	<b>pSa Y [g]</b>	<b>pSa X [g]</b>	<b>pSa Y [g]</b>
<b>Bare Frame</b>	0.694	0.915	0.490	0.799	0.546	0.618
<b>FVD Frame</b>	1.051	0.812	1.238	0.757	1.022	0.647
<b>VE Frame</b>	0.704	0.915	0.819	0.799	0.622	0.618
<b>FVD / VE</b>	1.493	0.887	1.512	0.948	1.643	1.047

Table 5.2b. Peak spectral acceleration of No-Pulse like earthquake records.

	<b>Landers</b>		<b>Tottori</b>	
	<b>pSa X [g]</b>	<b>pSa Y [g]</b>	<b>pSa X [g]</b>	<b>pSa Y [g]</b>
<b>Bare Frame</b>	0.578	0.755	0.449	0.546
<b>FVD Frame</b>	0.927	0.876	0.906	0.846
<b>VE Frame</b>	0.648	0.755	0.446	0.546
<b>FVD / VE</b>	1.432	1.161	2.031	1.550

Table 5.3a. Peak spectral acceleration of Pulse like earthquake records.

	Morgan		Chi-Chi		Parkfield	
	pSa X [g]	pSa Y [g]	pSa X [g]	pSa Y [g]	pSa X [g]	pSa Y [g]
<b>Bare Frame</b>	0.831	0.742	0.695	0.947	0.554	0.743
<b>FVD Frame</b>	0.568	0.719	1.126	1.068	1.202	0.974
<b>VE Frame</b>	0.817	0.742	0.824	0.947	0.672	0.743
<b>FVD / VE</b>	0.696	0.969	1.367	1.128	1.788	1.312

Table 5.3b. Peak spectral acceleration of Pulse like earthquake records.

	Darfield		Duzce	
	pSa X [g]	pSa Y [g]	pSa X [g]	pSa Y [g]
<b>Bare Frame</b>	0.415	0.727	0.359	0.643
<b>FVD Frame</b>	0.862	0.734	1.431	0.852
<b>VE Frame</b>	0.621	0.727	0.444	0.643
<b>FVD / VE</b>	1.390	1.011	3.225	1.325

Table 5.4. Total number of plastic hinges for No-Pulse like earthquake records.

	Total # of Plastic Hinges						
	Imperial	Superstitions	Manjil	Landers	Tottori	Geo. Mean	% Reduct.
<b>BARE</b>	95	71	108	159	85	99.69	41.19
<b>FVD</b>	65	61	22	80	59	52.83	21.83
<b>VE</b>	71	66	72	75	44	64.47	26.64

Table 5.5. Total number of plastic hinges for Pulse like earthquake records.

	Total # of Plastic Hinges						
	Morgan	Chi-Chi	Parkfield	Darfield	Düzce	Geo. Mean	% Reduct.
<b>BARE</b>	121	129	99	103	56	97.73	40.38
<b>FVD</b>	73	75	75	59	44	63.91	26.41
<b>VE</b>	73	95	75	74	52	72.49	29.95

### 5.3. Maximum Link Forces and Links' Force-Deformation Graphs

The link elements lay along the same direction showed almost the same behavior because of the rigid diaphragms in the X and Y directions. Because of that reason, only one link element was presented for each direction. One for the shorter side of the Building Block-1 and one for the longer side of the Building Block-1. The maximum link forces during a specific earthquake were tabulated in tables 5.6., 5.7., 5.8., and 5.9.

Table 5.6. Maximum link forces under No-Pulse like records (FVD).

NO-Pulse Like Records [FVD]						
Link Direction	Imperial Max Force [kN]	Supersition Max Force [kN]	Manjil Max Force [kN]	Landers Max Force [kN]	Tottori Max Force [kN]	Geometric Mean [kN]
X (Longer)	237.20	210.90	226.90	240.80	254.70	233.64
Y (Shorter)	242.10	238.50	238.60	247.40	228.70	238.98

Table 5.7. Maximum link forces under Pulse like records (FVD).

Pulse Like Records [FVD]						
Link Direction	Morgan Max Force [kN]	ChiChi Max Force [kN]	Parkfield Max Force [kN]	Darfield Max Force [kN]	Düzce Max Force [kN]	Geometric Mean [kN]
X (Longer)	187.20	250.90	291.30	247.30	243.80	241.70
Y (Shorter)	250.20	235.40	266.20	232.00	233.30	243.08

Table 5.8. Maximum link forces under No-Pulse like records (VE).

<b>NO-Pulse Like Records [VE]</b>						
<b>Link Direction</b>	<b>Imperial Max Force [kN]</b>	<b>Supersition Max Force [kN]</b>	<b>Manjil Max Force [kN]</b>	<b>Landers Max Force [kN]</b>	<b>Tottori Max Force [kN]</b>	<b>Geometric Mean [kN]</b>
X (Longer)	244.70	181.90	251.70	309.30	288.50	251.17
Y (Shorter)	229.70	248.20	199.10	247.20	193.80	222.38

Table 5.9. Maximum link forces under Pulse like records (VE).

<b>Pulse Like Records [VE]</b>						
<b>Link Direction</b>	<b>Morgan Max Force [kN]</b>	<b>ChiChi Max Force [kN]</b>	<b>Parkfield Max Force [kN]</b>	<b>Darfield Max Force [kN]</b>	<b>Düzce Max Force [kN]</b>	<b>Geometric Mean [kN]</b>
X (Longer)	147.70	316.40	428.40	263.80	253.40	266.26
Y (Shorter)	380.70	253.80	298.00	200.00	200.70	258.57

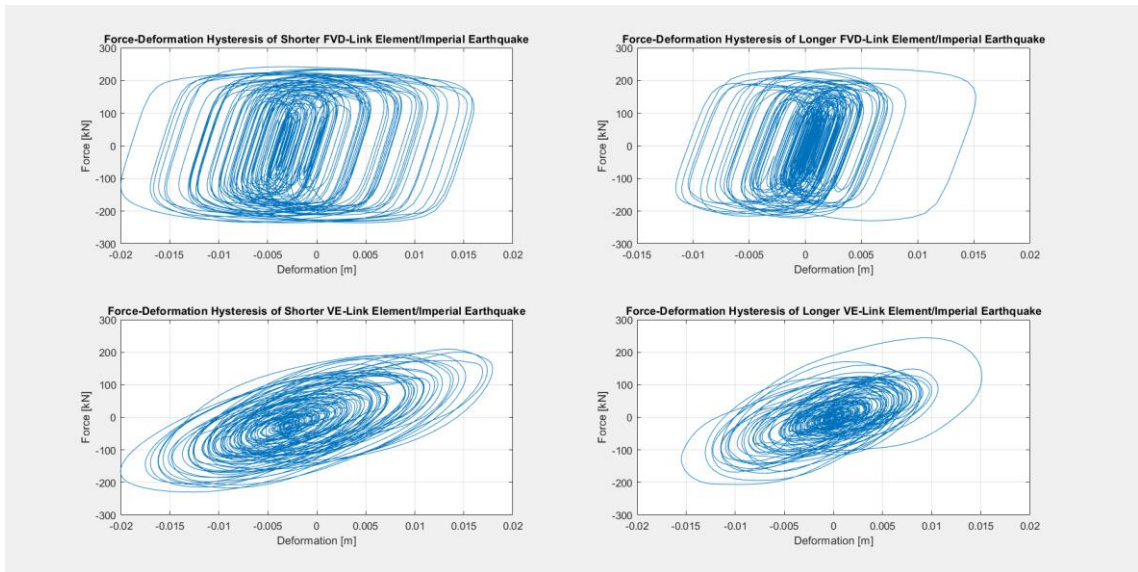


Figure 5.30. Hysteresis behavior of link elements (Imperial Earthquake) [43].

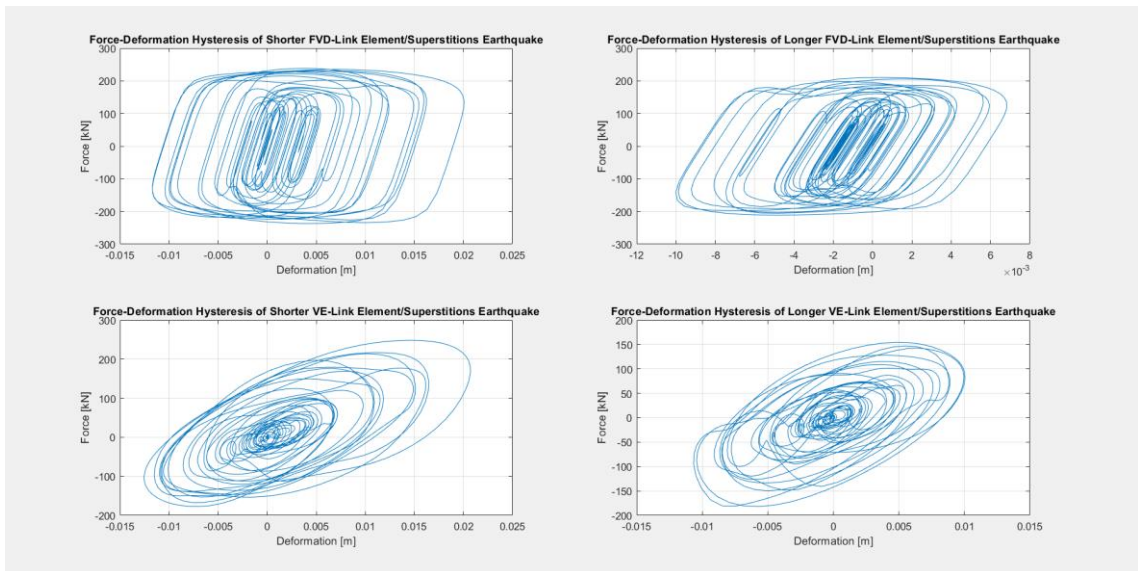


Figure 5.31. Hysteresis behavior of link elements (Superstitions Earthquake).

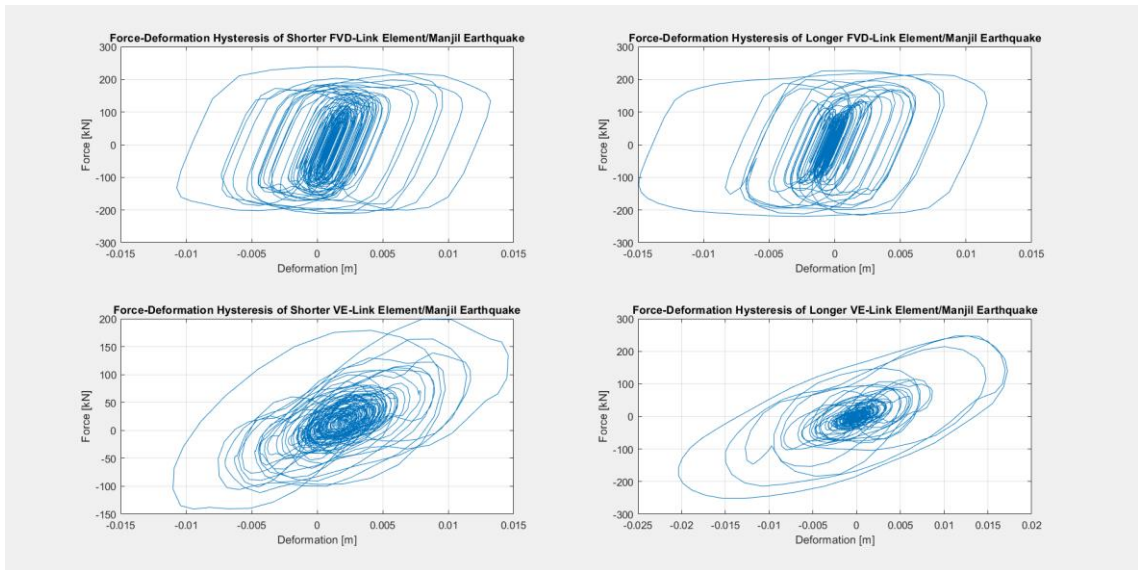


Figure 5.32. Hysteresis behavior of link elements (Manjil Earthquake).

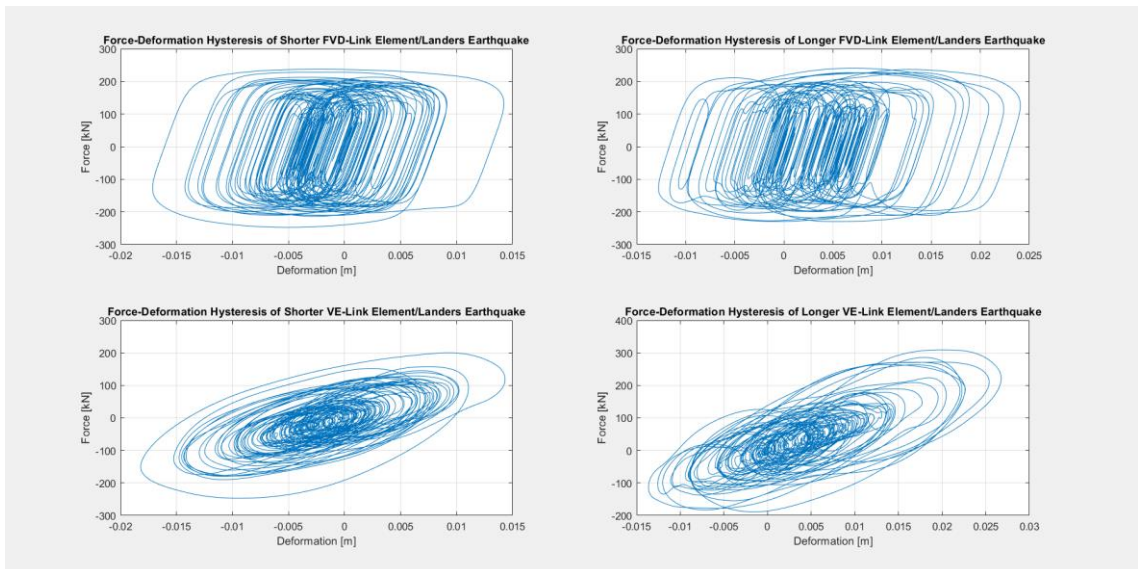


Figure 5.33. Hysteresis behavior of link elements (Landers Earthquake).

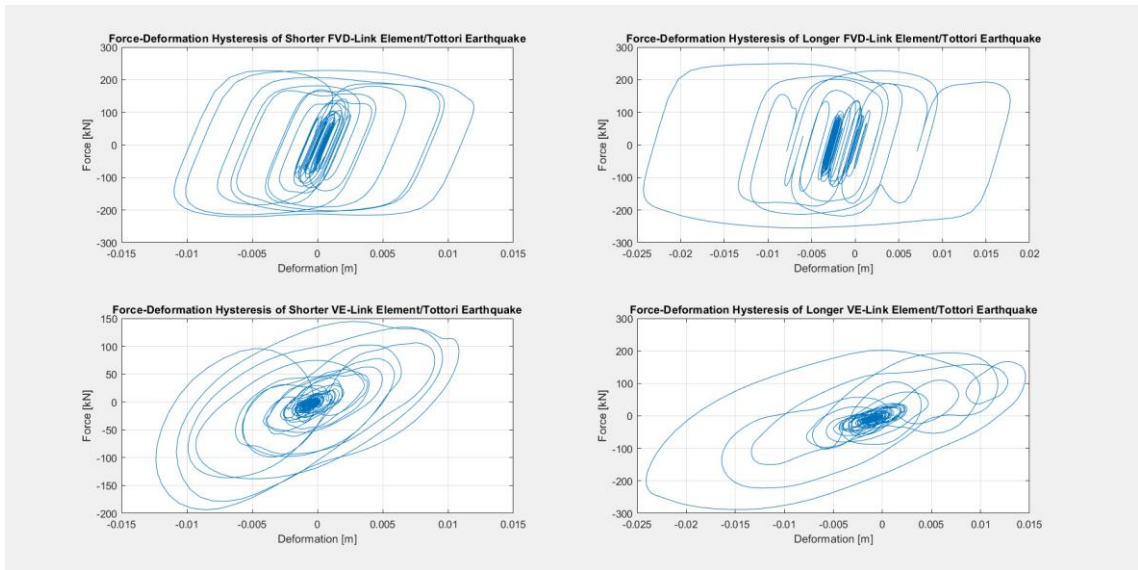


Figure 5.34. Hysteresis behavior of link elements (Tottori Earthquake).

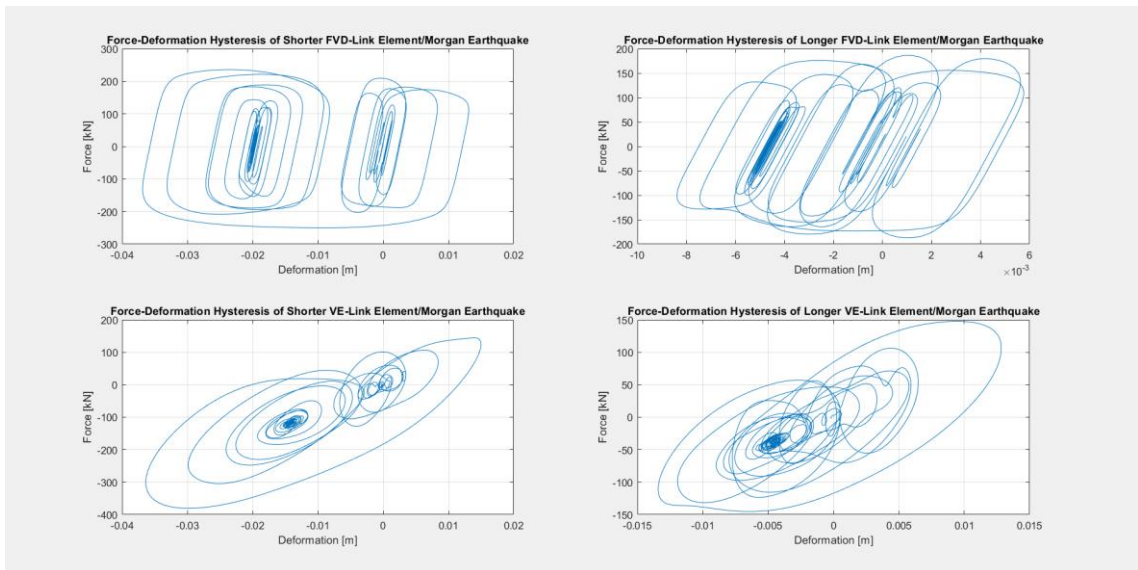


Figure 5.35. Hysteresis behavior of link elements (Morgan Earthquake).

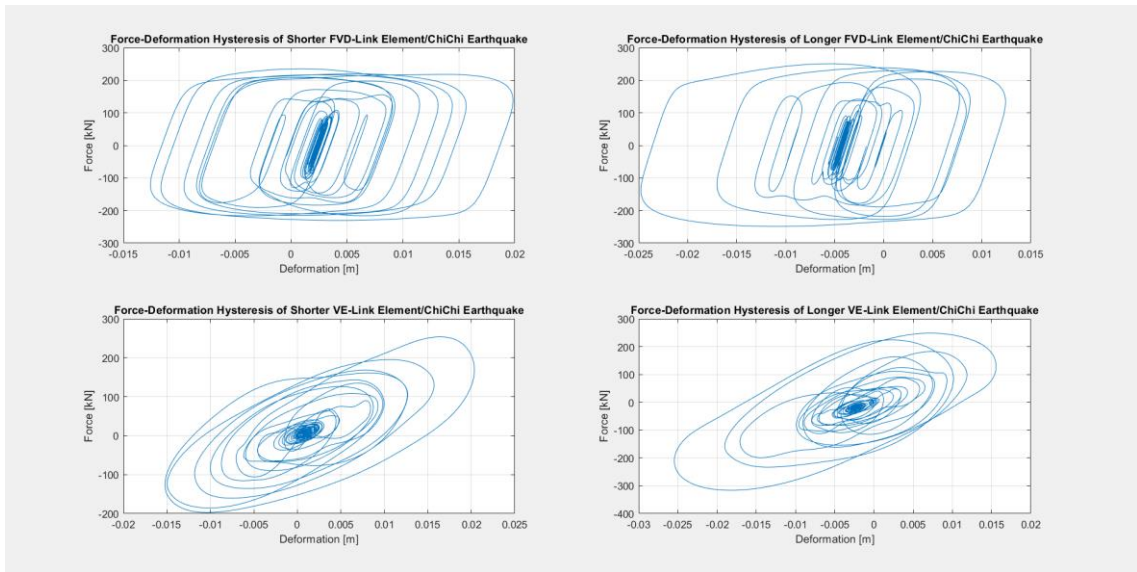


Figure 5.36. Hysteresis behavior of link elements (Chi-Chi Earthquake).

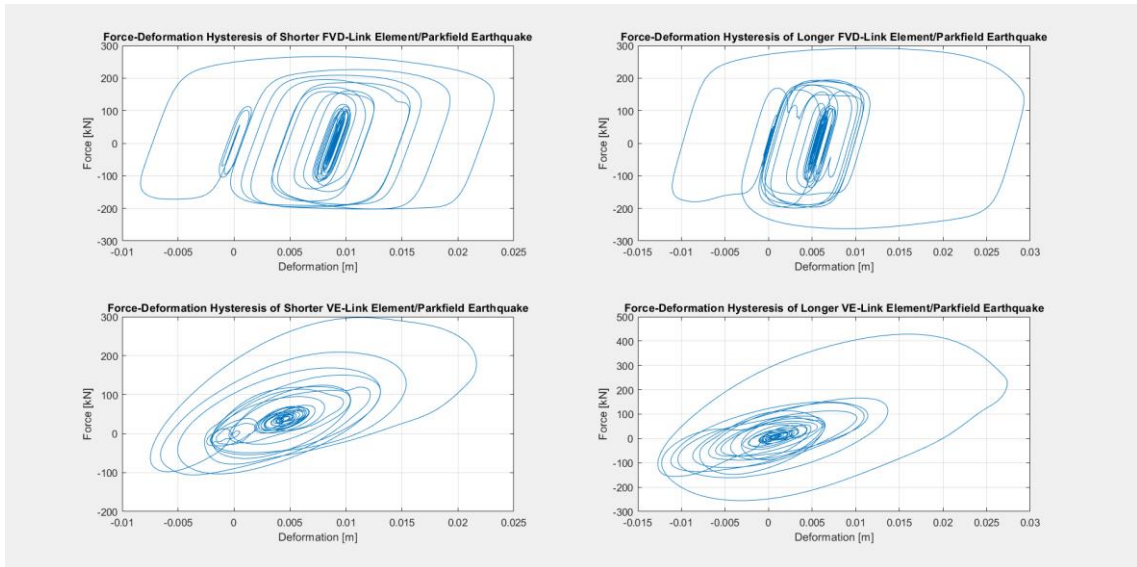


Figure 5.37. Hysteresis behavior of link elements (Parkfield Earthquake).

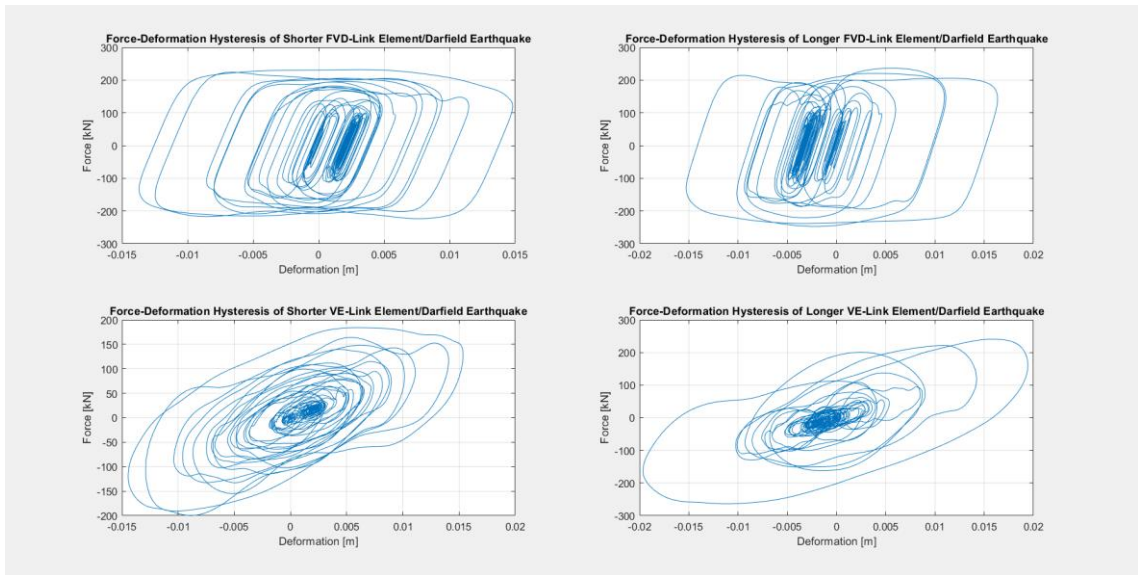


Figure 5.38. Hysteresis behavior of link elements (Darfield Earthquake).

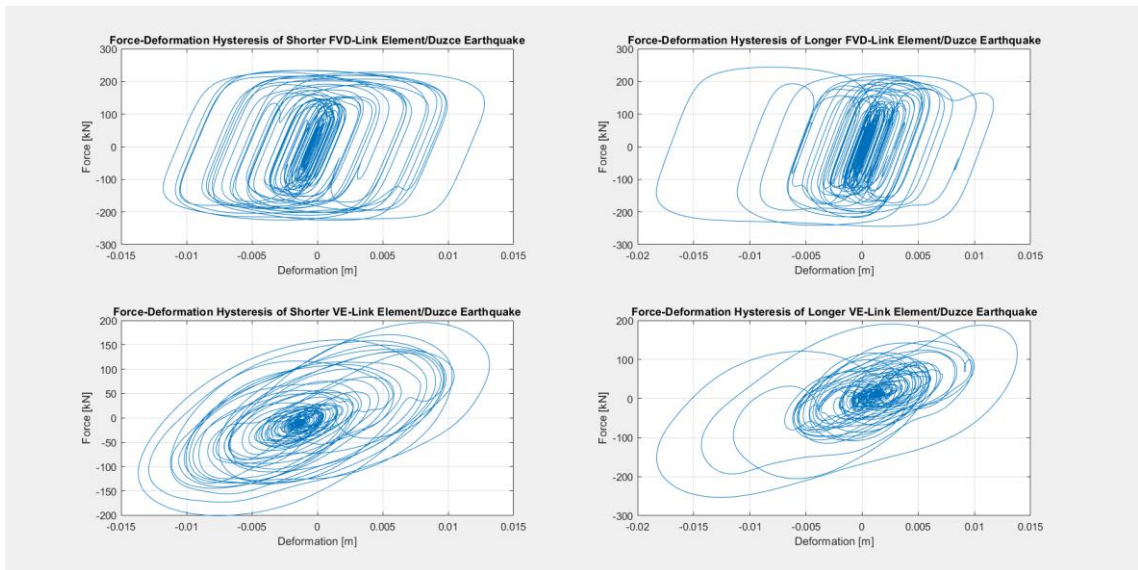


Figure 5.39. Hysteresis behavior of link elements (Duzce Earthquake).

## 6. EVALUATION OF THE ANALYSIS RESULTS and COMMENTS

For all earthquake records, the decrease in R3 plastic rotations of columns is more than the decrease in R2 plastic rotations of columns. This can be explained by the total number of dampers along the sides of the Building Block-1. There are 16 dampers along the longer side of the Building Block-1, whereas there are eight dampers along the shorter side of the Building Block-1. Because R3 rotations are occurred due to displacement in the X direction (parallel to the longer dimension), the decrease in the amount of R3 plastic rotation of columns for FVD and VE frames is greater than the decrease in the amount of R2 plastic rotation.

For the No-Pulse like earthquakes, FVDs are obviously more effective in reducing the response than VEs. For evaluating the effectiveness of damper types, spectral acceleration was also considered. Table 5.2 shows that peak spectral accelerations are more for the structure having FVDs, and therefore it is certain that FVDs are more effective in reducing the plastic rotation demands on the columns compared to VEs for the No-Pulse like earthquake records.

On the other hand, for the pulse-like records, the effectiveness of FVDs and VEs are very close to each other. Moreover, although the reduction in plastic rotations is very close for FVDs and VEs, VEs show relatively better performance compared to FVDs. However, this disposition is not observed in the Darfield, Duzce, and Morgan R3 plastic rotation results. The Morgan base excitation led to less R3 plastic rotation demand on the FVD case members, which can be explained by the change in the spectral acceleration value in the X direction, which causes R3 rotations. Table 5.3 shows that the experienced peak spectral acceleration of the structure having FVD under the Morgan Earthquake is less compared to the structure having VE. However, other pulse-like earthquake records cause more peak spectral acceleration in the X direction for the FVD case. Because of that, less R3 plastic rotation demands for the Morgan Earthquake can be explained by experiencing less spectral acceleration compared to the structure with VE. Moreover, the results of the Darfield Earthquake resemble the results of the no-pulse like earthquake records, although the Darfield earthquake record contains velocity pulses. However, because Darfield Earthquake

has a pulse period of 10.63 seconds which is not close enough to the structure's fundamental period, Darfield Earthquake works as a no-pulse-like earthquake record. Therefore, the earthquake records should be selected by considering the fundamental period of the structure and the pulse period of earthquakes. They need to be sufficiently close to observe the pulse effect on the response. Furthermore, at first glance, we can say that the results of the FVD and VE dampers are very close to each other for the Duzce earthquake like the results of other pulse-like earthquakes. Duzce Earthquake has a pulse period of 10.052 seconds which is not close enough to the structure's fundamental period just like the Darfield Earthquake. However, although the results of the Darfield Earthquake resemble the results of no-pulse like records, the results of the Duzce Earthquake are similar to the results of other pulse like records. Table 5.3 shows that, the ratio of the peak spectral acceleration values in the X and Y direction is 3.225 and 1.55, respectively. These ratios are obviously bigger for Duzce Earthquake than the other pulse-like earthquake records: Morgan, ChiChi, Parkfield, and Darfield. Because of that reason, although the pulse period of the Duzce Earthquake is not close enough to the structure's fundamental period, the effectiveness of the FVDs and VEs for Duzce Earthquake might be interpreted as similar due to the change in the peak spectral acceleration values.

The maximum force that occurred on the link elements during the no-pulse like earthquake excitations is smaller than during the pulse like excitations. Although the maximum link forces are smaller for the no-pulse like records than the damper capacity which is 250 KN, the pulse-like records led to the maximum link force of more than 250 KN which is designated as the failure of the connection joints and link elements. It is known that most of the energy in a pulse motion is transmitted to the structure in one or two cycles of the velocity-time series, and structural responses are magnified in case of close matching of the pulse period and the structure's fundamental period. This situation can be easily observed from the maximum force that occurred on the link elements during the pulse-like records. Morgan, Chi-Chi, and Parkfield earthquakes have pulse periods 1.23s, 2.44s and 0.7s, respectively. These are close to the fundamental period of the structure shown in table 5.1. Especially, the maximum force that occurred on the VE link element laying along the X direction during the Parkfield Earthquake is 428 KN, shown in table 5.9., which is obviously bigger than other maximum occurred forces on the link elements. This result shows us the importance of the closeness of the pulse period and the structure's fundamental period since

the period of the Building Block-1 with VEs in the X direction is 0.7s which is exactly the same as the pulse period of the Parkfield Earthquake, which 0.7s.

Tables 5.4 and 5.5 show that fluid viscous and viscoelastic dampers having 250 KN capacity reduced the total number of plastic hinges significantly. However, this reduction in the total number of plastic hinges does not change the performance level of the structure much since for both cases, which are retrofitting with FVD and retrofitting with VE, the percentage of the columns having plastic deformation is higher than 30% which directly indicates that the structure is at least at a performance level of Collapse Prevention according to the TBDY2018, which is same with the performance level of the current structure explained in section 2.4. In that context, although the using passive control devices led to a significant reduction in plastic rotation demands on the column members, retrofitting methodologies using FVDs and VEs do not change the performance level of the structure, and therefore these methodologies are redundant just like other tries.

The Building Block-1 was constructed so that when the structure is displaced in the X direction, rotations occur about the strong axis of each column member, and these rotations are designated as R3 rotation on the bar charts. On the other hand, when the structure is displaced in the Y direction, rotations occur about the weak axis of each column member, and these rotations are designated as R2 rotation on the bar charts. Therefore, R2 rotations shown on the bar charts are larger than R3 rotations since the sections rotate more easily about the weak axis and R2 rotations are about the weak axis.

For the no-pulse like records and the pulse like records, the ratios of the spectral acceleration of FVD case to the VE case in the X and Y direction are in a similar tendency for most of the earthquake records, and this was shown in tables 5.2. and 5.3. You can also find the geometric mean of these ratios in table 6.1. Although these ratios are closer to each other, the structure with FVDs, obviously, has less plastic deformation on members than the structure with VEs for the no-pulse like earthquake records. However, the structure with FVDs and VEs exhibit similar plastic responses for the pulse-like records. The peak spectral acceleration ratios are very close for the no-pulse like records and the pulse like records, however the plastic rotation demand on the members for the FVD and VE cases are not in line with these peak spectral acceleration ratios. Because of that, we might say that the

closeness of the plastic rotation demands for the structures with FVDs and VEs under the pulse like excitations, whereas the plastic rotation demands are higher for the structure retrofitted with VEs under the no-pulse like excitations, is not explained by the change in the spectral acceleration values, and therefore a different explanation needs to be searched.

Table 6.1. Geometric mean of the ratios.

	<b>Geometric Mean</b>	
<b>FVD/VE</b>	<b>pSa_X [g]</b>	<b>pSa_Y [g]</b>
No-Pulse	1.609	1.097
Pulse	1.501	1.139

As stated in the previous paragraph, we observe similar plastic rotation demands on the members for the pulse like records. On the other hand, the members of structure with FVDs have less plastic demand than those with VEs for the no-pulse like records. That was investigated and concluded that the earthquakes' peak spectral accelerations do not cause this difference. Characteristics of pulse like records should be the reason for that. It is known from previous researches that records containing velocity pulses are known to lead to disproportionately large nonlinear responses [44-46]. It was observed from the analysis result, larger plastic deformations in both R2 and R3 directions occurred for pulse like records than the no-pulse like records. You can check the sections 5.1.1., 5.1.2., and 5.1.3. and see the results of plastic rotation demands of the no-pulse like records, pulse-records, and the geometric mean of results. It should be remembered that although the Darfield and Duzce Earthquakes are classified as the pulse like records, their effect on the structure is similar to the no-pulse like records since the pulse periods of Darfield and Duzce Earthquakes are approximately 10 seconds which is considerably larger than the fundamental period of the Building Block-1.

It is known that most of the energy in a pulse motion is concentrated in one or two cycles of the velocity-time series, and this may account for disproportionately larger inelastic deformations for the pulse like records because as the pulse period approaches the period of structure, all the energy embedded in one or two cycles of the velocity time-series is transmitted to the structure in a most dangerous form known as resonance. For the pulse like records, structure experiences more deformation, and therefore structure oscillates between

two distant points compared to oscillation due to no-pulse like excitations. So, this leads to less hysteretic behavior because the oscillation distance increases, and oscillation takes place more in the plastic region since the pulse like records cause disproportionately larger inelastic deformations and velocities are low when the sections are in the inelastic region. We can observe that from the force deformation graphs of link elements. You can check section 5.3 to compare the force-deformation graphs of link elements.

In summary:

- Structures experience more deformation under pulse like earthquakes whose pulse period is closer to the period of the structure.
- It leads to less hysteretic behavior because of the amount of deformation and low velocity content in the inelastic region.
- The structure occupies mostly in the inelastic region. In the inelastic region, the velocity of the joints is very low since the velocity of the joints is zero at the maximum deformation, and velocity increases as the joints approach the initial state. Because of that, in the inelastic region, the velocity of the joints is closer to zero, and this region determines the maximum plastic deformation.
- As shown in figure 6.1., we can observe that the difference between FVD and VE is getting smaller and smaller for small velocities, which we mainly observe in inelastic regions.
- When we draw the velocity time histories of the joint 50 (a joint on the top floor) for Morgan, Chi-Chi and Parkfield Earthquakes for FVD and VE cases together, it is observed that velocity graphs well coincide, and this eliminates the effect of velocity difference in explaining the why the cases FVD and VE show similar results under the pulse like excitations.

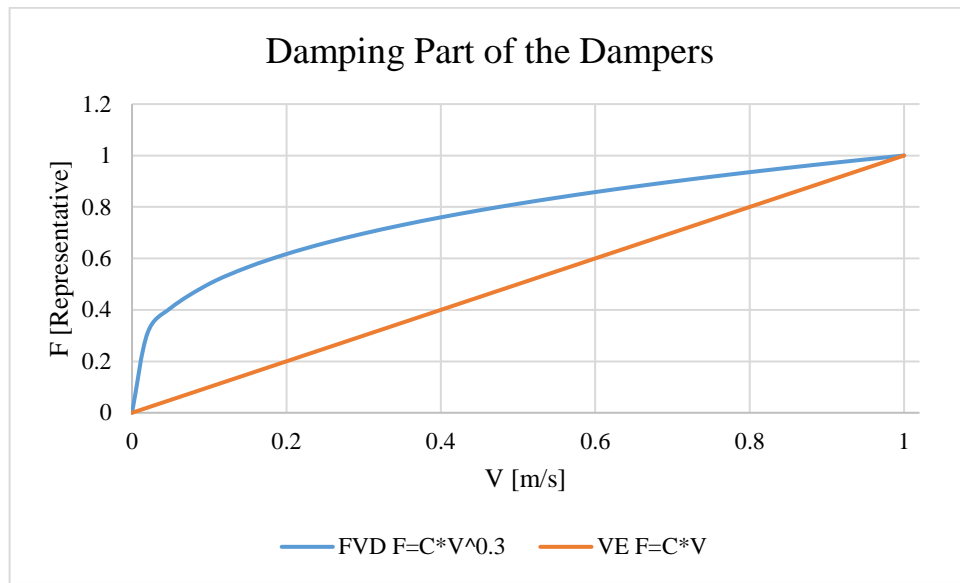


Figure 6.1. Velocity-Force graph of the Fluid Viscous Dampers having 0.3 nonlinearity coefficient and Velocity-Force graph of damping part of the Viscoelastic Dampers.

The velocity time histories of the joint 50 (a joint on the top floor) for Morgan, Chi-Chi, and Parkfield Earthquakes are shared below.

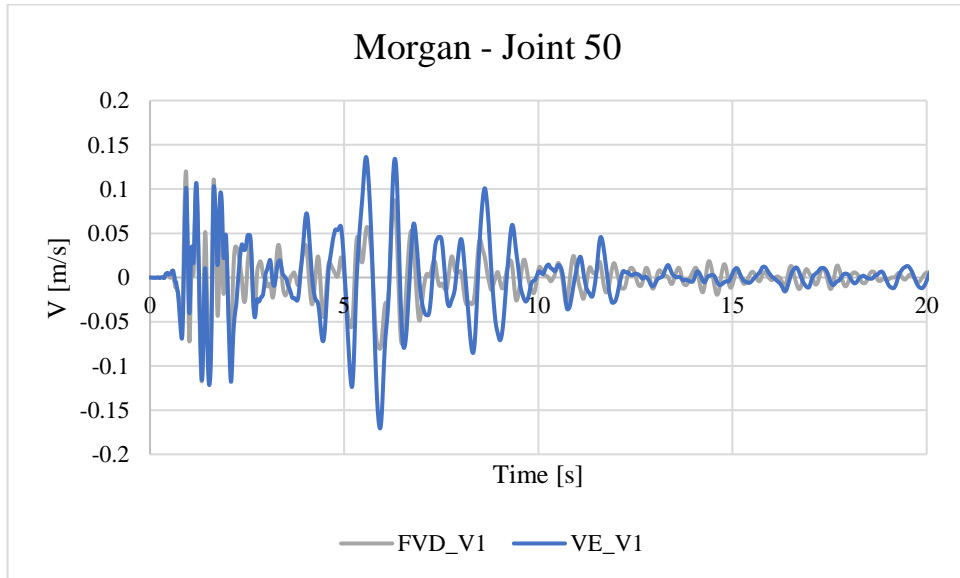


Figure 6.2. Velocity-X time history (Morgan Earthquake).

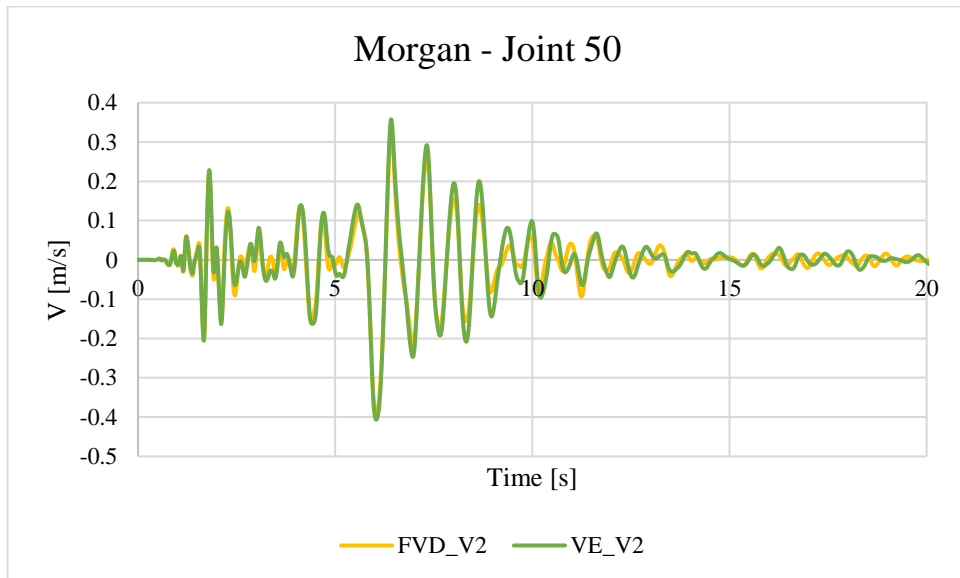


Figure 6.3. Velocity-Y Time History (Morgan Earthquake).

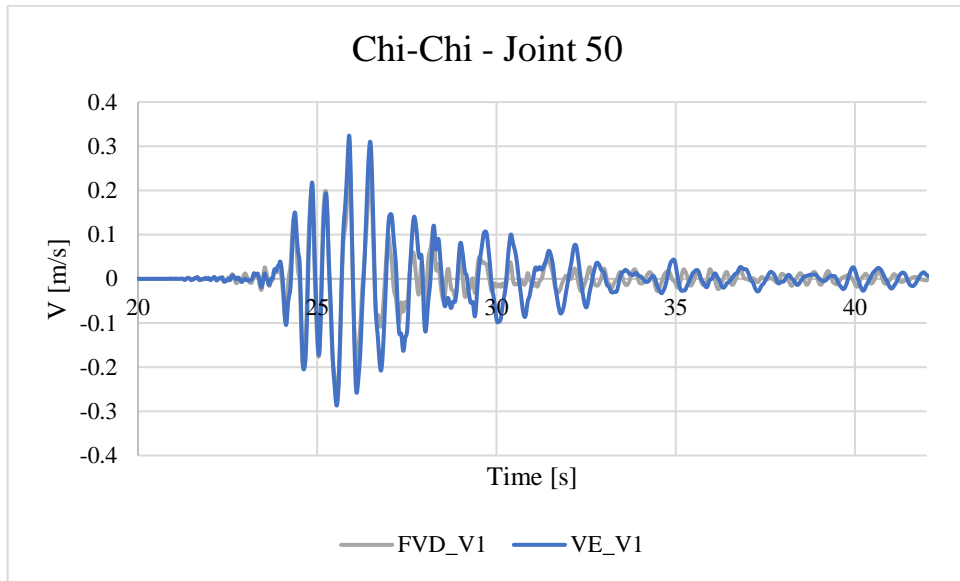


Figure 6.4. Velocity-X Time History (Chi-Chi Earthquake).

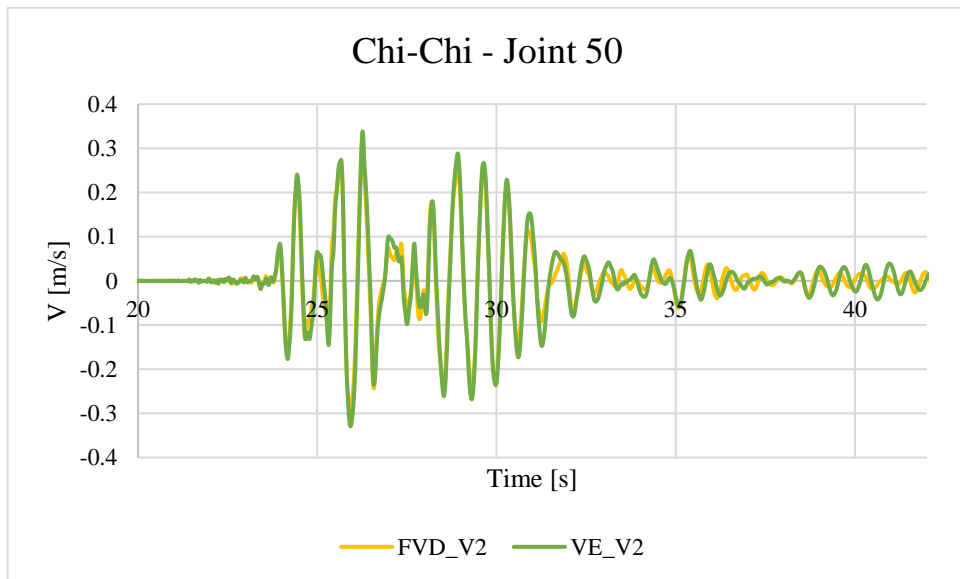


Figure 6.5. Velocity-Y Time History (Chi-Chi Earthquake).

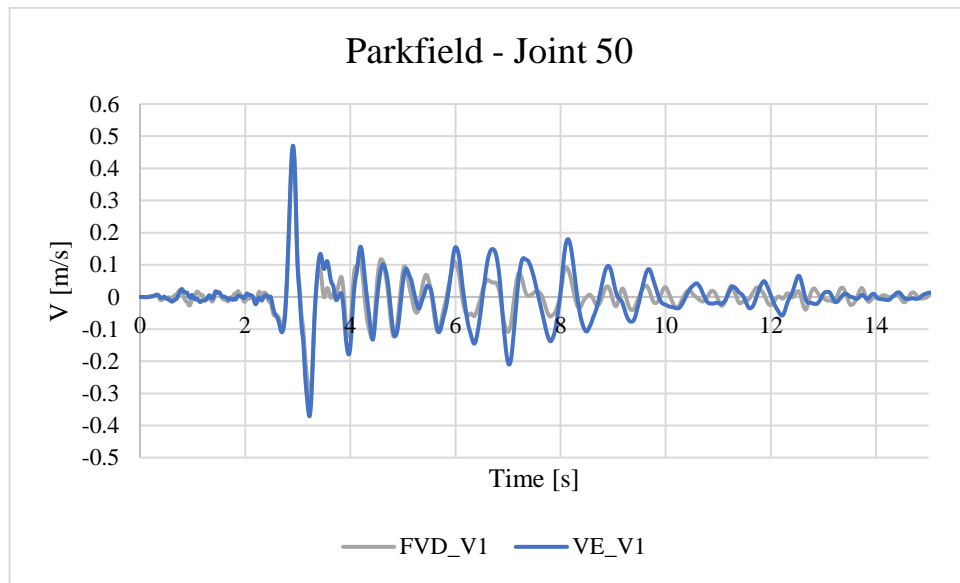


Figure 6.6. Velocity-X Time History (Parkfield Earthquake).

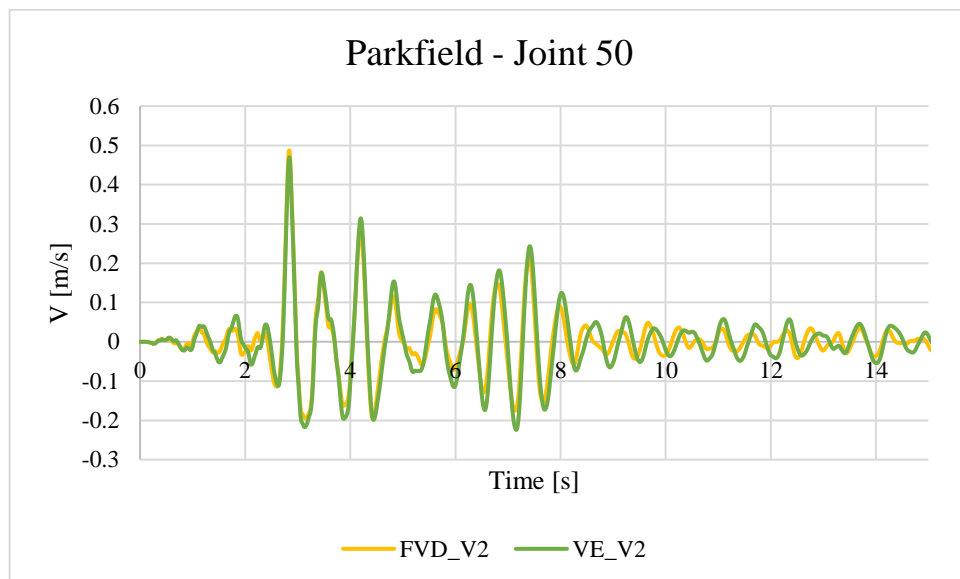


Figure 6.7. Velocity-Y Time History (Parkfield Earthquake).

The velocity time histories of the joint 50, which represents all joints since the rigid diaphragms were assigned in the X and Y directions, are very similar for FVD and VE cases under the pulse like excitations.

All in all, under the pulse like excitations, the structure occupies more in the inelastic region with higher deformation. In that region, plastic deformations occur, and velocities are closer to zero. Because of these reasons, under the pulse like excitations, dampers work under very low velocities, and the behavior of dampers is getting closer to each other for very low velocities. Also, because the structure occupies mostly in the inelastic region, dampers' responses are similar for a larger time interval under the pulse like excitations, and plastic deformations occurs in the interval which dampers' response are very similar. These are the successive explanations for why FVDs and VEs give similar plastic deformation demands under the pulse like excitations.

Most briefly, fluid viscous dampers and viscoelastic dampers are rate dependent, and their response is out of phase with structural strains. Therefore, under the pulse like excitations, their influence on the plastic rotation demands is very similar.

## 7. CONCLUSION

### 7.1. Summary and Results

In this study, passive control devices, fluid viscous dampers and viscoelastic dampers, were used for the retrofitting process of the industrial building located in Malatya, Yeşilyurt. Within the scope of the study, firstly, performance level of the Building Block-1 was figured out according to TBDY 2018 by using nonlinear static analysis (NSA) method. It was demonstrated that the Building Block-1 is at the Collapse Prevention Level, which means that the building possesses a risk of life safety, and therefore should be rehabilitated. For that purpose, fluid viscos dampers (FVDs) and viscoelastic Dampers (VEs) were added to the building, and NLTHA under ten different earthquake records were conducted. Due to the closeness of the structure to the East Anatolian Fault, five of these records were chosen so that they comprise velocity-pulse characteristics. The members' plastic rotation demands were determined as the performance index (PI). Based on the results of NLTHA and maximum plastic rotation demands, important conclusions were obtained and are listed as follows:

- i. For all earthquake records, the dampers caused more reduction in maximum R3 plastic rotations than maximum R2 plastic rotations. This is because the total number of dampers along the longer side of the Building Block-1 is twice the total number of dampers along the shorter side.
- ii. For the no-pulse like records, FVDs led to more reduction in maximum plastic rotations than VEs.
- iii. For the pulse like records, FVDs and VEs gave very close maximum plastic rotation demands.

- iv. Although the Düzce and Darfield earthquakes are classified as pulse-like records, their effect on the response resembles the no-pulse like records. This is because the pulse period of these earthquake records is considerably greater than the period of the structure.
- v. Maximum forces on the link elements during the no-pulse like earthquake excitations are smaller than 250 KN which is the specified damper capacity. On the other hand, the maximum forces on the link elements during the pulse like earthquake excitations are very close to 250 KN or bigger than 250 KN. As the pulse period of earthquake records approaches the period of the structure, the maximum damper force is magnified for example Parkfield Earthquake.
- vi. Although the dampers decreased the plastic rotation demands and the total number of plastic hinges considerably, the structure is still at the Collapse Prevention Level after the retrofitting processes with FVDs and VEs. This is because maximum damper force capacity was determined as 250 KN due to low shear strength of the members. Therefore, to depict the magnitude of damper capacity of 250 KN, it should be said that an FVD having capacity of 250 KN is considered as the minimum damper force capacity in the damper catalog.
- vii. R2 rotations shown on the bar charts are larger than R3 rotations since R2 rotations are about the weak axis.
- viii. Fluid viscous and viscoelastic dampers are rate dependent and their response is out of phase with structural strains. Therefore, FVDs and VEs gave very close maximum plastic rotation demands under the pulse-like excitations.

## 7.2. Future Works

As an extension to this study:

- Different damper configurations, such as scissor jack, toggle brace or chevron brace, can be adopted, and a comparative study evaluating the performance of different damper configurations under no-pulse and pulse like excitations can be conducted.
- Earthquake records, especially pulse like records, can be increased since some of them have very big pulse periods, so they work as a no-pulse like record. However, it is hard to find a pulse-like record that is compatible with the target spectrum, and therefore artificial records can be used.
- Fragility Curves of the building with and without dampers can be developed and decrease in failure probability under different level of input motions can be quantified.
- If possible, an experimental study at the component scale, which includes only the damper and connection part, can be carried through to validate the analytical study results.

## REFERENCES

1. Symans, M. D., F. A. Charney, A. S. Whittaker, M. C. Constantinou, C. A. Kircher, M. W. Johnson and R. J. McNamara, “Energy Dissipation Systems for Seismic Applications: Current Practice and Recent Developments”, *Journal of Structural Engineering*, Vol. 134, No. 1, pp. 3-21, 2008.
2. Braz-César, M. T. and R. Barros, “Passive Control of Civil Engineering Structures”, *IRF2013-Integrity, Reliability and Failure of Mechanical Systems*, 2013.
3. Akcelyan, S., D. G. Lignos, T. Hikino and M. Nakashima, “Evaluation of Simplified and State-of-the-Art Analysis Procedures for Steel Frame Buildings Equipped with Supplemental Damping Devices Based on E-Defense Full-Scale Shake Table Tests”, *Journal of Structural Engineering*, Vol. 142, No. 6, 2016.
4. Dong, B., R. Sause and J. M. Ricles, “Seismic Response and Damage of Reduced-Strength Steel MRF Structures with Nonlinear Viscous Dampers”, *Journal of Structural Engineering*, Vol. 144, No. 12, 2018.
5. Lin, W. H. and A. K. Chopra, “Earthquake Response of Elastic SDF Systems with Non-linear Fluid Viscous Dampers”, *Earthquake Engineering and Structural Dynamics*, Vol. 31, No. 9, pp. 1623-1642, 2002.
6. Singh, M. P. and L. M. Moreschi, “Optimal Seismic Response Control with Dampers”, *Earthquake Engineering and Structural Dynamics*, Vol. 30, No. 4, pp. 553-572, 2001.
7. Lin, W. H. and A. K. Chopra, “Understanding and Predicting Effects of Supplemental Viscous Damping on Seismic Response of Asymmetric One-Storey Systems”, *Earthquake Engineering and Structural Dynamics*, Vol. 30, No. 10, pp. 1475-1494, 2001.

8. Singh, M. P. and L. M. Moreschi, "Optimal Placement of Dampers for Passive Response Control", *Earthquake Engineering and Structural Dynamics*, Vol. 31, No. 4, pp. 955-976, 2002.
9. Cardone, D., M. Dolce, F. C. Ponzo and E. Coelho, "Experimental Behaviour of R/C Frames Retrofitted with Dissipating and Re-Centring Braces", *Journal of Earthquake Engineering*, Vol. 8, No. 3, pp. 361-396, 2004.
10. Rama Raju, K., M. Ansu and N. R. Iyer, "A Methodology of Design for Seismic Performance Enhancement of Buildings Using Viscous Fluid Dampers", *Structural Control and Health Monitoring*, Vol. 21, No. 3, pp. 342-355, 2014.
11. Pan, C., R. Zhang, H. Luo, C. Li and H. Shen, "Demand-Based Optimal Design of Oscillator with Parallel-Layout Viscous Inerter Damper", *Structural Control and Health Monitoring*, Vol. 25, No. 1, 2018.
12. Tubaldi, E., "Dynamic Behavior of Adjacent Buildings Connected by Linear Viscous/Viscoelastic Dampers", *Structural Control and Health Monitoring*, Vol. 22, No. 8, pp. 1086-1102, 2015.
13. Patel, C. C. and R. S. Jangid, "Dynamic Response of Identical Adjacent Structures Connected by Viscous Damper", *Structural Control and Health Monitoring*, Vol. 21, No. 2, pp. 205-224, 2014.
14. Mazza, F. and A. Vulcano, "Equivalent Viscous Damping for Displacement-Based Seismic Design of Hysteretic Damped Braces for Retrofitting Framed Buildings", *Bulletin of Earthquake Engineering*, Vol. 12, No. 6, pp. 2797-2819, 2014.
15. Mazza, F. and A. Vulcano, "Displacement-Based Design Procedure of Damped Braces for the Seismic Retrofitting of RC Framed Buildings", *Bulletin of Earthquake Engineering*, Vol. 13, No. 7, pp. 2121-2143, 2015.

16. Del Gobbo, G. M., A. Blakeborough and M. S. Williams, "Improving Total-Building Seismic Performance Using Linear Fluid Viscous Dampers", *Bulletin of Earthquake Engineering*, Vol. 16, No. 9, pp. 4249-4272, 2018.
17. Lin, Y. Y., K. C. Chang and C. Y. Chen, "Direct Displacement-Based Design for Seismic Retrofit of Existing Buildings Using Nonlinear Viscous Dampers", *Bulletin of Earthquake Engineering*, Vol. 6, No. 3, pp. 535-552, 2008.
18. Jankowski, R. and S. Mahmoud, "Linking of Adjacent Three-Storey Buildings for Mitigation of Structural Pounding During Earthquakes", *Bulletin of Earthquake Engineering*, Vol. 14, No. 11, pp. 3075-3097, 2016.
19. Aiken, I. D., D. K. Nims, A. S. Whittaker and J. M. Kelly, "Testing of Passive Energy Dissipation Systems", *Earthquake Spectra*, Vol. 9, No. 3, pp. 335-370, 1993.
20. Tsai, K. C., H. W. Chen, C. P. Hong and Y. F. Su, "Design of Steel Triangular Plate Energy Absorbers for Seismic-Resistant Construction", *Earthquake Spectra*, Vol. 9, No. 3, pp. 505-528, 1993.
21. Whittaker, A. S., V. V. Bertero, C. L. Thompson and L. J. Alonso, "Seismic Testing of Steel Plate Energy Dissipation Devices", *Earthquake Spectra*, Vol. 7, No. 4, pp. 563-604, 1991.
22. Chang, K. C., T. T. Soong, M. L. Lai and E. J. Nielsen, "Viscoelastic Dampers as Energy Dissipation Devices for Seismic Applications", *Earthquake Spectra*, Vol. 9, No. 3, pp. 371-387, 1993.
23. Ramirez, O. M., M. C. Constantinou, A. S. Whittaker, C. A. Kircher and C. Z. Chrysostomou, "Elastic and Inelastic Seismic Response of Buildings with Damping Systems", *Earthquake Spectra*, Vol. 18, No. 3, pp. 531-547, 2002.
24. Martinez-Romero, E., "Experiences on the Use of Supplementary Energy Dissipators on Building Structures", *Earthquake Spectra*, Vol. 9, No. 3, pp. 581-625, 1993.

25. Ramirez, O. M., M. C. Constantinou, J. D. Gomez, A. S. Whittaker and C. Z. Chrysostomou, "Evaluation of Simplified Methods of Analysis of Yielding Structures with Damping Systems", *Earthquake Spectra*, Vol. 18, No. 3, pp. 501-530, 2002.
26. Whittaker, A. S., M. C. Constantinou, O. M. Ramirez, M. W. Johnson and C. Z. Chrysostomou, "Equivalent Lateral Force and Modal Analysis Procedures of the 2000 NEHRP Provisions for Buildings with Damping Systems", *Earthquake Spectra*, Vol. 19, No. 4, pp. 959-980, 2003.
27. AFAD, "Turkey Earthquake Risk Map", 2018, <https://depem.afad.gov.tr/depem-tehlike-haritasi>, accessed on April 28, 2022.
28. AFAD, "Turkey Earthquake Hazard Maps Application", <https://tdth.afad.gov.tr>, accessed on April 29, 2022.
29. Earthquake Regulation of Buildings in Turkey (TBDY 2018), Government Gazette of Turkey, Ankara, March, 2018. Accessed on: 02,01,2022.
30. Regulation on Buildings to be Built in Earthquake Zones (DBYBHY 2007), Government Gazette of Turkey, Ankara, March 2007. Accessed on: 02,01,2022.
31. A Tool for Section Analysis, TRC-XTRACT Collaboration, Connecticut, July, 2017. Accessed on: 02,18,2022.
32. TS 498 Design Loads for Buildings, Turkish Standards Institute, Ankara, November, 1987. Accessed on: 02,01,2022.
33. Fluid Viscous Dampers General Guidelines for Engineers Including Brief History, 3th ed. Taylor Device Inc., North Tonawanda, New York, 2020. Accessed on: 03,01,2022.
34. Shedbale, N. and P. V. Muley, "Review on Viscoelastic Materials Used in Viscoelastic Dampers", *Int. Res. J. Eng. Technol. (IRJET)*, Vol. 4, No. 7, pp. 3375-3381, 2017.

35. Gosline, A. H. and V. Hayward, “Dual-Channel Haptic Synthesis of Viscoelastic Tissue Properties Using Programmable Eddy Current Brakes”, *The International Journal of Robotics Research*, Vol. 28, No. 10, pp. 1387-1399, 2009.
36. Lobo, R. F., J. M. Bracci, K. L. Shen, A. M. Reinhorn and T. T. Soong, “Inelastic Response of R/C Structures with Viscoelastic Braces”, *Earthquake Spectra*, Vol. 9, No. 3, pp. 419-446, 1993.
37. TS 500 Requirements for Design and Construction of Reinforced Concrete Structures, Turkish Standards Institute, Ankara, February, 2000. Accessed on: 02,01,2022.
38. Abbas, H. and J. M. Kelly, “A Methodology for Design of Viscoelastic Dampers in Earthquake-Resistant Structures”, *Earthquake Engineering Research Center, College of Engineering, University of California*, 1993.
39. Autodesk Inc., AutoCAD, 2022.
40. Software Verification Examples, Computers and Structures Inc., California, January, 2020. Accessed on: 01,01,2022.
41. Selecting and Scaling Earthquake Ground Motions for Performing Response-History Analyses, National Institute of Standard and Technology U.S. Department of Commerce, Maryland, November, 2011. Accessed on: 05,01,2022.
42. The Pacific Earthquake Engineering Research Center (PEER), “PEER Ground Motion Database”, <https://ngawest2.berkeley.edu/>, accessed on April 03,2022.
43. MATLAB Graphics, The MathWorks Inc., Massachusetts, September, 2021. Accessed on: 05,23,2022.
44. Krawinkler, H., B. Alavi and F. Zareian, “Impact of Near-Fault Pulses on Engineering Design”, *In Directions in Strong Motion Instrumentation*, Springer, Dordrecht, pp. 83-106, 2005.

45. Mavroeidis, G. P., G. Dong and A. S. Papageorgiou, “Near-Fault Ground Motions, and the Response of Elastic and Inelastic Single-Degree-of-Freedom (SDOF) Systems”, *Earthquake Engineering and Structural Dynamics*, Vol. 33, No. 9, pp. 1023-1049, 2004.
46. Akkar, S., U. Yazgan and P. Gülkan, “Drift Estimates in Frame Buildings Subjected to Near-Fault Ground Motions”, *Journal of Structural Engineering*, Vol. 131, No. 7, pp. 1014-1024, 2005.